NONLINEAR SPIN WAVE CALCULATION

Spin Wave Analysis of Quasi Two-dimensional Quantum Magnet Cs_2CuCl_4

By

JUNHUA ZHANG, M.Sc.

A Thesis
Submitted to the School of Graduate Studies
in Partial Fulfilment of the Requirements
for the Degree
Master of Science

McMaster University

MASTER OF SCIENCE (2005) McMaster University
(Condensed Matter) Hamilton, Ontario

TITLE: Spin Wave Analysis of Quasi Two-dimensional Quantum Magnet Cs_2CuCl_4

AUTHOR: Junhua Zhang,M.Sc.(Peking University)

SUPERVISOR: Dr. C. Kallin, Dr. A. J. Berlinsky

NUMBER OF PAGES: viii, 100

Abstract

The inelastic neutron scattering measurements by Coldea and co-workers on Cs_2CuCl_4 have attracted intense attention due to the anomalous spin correlation properties revealed. The debate on the low-temperature magnetic phase, spiral ordered phase or spin liquid phase, of this material has triggered mainly two theoretical scenarios, a spin wave scenario and a spinon scenario, for the origin of the unusual scattering continua and large quantum effects. Since there is evidence of low-energy spin wave modes in the experimental data, a study of the spiral ordered phase using perturbation theory, taking into account spin wave interactions, becomes important to determine the nature of the magnetic excitations in this spin system.

Motivated by this situation, we have carried out a perturbation calculation within the nonlinear spin wave theory framework by means of the $1/S$ expansion scheme. In this work, we first develop the general formalism for a class of spiral ordered spin systems. Then we explain how to make contact between our theoretical calculation and experiment. After establishing the necessary formulae, we perform numerical evaluations for Cs_2CuCl_4 to compare with experimental data. We find that a nonlinear spin wave analysis of this material results in significant continua in the scattering spectra as well as large quantum renormalization of the excitation energy. However, our results are quantitatively different from the experimental data. Further numerical work needs to be done to better understand the remaining discrepancies between theory and experiment.

Contents

List of Tables

List of Figures

Chapter 1

Introduction

Recently, there has been intense work in the exploration of two-dimensional (2D) spin liquids in condensed matter physics. Since Anderson postulated a quantum-disordered "resonating-valence-bond" (RVB) ground state in the spin-1/2 Heisenberg triangular antiferromagnet[1, 2], many theoretical advances [3, 4, 5] have made this a promising direction to search for 2D spin liquid states of spin-1/2 frustrated quantum magnets. However, nearly all experimentally studied 2D quantum magnets exhibit conventional magnetic order. In this respect the recent discovery of a 2D quantum magnet Cs_2CuCl_4, whose inelastic neutron scattering measurements revealed unconventional features, has stimulated several studies of the nature of the magnetic excitations in this spin system.

Although previously considered as a quasi-1D spin-1/2 antiferromagnet [6, 7, 8], Cs_2CuCl_4, which is geometrically frustrated with low spin, can also be described as a layered Heisenberg antiferromagnet on a spatially anisotropic triangular lattice [9, 10, 11]. The crystal structure of Cs_2CuCl_4 is orthorhombic (Pnma) with lattice spacings $a = 9.65$Å, $b = 7.48$Å, $c = 12.26$Å, as shown in Fig.1.1. Its quasi-2D character restricts the main superexchange routes to neighboring spin sites in the (bc) plane, and the exchange energies are low $\sim 1 - 4\mathbf{K}$. Experiments suggest a minimal spin Hamiltonian [9] of the form

$$H = \sum_{<i,i'>} J\mathbf{S}_i \cdot \mathbf{S}_{i'} + \sum_{<i,j>} J'\mathbf{S}_i \cdot \mathbf{S}_j,$$

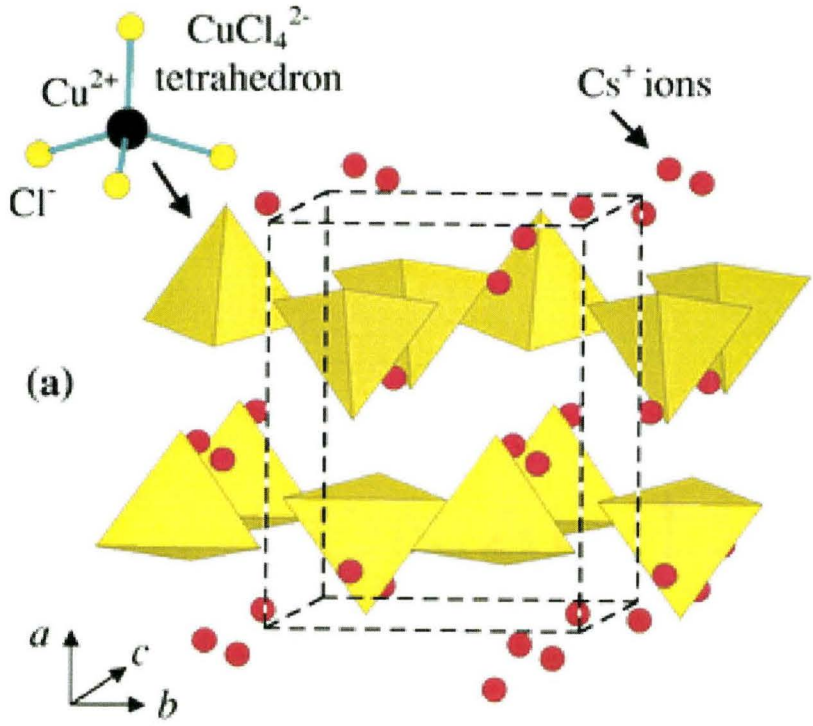

Figure 1.1: Crystal structure in Cs_2CuCl_4 from Ref.[11].

describing an isotropic Heisenberg spin on each site with nearest neighbor coupling J along the b axis and $J'/J = 0.34(3)$ along the zig-zag bonds. The significant dispersion observed along both $[0k0]$ and $[00l]$ directions confirms the two dimensionality of the spin correlations.

What the scattering measurements show is that, although there is incommensurate spiral magnetic order below the Neel temperature $T_N = 0.62\mathbf{K}$, a broad continuum shows up and extends to reasonably high frequencies in the inelastic scattering spectrum in addition to sharp low-energy spin-wave peaks. Linear spin wave theory fails to quantitatively describe the scattering line shape[11].

As the remarkable continuum is reminiscent of spinon excitations in a 1D Heisenberg antiferromagnetic chain, many theoretical investigations of the excitation properties have been carried out and several scenarios have been proposed. In the conventional spin-wave theory (SWT) framework, after the linear spin-wave theory (LSWT)

was exploited[12, 13] on the J_1-J_2 Heisenberg model, a $1/S$-expansion calculation[14, 15] was performed, beyond LSWT, including spin-wave interaction effects. Series expansion studies[16, 17, 18] calculated the excitation spectra of 2D frustrated spin-1/2 Heisenberg antiferromagnets (HAFM's) and found quantitative agreement with experiment. Meanwhile, quasi-1D effects have been explored by treating the triangular lattice as coupled 1D Heisenberg antiferromagnetic chains[19]. Based on the RVB picture, a variational wave-function was constructed as an ansatz for the 2D spin liquid phase[20, 21]. Interestingly, a projective symmetry group (PSG) method was introduced to classify the symmetric spin liquids on triangular lattice[22]. On the other hand, Chung et al.[23, 24, 25] used large-N and slave-boson mean-field theories to study the possible spin-liquid phase in this material.

More recently, Isakov et al.[26] discussed the possibility of the Cs_2CuCl_4 phenomenology controlled by a quantum critical point (QCP) separating the Z_2 spin liquid and the spiral ordered state inspired by the suggested phase diagram (as shown in Fig.1.2) in Ref.[11]. Afterwards, Florens et al.[27] outlined a bosonic version of the Kondo effect in magnetic systems with deconfined bosonic spinons and suggested employing magnetic impurities as a probe of deconfined criticality. Furthermore, based on exact diagonalization and density matrix renormalization group (DMRG) method, Weng et al.[28] studied the phase diagram of an anisotropic triangular lattice Heisenberg spin model and found a spin-liquid phase in the weak interchain coupling regime. Also, a new theoretical approach to the triangular antiferromagnet was exploited[29] to yield a new critical spin liquid—an "algebraic vortex liquid", which was applied to Cs_2CuCl_4.

In spite of the great amount of progress made in the theoretical understanding of spin liquid phases, it is still not clear whether the low-temperature phase of Cs_2CuCl_4, in which low-energy peaks and high-energy continua coexist, is a 2D spin liquid, a quasi-1D spin liquid, or, in fact a conventional magnetically ordered phase. The last possibility is not excluded, though LSWT fails, because when strong magnon interactions are included in the dynamics, a broad continuum appears due to multi-magnon processes. In particular, for a frustrated 2D system, the traditional $1/S$-expansion generates a coupling between transverse and longitudinal excitations such that some

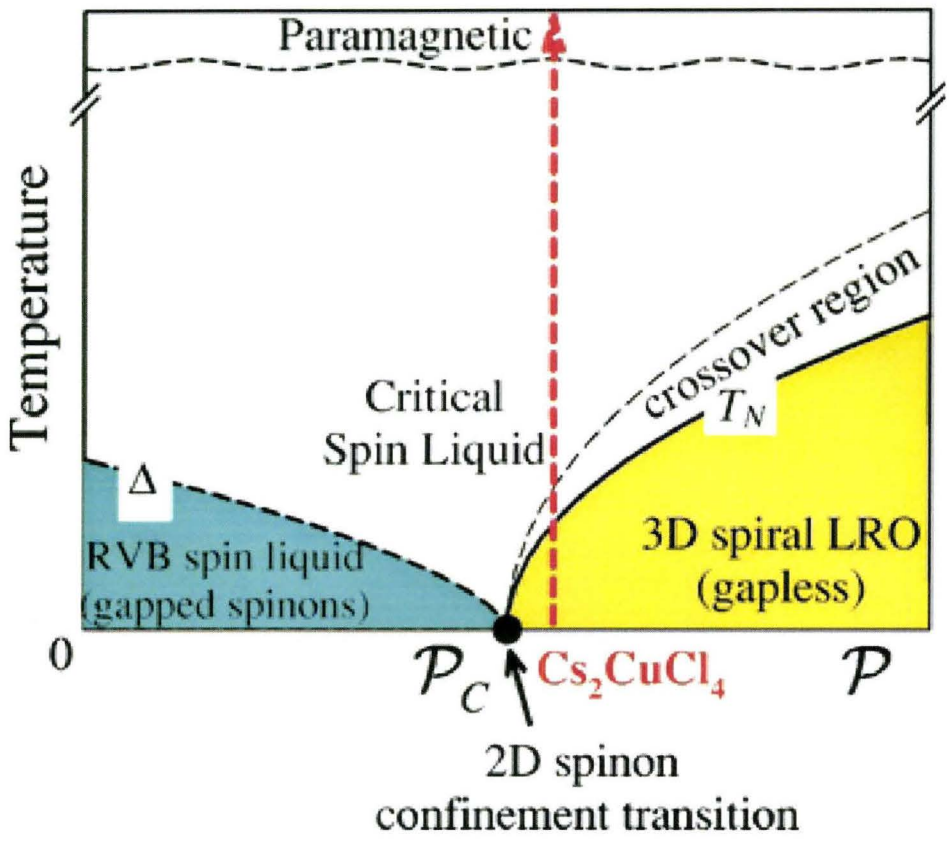

Figure 1.2: Phase diagram of Cs_2CuCl_4 suggested in Ref.[11].

scattering weight from one-magnon processes will be shifted to two-magnon processes. Qualitatively, this reduces the spin-wave peak and enhances the two-particle continuum in the scattering spectra. Also due to the geometric frustration and low spin value, even in the ordered phase the conventional magnetic fluctuations are not expected to be small, which could cause a large renormalization of the bare parameters in the Hamiltonian. Hence it is worthwhile to perform a higher-order calculation to study the quantum effects within non-linear SWT for this spin system.

Motivated by this consideration, Veillette et al.[15] has applied the $1/S$-expansion approach to Cs_2CuCl_4 at zero temperature. They calculated the dynamical spin correlations as well as the renormalized magnon spectrum for the Hamiltonian including the Dzyaloshinskii-Moriya interaction, which creates an effective easy-plane

anisotropy that orients the ordered spins nearly in the (bc) plane. This symmetry breaking term suppresses some low-energy fluctuations and stabilizes the long-range order. However, things remain unclear for the minimal Hamiltonian, where the fluctuations are much stronger. Whether there is still well-established long-range order in SWT, and if there is, how the spin wave dispersion is renormalized by quantum fluctuations and what the dynamical spin correlations turn out to be, are all important issues to be addressed. These unsolved problems have stimulated the theoretical work presented in this thesis.

The remainder is organized as follows. In Chapter 2 after introducing the bosonic Hamiltonian, the LSWT calculation is briefly reviewed with some discussion of the ground state properties. Then beyond LSWT we calculate the zero temperature Green's function to first sub-leading order in $1/S$ expansion, from which the renormalized magnon dispersion is obtained. To make a connection to experimental measurements, we develop expressions for the dynamical structure factor in Chapter 3. In Chapter 4, the established theoretical formalism is applied to a quasi-2D quantum magnet Cs_2CuCl_4. We show our numerical results on the $1/S$ renormalized magnon dispersion and the spin structure factor at different wavevectors to compare with the experimental data. A short conclusion is drawn in Chapter 5. Finally, the treatment of Goldstone modes is left to the Appendix.

Chapter 2

Spin Wave Analysis of J-J' HAFM on the Anisotropic Triangular Lattice

Here we present a general formalism of spin wave analysis for the J-J' Heisenberg antiferromagnet (HAFM) on the spatially anisotropic triangular lattice. The method we are using is the so-called $1/S$ expansion, which is implemented by the Green's function technique.

2.1 Statement of the Problem

We consider an anisotropic triangular lattice with N sites of lattice spacings b and c. The degrees of freedom are vector spin operators $\mathbf{S}_i$ attached to the site $\mathbf{R}_i$, which follow the usual commutation relations

$$[\mathbf{S}_j^{\alpha}\,,\,\mathbf{S}_k^{\beta}] = i\,\epsilon^{\alpha\beta\gamma}\,\mathbf{S}_j^{\gamma}\,\delta_{j,k},$$

where the superscripts α, β, and γ denote the x, y, and z components and $\epsilon^{\alpha\beta\gamma}$ is the totally antisymmetric tensor. We work with periodic boundary conditions and, at the end of the calculation, take the thermodynamic limit.

The dynamics of the degrees of freedom are controlled by the spin-$\frac{1}{2}$ antiferromagnetic Heisenberg Hamiltonian with the exchange coupling J along one bond and the coupling J' along the zigzag directions. Such a model Hamiltonian is expressed as ($\hbar \equiv 1$)

$$H = \sum_{<i,j>} J_{ij} \mathbf{S}_i \cdot \mathbf{S}_j, \tag{2.1}$$

which is invariant under rotations in spin space and where $J_{ij} > 0$ with each nearest neighbor $< i, j >$ counted once. The arrangement of the exchange couplings on the anisotropic triangular lattice, taken from Ref.[11], is shown in Fig.2.1.

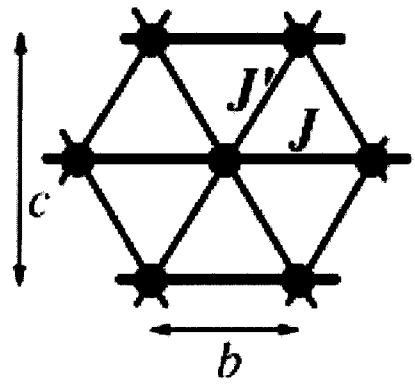

Figure 2.1: Schematic of the exchange couplings on the anisotropic triangular lattice from Ref.[11].

In two space dimensions (2D), the Heisenberg model cannot exhibit long-range order for any spin at finite temperature [30]. Even at zero temperature, it is still an open question whether the spin long-range order can survive quantum fluctuations when the system is frustrated and the amplitude of spin is small, which is the case of interest here. Early studies on the Hamiltonian (2.1) have shown that it exhibits a rich phase diagram with respect to the ratio of the two exchange couplings. In particular, when $J = 0$, it is in the collinearly long-range ordered phase as the case of the square lattice; and when $J' = 0$, it is in the magnetically disordered phase as the case of the 1D spin liquid. For $J = J'$, the frustrated 2D magnet, there has been more and more evidence[31, 32, 33, 34] for the robustness of the non-collinear order, although no rigorous proof is available for the existence or nonexistence of

long-range order in the ground state. It has been proved in the framework of linear spin wave theory[12, 13] that a spiral order, which is a classical configuration of the globally ordered spin structure, arises when J'/J lies between 0 and 2. It is necessary to investigate whether such a non-collinear order can survive quantum fluctuations when spin wave interactions are taken into account and how the physical properties are affected by the interactions.

Here we wish to study the ground-state and the dynamical properties of the Hamiltonian (2.1) on an anisotropic triangular lattice. Assuming that the ground state of the model possesses long-range order, we shall calculate the ground-state energy, the sublattice magnetization, the excitation spectrum and the dynamical spin correlations to the first sub-leading order.

2.2 Spin Wave Theory

Spin wave theory is one of the most powerful tools in the theory of magnetism. Originally proposed by Bloch [35, 36] and Holstein and Primakoff [37] as a theory of the ferromagnetic state, it was later extended to the antiferromagnetic Néel state by Anderson [38], Kubo [39], and Oguchi [40]. Dyson's profound analysis of spin-wave interactions [41, 42] demonstrated that spin waves may be used to obtain asymptotic expansions for the thermodynamic functions of the Heisenberg ferromagnet at low temperatures.[43]

In principle, the spin-wave approach is less effective for low-dimensional quantum spin systems, as quantum spin fluctuations typically increase in reduced space dimensions and for small spin quantum numbers S. Moreover, since at finite temperature thermal fluctuations completely destroy the magnetic long-range order in 1D and 2D Heisenberg models with isotropic short-range interactions [30], in such cases conventional spin wave theory completely fails. Hence all the following discussion is carried out at zero temperature.

The perturbation theory for spin waves is usually called a $1/S$ expansion since LSWT is exact in the limit $S \to \infty$. The Hamiltonian approach to the $1/S$ expansion is quite standard, basically following a few steps:

- Take a boson representation of spin operators;
- Transform the spin Hamiltonian into a boson Hamiltonian;
- Diagonalize the quadratic part by a Bogoliubov transformation to find the unperturbed ground state;
- Treat the higher order terms in the Hamiltonian as perturbations to perform the traditional perturbative calculation.

As a concrete application to our specific model, let us implement the procedures step by step.

2.2.1 Holstein-Primakoff Representation of Spin Operators

The angular momentum eigenstates obey

$$\begin{aligned} J^z|j,m\rangle &= m|j,m\rangle, \\ J^+|j,m\rangle &= \sqrt{(j-m)(j+m+1)}|j,m+1\rangle, \\ J^-|j,m\rangle &= \sqrt{(j+m)(j-m+1)}|j,m-1\rangle, \end{aligned}$$

where $|j,m\rangle$ is the eigenstate of the z component of the angular momentum. The spin operators obey the same rules and if we define a deviation operator $\hat{n} \equiv S - \hat{S}^z$, it has the same eigenstates as $\hat{S}^z$ with the eigenvalue $n = S - m$. Therefore the following properties hold

$$\hat{S}^z|S,n\rangle = (S-n)|S,n\rangle, \quad \hat{n}|S,n\rangle = n|S,n\rangle,$$

$$\hat{S}^+|S,n\rangle = \sqrt{n(2S+1-n)}|S,n-1\rangle = \sqrt{2S\left(1-\frac{n-1}{2S}\right)n}\,|S,n-1\rangle,$$

$$\hat{S}^-|S,n\rangle = \sqrt{(2S-n)(n+1)}|S,n+1\rangle = \sqrt{2S(n+1)\left(1-\frac{n}{2S}\right)}\,|S,n+1\rangle.$$

Introduce the operators

$$a^\dagger|n\rangle \equiv \sqrt{n+1}|n+1\rangle, \quad a|n\rangle \equiv \sqrt{n}|n-1\rangle,$$

where $[a, a^\dagger] = 1$, $[a, a] = [a^\dagger, a^\dagger] = 0$. Then we have

$$\begin{aligned}
\hat{S}^+ &= \sqrt{2S}\, f_S(\hat{n})\, a, \\
\hat{S}^- &= \sqrt{2S}\, a^\dagger\, f_S(\hat{n}), \\
\hat{S}^z &= S - \hat{n}, \\
\hat{n} &= a^\dagger a, \\
f_S(\hat{n}) &\equiv \left[1 - \frac{\hat{n}}{2S}\right]^{1/2}.
\end{aligned} \tag{2.2}$$

Expand the operator $f_S(\hat{n})$ as

$$f_S(\hat{n}) = 1 - \frac{\hat{n}}{4S} - \frac{\hat{n}^2}{32S^2} - \cdots . \tag{2.3}$$

The truncation of the series (2.3) to a finite order may lead to a spectrum that has admixtures of unphysical states with quanta of spin deviations $n > 2S$. This problem was first addressed by Dyson [41] for the ferromagnetic case. For the antiferromagnetic case, there is a perturbation-expansion treatment of the Hamiltonian (2.1) in the original spin-operator representation performed on the square lattice [44] to resolve the problem. Other approaches have also been investigated.

Since the foundation of spin-wave theory for our model is the assumption that antiferromagnetic long-range order exists in the ground state and that the amplitude of zero-point motion of quantum fluctuations about the classical Néel state is small, we directly use the Holstein-Primakoff [37] boson representation to transform the Hamiltonian (2.1) into a boson Hamiltonian kept to order S^0 for the study of spin-wave interaction effects.

2.2.2 Boson Hamiltonian

It is more convenient to transform the non-collinear magnetic structure into a ferromagnetic configuration by applying a uniform twist on the coordinate frame. By doing so we can describe the system in terms of a single boson field, as in the ferromagnetic case [34] [43].

Define local coordinates such that the mean spin direction at each site appears along the z direction. The coordinate transformation between the fixed laboratory reference frame (a, b, c) and the rotating local reference frame (x, y, z) is defined by

$$\begin{pmatrix} S^a_{\mathbf{R}} \\ S^b_{\mathbf{R}} \\ S^c_{\mathbf{R}} \end{pmatrix} = \begin{pmatrix} 1 & 0 & 0 \\ 0 & \cos(\phi_{\mathbf{R}}) & -\sin(\phi_{\mathbf{R}}) \\ 0 & \sin(\phi_{\mathbf{R}}) & \cos(\phi_{\mathbf{R}}) \end{pmatrix} \begin{pmatrix} S^x_{\mathbf{R}} \\ S^y_{\mathbf{R}} \\ S^z_{\mathbf{R}} \end{pmatrix} \tag{2.4}$$

where $\phi_{\mathbf{R}} = \mathbf{Q} \cdot \mathbf{R} + \phi_0$, ϕ_0 is an arbitrary angle. Here $\mathbf{Q}$ is the ordering wavevector describing the long-range spiral ordered configuration of the spins. Then the Hamiltonian $H = \sum J_{\boldsymbol{\delta}} \mathbf{S}_{\mathbf{R}} \cdot \mathbf{S}_{\mathbf{R}+\boldsymbol{\delta}}$ becomes

$$\begin{aligned} H = \sum_{\mathbf{R},\boldsymbol{\delta}} J_{\boldsymbol{\delta}} \Big[& S^x_{\mathbf{R}} S^x_{\mathbf{R}+\boldsymbol{\delta}} + \cos(\mathbf{Q}\cdot\boldsymbol{\delta}) \Big(S^y_{\mathbf{R}} S^y_{\mathbf{R}+\boldsymbol{\delta}} + S^z_{\mathbf{R}} S^z_{\mathbf{R}+\boldsymbol{\delta}} \Big) \\ & - \sin(\mathbf{Q}\cdot\boldsymbol{\delta}) \Big(S^y_{\mathbf{R}} S^z_{\mathbf{R}+\boldsymbol{\delta}} - S^z_{\mathbf{R}} S^y_{\mathbf{R}+\boldsymbol{\delta}} \Big) \Big] \\ = \sum_{\mathbf{R},\boldsymbol{\delta}} J_{\boldsymbol{\delta}} \Big[& S^x_{\mathbf{R}} S^x_{\mathbf{R}+\boldsymbol{\delta}} + \cos(\mathbf{Q}\cdot\boldsymbol{\delta}) \Big(S^y_{\mathbf{R}} S^y_{\mathbf{R}+\boldsymbol{\delta}} + S^z_{\mathbf{R}} S^z_{\mathbf{R}+\boldsymbol{\delta}} \Big) - 2\sin(\mathbf{Q}\cdot\boldsymbol{\delta}) S^y_{\mathbf{R}} S^z_{\mathbf{R}+\boldsymbol{\delta}} \Big] \\ = \sum_{\mathbf{R},\boldsymbol{\delta}} J_{\boldsymbol{\delta}} \Big[& \frac{1}{4}\Big(1 - \cos(\mathbf{Q}\cdot\boldsymbol{\delta})\Big) \Big(S^+_{\mathbf{R}} S^+_{\mathbf{R}+\boldsymbol{\delta}} + S^-_{\mathbf{R}} S^-_{\mathbf{R}+\boldsymbol{\delta}} \Big) \\ & + \frac{1}{4}\Big(1 + \cos(\mathbf{Q}\cdot\boldsymbol{\delta})\Big) \Big(S^+_{\mathbf{R}} S^-_{\mathbf{R}+\boldsymbol{\delta}} + S^-_{\mathbf{R}} S^+_{\mathbf{R}+\boldsymbol{\delta}} \Big) \\ & + \cos(\mathbf{Q}\cdot\boldsymbol{\delta}) S^z_{\mathbf{R}} S^z_{\mathbf{R}+\boldsymbol{\delta}} + i\sin(\mathbf{Q}\cdot\boldsymbol{\delta}) \Big(S^+_{\mathbf{R}} - S^-_{\mathbf{R}} \Big) S^z_{\mathbf{R}+\boldsymbol{\delta}} \Big]. \end{aligned}$$

Applying the Holstein-Primakoff transformation,

$$\begin{aligned} S^+_{\mathbf{R}} &= S^x_{\mathbf{R}} + iS^y_{\mathbf{R}} = \sqrt{2S} \left[1 - \frac{a^\dagger_{\mathbf{R}} a_{\mathbf{R}}}{2S} \right]^{1/2} a_{\mathbf{R}}, \\ S^-_{\mathbf{R}} &= S^x_{\mathbf{R}} - iS^y_{\mathbf{R}} = \sqrt{2S}\, a^\dagger_{\mathbf{R}} \left[1 - \frac{a^\dagger_{\mathbf{R}} a_{\mathbf{R}}}{2S} \right]^{1/2}, \\ S^z_{\mathbf{R}} &= S - a^\dagger_{\mathbf{R}} a_{\mathbf{R}}, \end{aligned} \tag{2.5}$$

the Hamiltonian is

$$H = H^{(0)} + H^{(2)} + H^{(3)} + H^{(4)} + \cdots,$$

where $H^{(n)}$ contains n boson operators and a pre-factor $S^{2-n/2}$,

$$
\begin{aligned}
H^{(0)} =& NS^2 \sum_{\boldsymbol{\delta}} J_{\boldsymbol{\delta}} \cos(\mathbf{Q}\cdot\boldsymbol{\delta}),\\
H^{(2)} =& 2S \sum_{\mathbf{R},\boldsymbol{\delta}} J_{\boldsymbol{\delta}} \Big\{ -\cos(\mathbf{Q}\cdot\boldsymbol{\delta})\, a^\dagger_{\mathbf{R}} a_{\mathbf{R}} + \frac{1}{4}\Big[1+\cos(\mathbf{Q}\cdot\boldsymbol{\delta})\Big]\Big(a^\dagger_{\mathbf{R}+\boldsymbol{\delta}} a_{\mathbf{R}} + a^\dagger_{\mathbf{R}} a_{\mathbf{R}+\boldsymbol{\delta}}\Big)\\
&\qquad + \frac{1}{4}\Big[1-\cos(\mathbf{Q}\cdot\boldsymbol{\delta})\Big]\Big(a^\dagger_{\mathbf{R}+\boldsymbol{\delta}} a^\dagger_{\mathbf{R}} + a_{\mathbf{R}} a_{\mathbf{R}+\boldsymbol{\delta}}\Big)\Big\},\\
H^{(3)} =& \sqrt{2S} \sum_{\mathbf{R},\boldsymbol{\delta}} J_{\boldsymbol{\delta}} \sin(\mathbf{Q}\cdot\boldsymbol{\delta})\, i\Big(a^\dagger_{\mathbf{R}} a^\dagger_{\mathbf{R}+\boldsymbol{\delta}} a_{\mathbf{R}+\boldsymbol{\delta}} - a^\dagger_{\mathbf{R}+\boldsymbol{\delta}} a_{\mathbf{R}+\boldsymbol{\delta}} a_{\mathbf{R}}\Big),\\
H^{(4)} =& \sum_{\mathbf{R},\boldsymbol{\delta}} J_{\boldsymbol{\delta}} \Big\{ \cos(\mathbf{Q}\cdot\boldsymbol{\delta})\, a^\dagger_{\mathbf{R}+\boldsymbol{\delta}} a^\dagger_{\mathbf{R}} a_{\mathbf{R}+\boldsymbol{\delta}} a_{\mathbf{R}}\\
&\quad - \frac{1}{8}\Big[1+\cos(\mathbf{Q}\cdot\boldsymbol{\delta})\Big]\Big(a^\dagger_{\mathbf{R}+\boldsymbol{\delta}} a^\dagger_{\mathbf{R}} a_{\mathbf{R}} a_{\mathbf{R}} + a^\dagger_{\mathbf{R}} a^\dagger_{\mathbf{R}} a_{\mathbf{R}} a_{\mathbf{R}-\boldsymbol{\delta}} + h.c.\Big)\\
&\quad - \frac{1}{8}\Big[1-\cos(\mathbf{Q}\cdot\boldsymbol{\delta})\Big]\Big(a^\dagger_{\mathbf{R}} a_{\mathbf{R}} a_{\mathbf{R}} a_{\mathbf{R}+\boldsymbol{\delta}} + a^\dagger_{\mathbf{R}} a_{\mathbf{R}} a_{\mathbf{R}} a_{\mathbf{R}-\boldsymbol{\delta}} + h.c.\Big)\Big\}.
\end{aligned}
$$

Since the system possesses translational symmetry it is more convenient to perform calculation in momentum space. Take the Fourier transform of the boson operators

$$
a^\dagger_{\mathbf{R}} = \frac{1}{\sqrt{N}} \sum_{\mathbf{k}} a^\dagger_{\mathbf{k}} e^{-i\mathbf{k}\cdot\mathbf{R}}, \quad a_{\mathbf{R}} = \frac{1}{\sqrt{N}} \sum_{\mathbf{k}} a_{\mathbf{k}} e^{i\mathbf{k}\cdot\mathbf{R}}, \tag{2.6}
$$

then the inverse transformation reads:

$$
a^\dagger_{\mathbf{k}} = \frac{1}{\sqrt{N}} \sum_{\mathbf{R}} a^\dagger_{\mathbf{R}} e^{i\mathbf{k}\cdot\mathbf{R}}, \quad a_{\mathbf{k}} = \frac{1}{\sqrt{N}} \sum_{\mathbf{R}} a_{\mathbf{R}} e^{-i\mathbf{k}\cdot\mathbf{R}}. \tag{2.7}
$$

And define

$$
J_{\mathbf{k}} \equiv \sum_{\boldsymbol{\delta}} J_{\boldsymbol{\delta}}\, e^{i\mathbf{k}\cdot\boldsymbol{\delta}} = \sum_{\boldsymbol{\delta}} J_{\boldsymbol{\delta}} \cos(\mathbf{k}\cdot\boldsymbol{\delta}), \tag{2.8}
$$

which is the Fourier transform of the exchange coupling. The Hamiltonian is repre-

sented in momentum space as

$$H^{(0)} = NS^2 J_{\mathbf{Q}}, \tag{2.9}$$

$$H^{(2)} = 2S \sum_{\mathbf{k}} A_{\mathbf{k}} a_{\mathbf{k}}^\dagger a_{\mathbf{k}} + \frac{1}{2} B_{\mathbf{k}} \left(a_{\mathbf{k}}^\dagger a_{-\mathbf{k}}^\dagger + a_{\mathbf{k}} a_{-\mathbf{k}} \right), \tag{2.10}$$

$$H^{(3)} = \frac{\sqrt{2S}}{\sqrt{N}} \sum_{\mathbf{1,2,3}} \delta_{\mathbf{1+2,3}} \frac{1}{2} (C_1 + C_2) \left(a_{\mathbf{1}}^\dagger a_{\mathbf{2}}^\dagger a_{\mathbf{3}} + a_{\mathbf{3}}^\dagger a_{\mathbf{2}} a_{\mathbf{1}} \right), \tag{2.11}$$

$$H^{(4)} = \frac{1}{N} \sum_{\mathbf{1,2,3,4}} \delta_{\mathbf{1+2,3+4}} \left(\frac{1}{2} \right)^2 \Upsilon^{(1)}_{12;34} a_{\mathbf{1}}^\dagger a_{\mathbf{2}}^\dagger a_{\mathbf{3}} a_{\mathbf{4}} \tag{2.12}$$

$$+ \delta_{\mathbf{1+2+3,4}} \frac{1}{3!} \Upsilon^{(2)}_{123} \left(a_{\mathbf{1}}^\dagger a_{\mathbf{2}}^\dagger a_{\mathbf{3}}^\dagger a_{\mathbf{4}} + a_{\mathbf{4}}^\dagger a_{\mathbf{3}} a_{\mathbf{2}} a_{\mathbf{1}} \right), \tag{2.13}$$

where the sum over $\mathbf{k}$ is performed in the first Brillouin zone and the subscripts $\mathbf{1}, \ldots, \mathbf{4}$ denote $\mathbf{k_1}, \ldots, \mathbf{k_4}$. The coefficients are expressed as

$$\begin{aligned}
A_{\mathbf{k}} &\equiv \frac{1}{2} \sum_{\boldsymbol{\delta}} J_{\boldsymbol{\delta}} \cos(\mathbf{k} \cdot \boldsymbol{\delta}) \Big[1 + \cos(\mathbf{Q} \cdot \boldsymbol{\delta}) \Big] - J_{\mathbf{Q}} \\
&= \frac{1}{4} \Big[2J_{\mathbf{k}} + \left(J_{\mathbf{k+Q}} + J_{\mathbf{k-Q}} \right) \Big] - J_{\mathbf{Q}}, \\
B_{\mathbf{k}} &\equiv \frac{1}{2} \sum_{\boldsymbol{\delta}} J_{\boldsymbol{\delta}} \cos(\mathbf{k} \cdot \boldsymbol{\delta}) \Big[1 - \cos(\mathbf{Q} \cdot \boldsymbol{\delta}) \Big] \\
&= \frac{1}{4} \Big[2J_{\mathbf{k}} - \left(J_{\mathbf{k+Q}} + J_{\mathbf{k-Q}} \right) \Big], \\
C_{\mathbf{k}} &\equiv - \sum_{\boldsymbol{\delta}} J_{\boldsymbol{\delta}} \sin(\mathbf{k} \cdot \boldsymbol{\delta}) \sin(\mathbf{Q} \cdot \boldsymbol{\delta}) \\
&= \frac{1}{2} \Big[J_{\mathbf{k+Q}} - J_{\mathbf{k-Q}} \Big], \\
D_{\mathbf{k}} &\equiv \sum_{\boldsymbol{\delta}} J_{\boldsymbol{\delta}} \cos(\mathbf{k} \cdot \boldsymbol{\delta}) \cos(\mathbf{Q} \cdot \boldsymbol{\delta}) \\
&= \frac{1}{2} \Big[J_{\mathbf{k+Q}} + J_{\mathbf{k-Q}} \Big], \\
\Upsilon^{(1)}_{12;34} &\equiv \left(D_{\mathbf{1-3}} + D_{\mathbf{2-3}} + D_{\mathbf{1-4}} + D_{\mathbf{2-4}} \right) - \left(A_1 + A_2 + A_3 + A_4 \right) - 4J_{\mathbf{Q}}, \\
\Upsilon^{(2)}_{123} &\equiv -\left(B_1 + B_2 + B_3 \right).
\end{aligned} \tag{2.14}$$

Using the relation between the coefficients,

$$D_{\mathbf{k}} - J_{\mathbf{Q}} = A_{\mathbf{k}} - B_{\mathbf{k}},$$

we have

$$\begin{aligned}\Upsilon^{(1)}_{12;34} =& (A_{\mathbf{1-3}} + A_{\mathbf{2-3}} + A_{\mathbf{1-4}} + A_{\mathbf{2-4}}) - (B_{\mathbf{1-3}} + B_{\mathbf{2-3}} + B_{\mathbf{1-4}} + B_{\mathbf{2-4}}) \\ & - (A_{\mathbf{1}} + A_{\mathbf{2}} + A_{\mathbf{3}} + A_{\mathbf{4}}), \\ \Upsilon^{(2)}_{123} =& - (B_{\mathbf{1}} + B_{\mathbf{2}} + B_{\mathbf{3}}); \end{aligned} \tag{2.15}$$

Using as well the relations:

$$D_{\mathbf{k}} - C_{\mathbf{k}} = J_{\mathbf{k-Q}}, \qquad D_{\mathbf{k}} + C_{\mathbf{k}} = J_{\mathbf{k+Q}}, \qquad J_{\mathbf{k}} = A_{\mathbf{k}} + B_{\mathbf{k}} + J_{\mathbf{Q}},$$

we find

$$C_{\mathbf{k}} = (A_{\mathbf{k}} - B_{\mathbf{k}}) - (A_{\mathbf{k-Q}} + B_{\mathbf{k-Q}}) = (A_{\mathbf{k+Q}} + B_{\mathbf{k+Q}}) - (A_{\mathbf{k}} - B_{\mathbf{k}}), \tag{2.16}$$

which turns out to be very helpful for the analysis of the Goldstone mode at $\mathbf{k} = \mathbf{Q}$ (see the Appendix).

2.2.3 Linear Spin Wave Theory

Linear spin wave theory only considers the quadratic Hamiltonian which is diagonalized by a Bogoliubov transformation

$$\begin{aligned} a_{\mathbf{k}} = u_{\mathbf{k}}\alpha_{\mathbf{k}} + v_{\mathbf{k}}\alpha^{\dagger}_{\mathbf{-k}}, \qquad a^{\dagger}_{\mathbf{-k}} = v_{\mathbf{k}}\alpha_{\mathbf{k}} + u_{\mathbf{k}}\alpha^{\dagger}_{\mathbf{-k}}; \\ u^2_{\mathbf{k}} - v^2_{\mathbf{k}} = 1. \end{aligned} \tag{2.17}$$

This is a canonical transformation of the second quantized operators such that the commutation relation remains the same. In terms of $\alpha_{\mathbf{k}}, \alpha^{\dagger}_{\mathbf{k}}$ boson operators the quadratic Hamiltonian reads

$$\begin{aligned} H^{(2)} =& 2S \sum_{\mathbf{k}} \Big\{ \left(A_{\mathbf{k}} v^2_{\mathbf{k}} + B_{\mathbf{k}} u_{\mathbf{k}} v_{\mathbf{k}}\right) + \left[A_{\mathbf{k}} \left(u^2_{\mathbf{k}} + v^2_{\mathbf{k}}\right) + B_{\mathbf{k}} 2 u_{\mathbf{k}} v_{\mathbf{k}}\right] \alpha^{\dagger}_{\mathbf{k}} \alpha_{\mathbf{k}} \\ & + \left[A_{\mathbf{k}} u_{\mathbf{k}} v_{\mathbf{k}} + \frac{B_{\mathbf{k}}}{2} \left(u^2_{\mathbf{k}} + v^2_{\mathbf{k}}\right)\right] \left(\alpha^{\dagger}_{\mathbf{k}} \alpha^{\dagger}_{\mathbf{-k}} + \alpha_{\mathbf{k}} \alpha_{\mathbf{-k}}\right) \Big\}. \end{aligned}$$

Setting the off-diagonal part equal to zero, we get

$$H^{(2)} = NSJ_{\mathbf{Q}} + \frac{1}{2} \sum_{\mathbf{k}} \omega_{\mathbf{k}} + \sum_{\mathbf{k}} \omega_{\mathbf{k}} \alpha^{\dagger}_{\mathbf{k}} \alpha_{\mathbf{k}}, \tag{2.18}$$

where $\omega_{\mathbf{k}} = 2S\sqrt{A_{\mathbf{k}}^2 - B_{\mathbf{k}}^2} \equiv 2S\Omega_{\mathbf{k}}$ is the linear spin wave dispersion relation, and

$$u_{\mathbf{k}} = \left[\frac{1}{2}\left(\frac{A_{\mathbf{k}}}{\Omega_{\mathbf{k}}} + 1\right)\right]^{1/2}, \qquad v_{\mathbf{k}} = -\frac{B_{\mathbf{k}}}{|B_{\mathbf{k}}|}\left[\frac{1}{2}\left(\frac{A_{\mathbf{k}}}{\Omega_{\mathbf{k}}} - 1\right)\right]^{1/2}, \tag{2.19}$$

or

$$u_{\mathbf{k}}^2 + v_{\mathbf{k}}^2 = \frac{A_{\mathbf{k}}}{\Omega_{\mathbf{k}}}, \qquad 2u_{\mathbf{k}}v_{\mathbf{k}} = -\frac{B_{\mathbf{k}}}{\Omega_{\mathbf{k}}}. \tag{2.20}$$

Properties of the Ground State

Our perturbative $1/S$ expansion is based on the quadratic Hamiltonian, which is taken as the unperturbed part, and treats the cubic and quartic parts as perturbations. Thus it is necessary to understand the properties of the unperturbed ground state and excitation spectrum. As shown in (2.18), the ground state energy of the quadratic Hamiltonian is different from that of the classical ground state by a quantity $NSJ_{\mathbf{Q}} + \frac{1}{2}\sum_{\mathbf{k}}\omega_{\mathbf{k}}$ and the annihilation and creation of the quasi-particle excitations is denoted by the boson operators $\alpha, \alpha^\dagger$. As the vacuum of the quasi-particle excitations, the ground state $|0\rangle$ satisfies

$$\alpha_{\mathbf{k}}|0\rangle = 0, \qquad \alpha_{\mathbf{k}}^\dagger|0\rangle = |1\rangle$$

and the pair expectation values of α particles with respect to the ground state are

$$\langle\alpha_{\mathbf{k}}\alpha_{\mathbf{k}}^\dagger\rangle = 1; \qquad \langle\alpha_{\mathbf{k}}^\dagger\alpha_{\mathbf{k}}\rangle = \langle\alpha_{\mathbf{k}}^\dagger\alpha_{-\mathbf{k}}^\dagger\rangle = \langle\alpha_{\mathbf{k}}\alpha_{-\mathbf{k}}\rangle = 0.$$

Therefore we obtain non-trivial expectation values of pairs of a and $a^\dagger$ operators in the ground state:

$$\begin{aligned}
\langle a_{\mathbf{k}}a_{\mathbf{k}}^\dagger\rangle &= u_{\mathbf{k}}^2 = \frac{1}{2}\left(\frac{A_{\mathbf{k}}}{\Omega_{\mathbf{k}}} + 1\right), \\
\langle a_{\mathbf{k}}^\dagger a_{\mathbf{k}}\rangle &= v_{\mathbf{k}}^2 = \frac{1}{2}\left(\frac{A_{\mathbf{k}}}{\Omega_{\mathbf{k}}} - 1\right), \\
\langle a_{\mathbf{k}}^\dagger a_{-\mathbf{k}}^\dagger\rangle &= \langle a_{\mathbf{k}}a_{-\mathbf{k}}\rangle = u_{\mathbf{k}}v_{\mathbf{k}} = -\frac{1}{2}\frac{B_{\mathbf{k}}}{\Omega_{\mathbf{k}}}.
\end{aligned} \tag{2.21}$$

Here $\langle a_{\mathbf{k}}^\dagger a_{\mathbf{k}}\rangle$ is simply the density of Holstein-Primakoff particles which is finite in the ground state. Therefore non-interacting spin waves reduce the local spin expectation

value to

$$\begin{aligned}\langle S^z_{\mathbf{R}}\rangle &= S - \frac{1}{N}\sum_{\mathbf{k}}\langle a^\dagger_{\mathbf{k}} a_{\mathbf{k}}\rangle \\ &= S - \frac{1}{N}\sum_{\mathbf{k}}\frac{1}{2}\left(\frac{A_{\mathbf{k}}}{\Omega_{\mathbf{k}}} - 1\right) \\ &= S + \frac{1}{2} - \frac{1}{2N}\sum_{\mathbf{k}}\frac{A_{\mathbf{k}}}{\Omega_{\mathbf{k}}}. \end{aligned} \tag{2.22}$$

Meanwhile quantum corrections to the classical value of $\mathbf{Q}$ can be obtained by minimizing the single site ground state energy, including the correction due to linear spin waves,

$$\frac{E_{LSW}}{N} = S(S+1)J_{\mathbf{Q}} + S\frac{1}{N}\sum_{\mathbf{k}}\Omega_{\mathbf{k}}. \tag{2.23}$$

The critical points are determined by the conditions, which are transcendental equations,

$$\frac{\partial E_{LSW}}{\partial Q_i} = S^2\frac{\partial J_{\mathbf{Q}}}{\partial Q_i} + S\left(1 + \frac{1}{N}\sum_{\mathbf{k}}\frac{A_{\mathbf{k}}}{\Omega_{\mathbf{k}}}\right)\frac{\partial J_{\mathbf{Q}}}{\partial Q_i} + S\,\frac{1}{2N}\sum_{\mathbf{k}}\frac{A_{\mathbf{k}} + B_{\mathbf{k}}}{\Omega_{\mathbf{k}}}\frac{\partial J_{\mathbf{k}+\mathbf{Q}}}{\partial Q_i} = 0,$$

where $i = x, y$. The classical ordering wavevector $\mathbf{Q}_c$ is obtained by keeping the $\mathcal{O}(S^2)$ part only, while the $\mathcal{O}(S^1)$ terms represent the corrections due to the linear spin wave zero-point energy which is a higher order $1/S$ effect. Since the formula holds for general spin amplitude S, perturbation effects are characterized and classified by their order of $1/S$. Thus in lowest order, it is natural to expect that the leading correction to the classical $\mathbf{Q}$ is of order $1/S$. Taking this as given, we expand $\frac{\partial E_{LSW}}{\partial Q_i}$ around $\mathbf{Q}_c$ to linear order and notice that $\frac{\partial J_{\mathbf{Q}}}{\partial Q_i}\Big|_{\mathbf{Q}=\mathbf{Q}_c} = 0$, $\Delta\mathbf{Q} \sim \mathcal{O}(1/S)$, such that

$$\frac{\partial E_{LSW}}{\partial Q_i} \approx S^2\left(\sum_j \frac{\partial^2 J_{\mathbf{Q}}}{\partial Q_i \partial Q_j}\Big|_{\mathbf{Q}=\mathbf{Q}_c}\Delta Q_j + \frac{1}{2S}\frac{1}{N}\sum_{\mathbf{k}}\frac{A_{\mathbf{k}} + B_{\mathbf{k}}}{\Omega_{\mathbf{k}}}\frac{\partial J_{\mathbf{k}+\mathbf{Q}}}{\partial Q_i}\Big|_{\mathbf{Q}=\mathbf{Q}_c}\right) = 0.$$

Hence

$$\Delta\mathbf{Q} = -\frac{1}{2S}\mathbb{M}^{-1}\mathbf{L}, \tag{2.24}$$

where

$$M_{ij} = \frac{\partial^2 J_{\mathbf{Q}}}{\partial Q_i \partial Q_j}\Big|_{\mathbf{Q}=\mathbf{Q}_c}, \quad \text{and} \quad L_i = \frac{1}{N}\sum_{\mathbf{k}}\frac{A_{\mathbf{k}} + B_{\mathbf{k}}}{\Omega_{\mathbf{k}}}\frac{\partial J_{\mathbf{k}+\mathbf{Q}}}{\partial Q_i}\Big|_{\mathbf{Q}=\mathbf{Q}_c}. \tag{2.25}$$

Properties of LSWT Excitations

The normal modes of the LSWT Hamiltonian, the so-called magnons, have the following dispersion relation

$$\omega_{\mathbf{k}} = 2S\sqrt{A_{\mathbf{k}}^2 - B_{\mathbf{k}}^2} = 2S\sqrt{(J_{\mathbf{k}} - J_{\mathbf{Q}})[(J_{\mathbf{k}-\mathbf{Q}} + J_{\mathbf{k}+\mathbf{Q}})/2 - J_{\mathbf{Q}}]}, \tag{2.26}$$

which contains three zero modes at $\mathbf{k} = \mathbf{0}$ and $\pm\mathbf{Q}$. This is no surprise. As we know, one of the consequences of spontaneous continuous symmetry breaking is the appearance of zero-energy excitations, Goldstone modes. We started with a Hamiltonian symmetric in spin space, but postulate a long-range ordered ground state for the system. Then the symmetric Hamiltonian controlled dynamics for this kind of system naturally generates arbitrarily low energy modes, as a reflection of the underlying symmetry.

2.2.4 Spin Wave Interactions

Effects of Quartic Interactions

The corrections due to quartic terms in the Hamiltonian are easy to compute. To leading order in $1/S$, one can just perform the simple one-loop diagrammatic calculation. Alternatively, it can be done by simply decoupling the fourth order term into all possible pair averages. The quadratic form allows for non-zero normal $\langle a_{\mathbf{k}}^\dagger a_{\mathbf{k}}\rangle$ and anomalous $\langle a_{\mathbf{k}}^\dagger a_{-\mathbf{k}}^\dagger\rangle$, $\langle a_{\mathbf{k}} a_{-\mathbf{k}}\rangle$ pair products of Bose particles, and the decoupling changes the quadratic coefficients and the zero-point energy [34].

The existence of off-diagonal terms in the quadratic Hamiltonian implies non-conservation of the number of particles. After the decoupling of quartic terms we are ready to achieve the renormalized ground state and quasi-particle, magnon, energy.

In terms of (2.21) it is straightforward to calculate the renormalized quadratic

coefficients

$$\begin{aligned}\bar{A}_{\mathbf{k}} =& A_{\mathbf{k}}\left[1-\frac{1}{2S}\left(\frac{1}{N}\sum_{\mathbf{q}}\frac{A_{\mathbf{q}}}{\Omega_{\mathbf{q}}}-1\right)\right]+\frac{1}{2S}\frac{1}{N}\sum_{\mathbf{q}}\frac{1}{\Omega_{\mathbf{q}}}\left[\frac{1}{2}B_{\mathbf{k}}B_{\mathbf{q}}+(A_{\mathbf{k}-\mathbf{q}}-B_{\mathbf{k}-\mathbf{q}})A_{\mathbf{q}}\right]\\ &-\frac{1}{2S}\frac{1}{N}\sum_{\mathbf{q}}\Omega_{\mathbf{q}},\\ \bar{B}_{\mathbf{k}} =& B_{\mathbf{k}}\left[1-\frac{1}{2S}\left(\frac{1}{N}\sum_{\mathbf{q}}\frac{A_{\mathbf{q}}}{\Omega_{\mathbf{q}}}-1\right)\right]+\frac{1}{2S}\frac{1}{N}\sum_{\mathbf{q}}\frac{1}{\Omega_{\mathbf{q}}}\left[\frac{1}{2}A_{\mathbf{k}}B_{\mathbf{q}}-(A_{\mathbf{k}-\mathbf{q}}-B_{\mathbf{k}-\mathbf{q}})B_{\mathbf{q}}\right],\end{aligned} \tag{2.27}$$

which do not have dynamical effects since they are frequency independent. There are still well-defined quasi-particle excitations with a modified spectrum $\bar{\omega}_{\mathbf{k}} = \sqrt{\bar{A}_{\mathbf{k}}^2 - \bar{B}_{\mathbf{k}}^2}$. It is easy to see that although the $\mathbf{k} = \mathbf{0}$ zero mode remains gapless, a gap appears at $\mathbf{k} = \pm\mathbf{Q}$ resulting from the fact that symmetry is not preserved unless we include all the contributions of the same order in $1/S$ in the Hamiltonian [45, 46, 47, 48]. Thus it is necessary to investigate the effects due to cubic interactions, which is the topic in the next section.

Other effects due to quartic interaction include the renormalization of the ground-state energy which comes from the completely paired terms, and the order $\mathcal{O}(S^{-2})$ correction to the ordering wavevector $\mathbf{Q}$.

Effects of Cubic Interactions

The contributions from the cubic interacting vertices, which are unique to non-collinear configurations, give rise to a couple of effects:

- Renormalized ground-state energy and the order $\mathcal{O}(S^{-2})$ correction to the ordering wavevector $\mathbf{Q}$;
- Renormalized magnon dispersion relations and associated finite life-times for quasi-particle excitations;
- Non-trivial correlations between one- and two-magnon processes.

We will discuss in detail how the cubic interactions modify excitation spectra and introduce new features to the dynamical spin correlations by coupling the transverse and longitudinal fluctuations.

Since our perturbation expansion is based on the LSWT ground state, i.e. the vacuum of the Bogoliubov transformed particles, on the one hand, one could proceed by transforming the cubic Hamiltonian from the Holstein-Primakoff boson representation $(a, a^\dagger)$ to the Bogoliubov boson basis $(\alpha, \alpha^\dagger)$ to perform the calculation of physical quantities. Alternatively, one may take the original simple form of the cubic vertices and use matrices of bare Green's functions.

2.3 Green's Function at $T = 0$

The Green's function technique is one of the most useful tools for studying the dynamics of many-body systems. Here for our specific problem we introduce the Holstein-Primakoff boson Green's function at zero temperature which has a 2×2 matrix form due to the property of the unperturbed ground state[49]:

$$\mathbb{G}(\mathbf{k},\omega) = \int_{-\infty}^{\infty} \mathrm{d}t e^{i\omega t}(-i) \left\langle T \begin{bmatrix} a_{\mathbf{k}}(t) \\ \\ a^\dagger_{-\mathbf{k}}(t) \end{bmatrix} \begin{bmatrix} a^\dagger_{\mathbf{k}}(0) & a_{-\mathbf{k}}(0) \end{bmatrix} \right\rangle \equiv \begin{bmatrix} G^{-+}(\mathbf{k},\omega) & G^{--}(\mathbf{k},\omega) \\ \\ G^{++}(\mathbf{k},\omega) & G^{+-}(\mathbf{k},\omega) \end{bmatrix}, \tag{2.28}$$

where T is the time-ordering operator. The Dyson equation is

$$\mathbb{G}(\mathbf{k},\omega) = \mathbb{G}_0(\mathbf{k},\omega) + \mathbb{G}_0(\mathbf{k},\omega)\mathbf{\Sigma}(\mathbf{k},\omega)\mathbb{G}(\mathbf{k},\omega), \tag{2.29}$$

where $\mathbb{G}_0(\mathbf{k},\omega)$ is the unperturbed Green's function and $\mathbf{\Sigma}(\mathbf{k},\omega)$ is the self-energy generated by the interaction vertices. From the quadratic Hamiltonian we have

$$\begin{aligned} G_0^{-+}(\mathbf{k},\omega) = G_0^{+-}(\mathbf{k},-\omega) &= \frac{u_{\mathbf{k}}^2}{\omega - \omega_{\mathbf{k}} + i0^+} + \frac{v_{\mathbf{k}}^2}{-\omega - \omega_{\mathbf{k}} + i0^+}, \\ G_0^{--}(\mathbf{k},\omega) = G_0^{++}(\mathbf{k},\omega) &= \frac{u_{\mathbf{k}} v_{\mathbf{k}}}{\omega - \omega_{\mathbf{k}} + i0^+} + \frac{u_{\mathbf{k}} v_{\mathbf{k}}}{-\omega - \omega_{\mathbf{k}} + i0^+}. \end{aligned} \tag{2.30}$$

It will be proved later that the following relations hold:

$$\Sigma^{+-}(\mathbf{k},\omega) = \Sigma^{-+}(\mathbf{k},-\omega) \equiv \Sigma(\mathbf{k},\omega),$$
$$\Sigma^{--}(\mathbf{k},\omega) = \Sigma^{++}(\mathbf{k},\omega) \equiv \Sigma_O(\mathbf{k},\omega),$$

where Σ_O refers to the off-diagonal self-energy. Hence the elements of the exact Green's function have the same relations as those of the unperturbed Green's function:

$$G^{-+}(\mathbf{k},\omega) = G^{+-}(\mathbf{k},-\omega), \quad G^{--}(\mathbf{k},\omega) = G^{++}(\mathbf{k},\omega).$$

Solving the Dyson equation formally we have

$$\begin{aligned}\mathbb{G}(\mathbf{k},\omega) &= \left[\mathbb{G}_0^{-1}(\mathbf{k},\omega) - \boldsymbol{\Sigma}(\mathbf{k},\omega)\right]^{-1} \\ &= \frac{1}{D(\mathbf{k},\omega)} \begin{bmatrix} -2SA_{\mathbf{k}} - \omega - \Sigma(\mathbf{k},-\omega), & 2SB_{\mathbf{k}} + \Sigma_O(\mathbf{k},\omega) \\ 2SB_{\mathbf{k}} + \Sigma_O(\mathbf{k},\omega), & -2SA_{\mathbf{k}} + \omega - \Sigma(\mathbf{k},\omega) \end{bmatrix}. \end{aligned} \tag{2.31}$$

In terms of the symmetric and antisymmetric combinations of the self-energy Σ

$$\Sigma_S(\mathbf{k},\omega) = \frac{1}{2}\left[\Sigma(\mathbf{k},\omega) + \Sigma(\mathbf{k},-\omega)\right], \quad \Sigma_A(\mathbf{k},\omega) = \frac{1}{2}\left[\Sigma(\mathbf{k},\omega) - \Sigma(\mathbf{k},-\omega)\right],$$
$$\Sigma(\mathbf{k},\omega) = \Sigma_S(\mathbf{k},\omega) + \Sigma_A(\mathbf{k},\omega), \quad \Sigma(\mathbf{k},-\omega) = \Sigma_S(\mathbf{k},\omega) - \Sigma_A(\mathbf{k},\omega),$$

we can express the denominator as

$$D(\mathbf{k},\omega) = \left[2SA_{\mathbf{k}} + \Sigma_S(\mathbf{k},\omega)\right]^2 - \left[2SB_{\mathbf{k}} + \Sigma_O(\mathbf{k},\omega)\right]^2 - \left[\omega - \Sigma_A(\mathbf{k},\omega)\right]^2. \tag{2.32}$$

2.3.1 Renormalized Excitation Spectrum

The singularities of the exact Green's function determine both the excitation energies and the corresponding damping. Looking into the pole structure equation

$$\left[\omega - \Sigma_A(\mathbf{k},\omega)\right]^2 = \left[2SA_{\mathbf{k}} + \Sigma_S(\mathbf{k},\omega)\right]^2 - \left[2SB_{\mathbf{k}} + \Sigma_O(\mathbf{k},\omega)\right]^2, \tag{2.33}$$

the linear (bare) dispersion relation is naturally recovered. Apparently, any $1/S$ corrections to the quadratic coefficients $A_{\mathbf{k}}$ and $B_{\mathbf{k}}$ contribute in the same order as the self-energies, i.e. $\mathcal{O}(S^0)$. Based on the earlier analysis, we see that there are two

sources. On the one hand, the shifted $\mathbf{Q}$, due to linear spin-wave fluctuation, results in:

$$\Delta A_{\mathbf{k}} = -\frac{1}{8S}\sum_{i,j}\left[\frac{\partial J(\mathbf{k}+\mathbf{Q})}{\partial Q_i}+\frac{\partial J(\mathbf{k}-\mathbf{Q})}{\partial Q_i}\right]_{\mathbf{Q}=\mathbf{Q}_c} M_{ij}^{-1}L_j,$$
$$\Delta B_{\mathbf{k}} = -\Delta A_{\mathbf{k}}. \tag{2.34}$$

On the other hand, the $1/S$ correction due to quartic vertices, the so called one-loop corrections in the sense of Feynman diagrammatic analysis, is purely real and frequency independent which can be incorporated into the redefinition of the quadratic coefficients denoted by $\bar{A}_{\mathbf{k}}$ and $\bar{B}_{\mathbf{k}}$ in (2.27). At this stage, we may include (2.34) into (2.27) such that $\bar{A}_{\mathbf{k}}$ and $\bar{B}_{\mathbf{k}}$ represent both of these two corrections. Then there are only cubic vertices involved in the diagrammatic perturbative calculation of the self-energies which are frequency dependent and consist of both real and imaginary parts. From this analysis we might write the above equation in the following way

$$\left[\omega-\Sigma_A^{(3)}(\mathbf{k},\omega)\right]^2=\left[2S\bar{A}_{\mathbf{k}}+\Sigma_S^{(3)}(\mathbf{k},\omega)\right]^2-\left[2S\bar{B}_{\mathbf{k}}+\Sigma_O^{(3)}(\mathbf{k},\omega)\right]^2. \tag{2.35}$$

However for the convenience of resolving the perturbative solution of the excitation we restore the contribution of the quartic interactions into the self-energy part to treat equation (2.33) as the starting point. Notice that the self-energies are of order $\mathcal{O}(S^0)$ explicitly, if we are pursuing the leading order correction to the excitation spectrum in a $1/S$ scheme, it is allowable to substitute the zeroth-order value of the excitation dispersion relation into the self-energy expressions. Assume

$$\omega=\omega_{\mathbf{k}}+\Delta\omega_{\mathbf{k}}-i\Gamma_{\mathbf{k}}=2S\Omega_{\mathbf{k}}+\Delta\omega_{\mathbf{k}}-i\Gamma_{\mathbf{k}}, \tag{2.36}$$

is the solution to (2.33), where $\Delta\omega_{\mathbf{k}}$, $\Gamma_{\mathbf{k}}\sim\mathcal{O}(S^0)$ are real. By keeping the terms to $\mathcal{O}(S^1)$ on both sides, order by order, we find that

$$\Delta\omega_{\mathbf{k}}=\frac{1}{\Omega_{\mathbf{k}}}\Big[A_{\mathbf{k}}\Big(2S\Delta A_{\mathbf{k}}+\mathrm{Re}\Sigma_S(\mathbf{k},\omega_{\mathbf{k}})\Big)-B_{\mathbf{k}}\Big(2S\Delta B_{\mathbf{k}}+\mathrm{Re}\Sigma_O(\mathbf{k},\omega_{\mathbf{k}})\Big)\Big]$$
$$+\mathrm{Re}\Sigma_A(\mathbf{k},\omega_{\mathbf{k}}),$$
$$\Gamma_{\mathbf{k}}=-\frac{1}{\Omega_{\mathbf{k}}}\Big[A_{\mathbf{k}}\,\mathrm{Im}\Sigma_S(\mathbf{k},\omega_{\mathbf{k}})-B_{\mathbf{k}}\,\mathrm{Im}\Sigma_O(\mathbf{k},\omega_{\mathbf{k}})\Big]-\mathrm{Im}\Sigma_A(\mathbf{k},\omega_{\mathbf{k}}), \tag{2.37}$$

which are of order $\mathcal{O}(S^0)$ as assumed. Therefore to leading order in the $1/S$ expansion, if $\Gamma_{\mathbf{k}}$, the damping rate, is small compared to the excitation energy $\widetilde{\omega}_{\mathbf{k}} = \omega_{\mathbf{k}} + \Delta\omega_{\mathbf{k}}$, there still exist single-particle type excitations (well-defined quasi-particles) in the interacting many-body system, but with a finite life-time which damps the quasi-particles.

It can be shown that the Goldstone modes are maintained (see the Appendix for details).

2.3.2 One-loop Self-energies

Quartic Self-energy

Our model Hamiltonian shows that the first order perturbation theory in quartic vertices and the second order perturbative calculation in cubic vertices contribute the same order self-energies in the $1/S$ criterion. As discussed in the last section, it is easy to obtain the self-energies due to the quartic interactions from the earlier result (2.27):

$$\begin{aligned}
\Sigma_S^{(4)}(\mathbf{k}) &= A_{\mathbf{k}} + \frac{2S}{N}\sum_{\mathbf{q}}\frac{1}{\omega_{\mathbf{q}}}\left[\left(A_{\mathbf{k}-\mathbf{q}} - B_{\mathbf{k}-\mathbf{q}} - A_{\mathbf{k}} - A_{\mathbf{q}}\right)A_{\mathbf{q}} + \left(\frac{1}{2}B_{\mathbf{k}} + B_{\mathbf{q}}\right)B_{\mathbf{q}}\right], \\
\Sigma_O^{(4)}(\mathbf{k}) &= B_{\mathbf{k}} + \frac{2S}{N}\sum_{\mathbf{q}}\frac{1}{\omega_{\mathbf{q}}}\left[\left(-A_{\mathbf{k}-\mathbf{q}} + B_{\mathbf{k}-\mathbf{q}} + \frac{1}{2}A_{\mathbf{k}} + A_{\mathbf{q}}\right)B_{\mathbf{q}} - \left(B_{\mathbf{k}} + B_{\mathbf{q}}\right)A_{\mathbf{q}}\right], \\
\Sigma_A^{(4)}(\mathbf{k}) &= 0.
\end{aligned} \tag{2.38}$$

Cubic Self-energy

Before evaluating the one-loop diagrams enabled by two cubic vertices, let us briefly recall some basic principles of diagrammatic perturbation theory. Instead of exactly solving interacting many-degree-of-freedom system, a much simpler and more generally applicable approach is: Treat the interaction term H_I as a perturbation, compute its effects as far in perturbation as is practicable, and hope that the perturbation is small enough that this gives a reasonable approximation to the exact answer. Through the use of Feynman diagrams it will be possible to visualize the

perturbation series which turns out to be very simple in structure. To illustrate this, let us consider the two-point correlation function, or two-point Green's function as defined earlier,

$$\langle\Omega|T\{\phi(x)\phi(y)\}|\Omega\rangle, \tag{2.39}$$

where the notation $|\Omega\rangle$ denotes the ground state of the interacting theory, which is generally different from $|0\rangle$, the ground state of the free theory, and $\phi(x)$ represents a field operator defined at space-time point $x = (\mathbf{x}, t)$. Using Gell-Mann and Low's theorem on the ground state, we arrive at an expression in the interaction picture:

$$\langle\Omega|T\{\phi(x)\phi(y)\}|\Omega\rangle = \frac{\langle 0|T\{\phi_I(x)\phi_I(y)\exp[-i\int_{-\infty}^{\infty}\mathrm{d}t\, H_I(t)]\}|0\rangle}{\langle 0|T\{\exp[-i\int_{-\infty}^{\infty}\mathrm{d}t\, H_I(t)]\}|0\rangle}. \tag{2.40}$$

So far this expression is exact. The virtue of it is that it is ideally suited to doing perturbative calculations; we need only retain as many terms as desired in the Taylor series expansions of the exponentials. Next, Wick's theorem states an operator identity:

$$T\{\phi(x_1)\phi(x_2)\cdots\phi(x_m)\} = N\{\phi(x_1)\phi(x_2)\cdots\phi(x_m) + \text{all possible contractions}\}. \tag{2.41}$$

For non-condensed particle ϕ, in the vacuum expectation value of this time-ordered operator product, any term in which there remain uncontracted operators gives zero, which allows us to turn any expression of the form

$$\langle 0|T\{\phi_I(x_1)\phi_I(x_2)\cdots\phi_I(x_n)\}|0\rangle \tag{2.42}$$

into a sum of products of free two-point correlations. Then, what follows is to develop a diagrammatic interpretation of such expressions. These diagrams are the so-called Feynman diagrams, each of which is built out of propagators, vertices, and external points. To write down the analytic formula for the diagrams, one needs to make certain rules for associating analytic expressions with pieces of diagrams. In most calculations, it is simpler to express the Feynman rules in momentum space. Finally, the disconnected diagrams exponentiate, factor, and cancel.

Applying to our case, we are concerned with the cubic interaction

$$H^{(3)} = \sqrt{\frac{2S}{N}} \sum_{\mathbf{1,2}} \delta_{\mathbf{1+2,3}} \frac{1}{2}(C_{\mathbf{1}} + C_{\mathbf{2}})(a^{\dagger}_{\mathbf{3}} a_{\mathbf{2}} a_{\mathbf{1}} + a^{\dagger}_{\mathbf{1}} a^{\dagger}_{\mathbf{2}} a_{\mathbf{3}}), \tag{2.43}$$

$$C_{\mathbf{k}} = \frac{1}{2}(J_{\mathbf{k+Q}} - J_{\mathbf{k-Q}}). \tag{2.44}$$

Since the procedure mentioned above is directly applied to non-condensed particles, it is more convenient to work with the quasiparticle α. Thus, changing particle basis from a to α, (2.43) becomes

$$H^{(3)} = \sqrt{\frac{2S}{N}} \sum_{\mathbf{1,2}} \delta_{\mathbf{1+2-3}} \left[\frac{1}{2} f^{(1)}_{\mathbf{1,2}} \left(\alpha^{\dagger}_{\mathbf{3}} \alpha_{\mathbf{2}} \alpha_{\mathbf{1}} + \alpha^{\dagger}_{\mathbf{1}} \alpha^{\dagger}_{\mathbf{2}} \alpha_{\mathbf{3}} \right) \right.$$
$$\left. + \frac{1}{3!} f^{(2)}_{\mathbf{1,2}} \left(\alpha_{\mathbf{-3}} \alpha_{\mathbf{2}} \alpha_{\mathbf{1}} + \alpha^{\dagger}_{\mathbf{1}} \alpha^{\dagger}_{\mathbf{2}} \alpha^{\dagger}_{\mathbf{-3}} \right) \right], \tag{2.45}$$

where

$$f^{(1)}_{\mathbf{1,2}} = (C_{\mathbf{1}} + C_{\mathbf{2}})(u_{\mathbf{1}} u_{\mathbf{2}} u_{\mathbf{3}} - v_{\mathbf{1}} v_{\mathbf{2}} v_{\mathbf{3}}) + (C_{\mathbf{1}} - C_{\mathbf{3}})(u_{\mathbf{1}} v_{\mathbf{2}} v_{\mathbf{3}} - v_{\mathbf{1}} u_{\mathbf{2}} u_{\mathbf{3}})$$
$$+ (C_{\mathbf{2}} - C_{\mathbf{3}})(v_{\mathbf{1}} u_{\mathbf{2}} v_{\mathbf{3}} - u_{\mathbf{1}} v_{\mathbf{2}} u_{\mathbf{3}}), \tag{2.46}$$

$$f^{(2)}_{\mathbf{1,2}} = (C_{\mathbf{1}} + C_{\mathbf{2}})(u_{\mathbf{1}} u_{\mathbf{2}} v_{\mathbf{3}} - v_{\mathbf{1}} v_{\mathbf{2}} u_{\mathbf{3}}) + (C_{\mathbf{1}} - C_{\mathbf{3}})(u_{\mathbf{1}} v_{\mathbf{2}} u_{\mathbf{3}} - v_{\mathbf{1}} u_{\mathbf{2}} v_{\mathbf{3}})$$
$$+ (C_{\mathbf{2}} - C_{\mathbf{3}})(v_{\mathbf{1}} u_{\mathbf{2}} u_{\mathbf{3}} - u_{\mathbf{1}} v_{\mathbf{2}} v_{\mathbf{3}}), \tag{2.47}$$

The prefactors 1/2 and 1/3! reflect the symmetries between the operators at the vertex and they will be cancelled by the number of ways to place contractions into this vertex when we evaluate Feynman diagrams. In the diagrams to be calculated, we may use an α-particle for the internal propagator whilst keeping the external particle in HP boson so as to connect with the originally defined Green's function. A further analysis shows that there are merely two bubble diagrams contributing, which relate to two types of cubic vertices. In light of this, the interaction Hamiltonian takes the following form after transforming one of the α-particle back to an a-particle,

$$H^{(3)} = \sqrt{\frac{2S}{N}} \sum_{\mathbf{1,2}} \delta_{\mathbf{1+2-3}} \left[\left(f^{(1)}_{\mathbf{1,2}} \cdot u_{\mathbf{3}} - f^{(2)}_{\mathbf{1,2}} \cdot v_{\mathbf{3}} \right) \left(a^{\dagger}_{\mathbf{3}} \alpha_{\mathbf{2}} \alpha_{\mathbf{1}} + \alpha^{\dagger}_{\mathbf{1}} \alpha^{\dagger}_{\mathbf{2}} a_{\mathbf{3}} \right) \right.$$
$$\left. + \left(- f^{(1)}_{\mathbf{1,2}} \cdot v_{\mathbf{3}} + f^{(2)}_{\mathbf{1,2}} \cdot u_{\mathbf{3}} \right) \left(a_{\mathbf{-3}} \alpha_{\mathbf{2}} \alpha_{\mathbf{1}} + \alpha^{\dagger}_{\mathbf{1}} \alpha^{\dagger}_{\mathbf{2}} a^{\dagger}_{\mathbf{-3}} \right) \right], \tag{2.48}$$

where we have dropped the prefactors 1/2 and 1/3! because they are naturally vanishing in the Feynman diagram calculation for the symmetry reason mentioned above. As a result, the two types of cubic vertex functions are

$$\begin{aligned}\Psi^{(1)}_{\mathbf{1,2}} =& f^{(1)}_{\mathbf{1,2}} \cdot u_{\mathbf{3}} - f^{(2)}_{\mathbf{1,2}} \cdot v_{\mathbf{3}} \\ =& (C_{\mathbf{1}} + C_{\mathbf{2}}) \cdot u_{\mathbf{1}} u_{\mathbf{2}} - (C_{\mathbf{1}} - C_{\mathbf{3}}) \cdot v_{\mathbf{1}} u_{\mathbf{2}} - (C_{\mathbf{2}} - C_{\mathbf{3}}) \cdot u_{\mathbf{1}} v_{\mathbf{2}},\end{aligned} \tag{2.49}$$

associating with such type of vertices as shown in Fig.2.2: and

Figure 2.2: Schematic of the first type of cubic vertices: The red lines represent the Bogoliubov transformed bosons and the black ones denote the HP bosons. To highlight the cubic interaction vertices, we draw them in blue.

$$\begin{aligned}\Psi^{(2)}_{\mathbf{1,2}} =& - f^{(1)}_{\mathbf{1,2}} \cdot v_{\mathbf{3}} + f^{(2)}_{\mathbf{1,2}} \cdot u_{\mathbf{3}} \\ =& - (C_{\mathbf{1}} + C_{\mathbf{2}}) \cdot v_{\mathbf{1}} v_{\mathbf{2}} + (C_{\mathbf{1}} - C_{\mathbf{3}}) \cdot u_{\mathbf{1}} v_{\mathbf{2}} + (C_{\mathbf{2}} - C_{\mathbf{3}}) \cdot v_{\mathbf{1}} u_{\mathbf{2}},\end{aligned} \tag{2.50}$$

associating with such type of vertices as shown in Fig.2.3:

Figure 2.3: Schematic of the second type of cubic vertices with the same color arrangement as that for the first type.

It is easy to see that these vertex functions are symmetric with respect to exchange between **1** and **2**, and are odd functions of **1** and **2**, i.e., $\Psi^{(j)}_{-\mathbf{1},-\mathbf{2}} = -\Psi^{(j)}_{\mathbf{1},\mathbf{2}}$.

We are left with the following momentum-space Feynman rules:

1. For each α-propagator, it has the expression $g_0(\mathbf{k},\omega) = \frac{1}{\omega-\omega_{\mathbf{k}}+i0^+}$;
2. For each vertex, it is associated with a factor function $i^{1/2}\sqrt{2S}\ \Psi^{(j)}_{\mathbf{1},\mathbf{2}}$, $j = 1, 2$;
3. For each external point, there is a momentum-flow $(\mathbf{k},\omega)$ in or out;
4. Impose momentum conservation at each vertex;
5. Integrate over each undetermined 4-momentum: $\frac{1}{N}\sum_{\mathbf{q}}\int_{-\infty}^{\infty}\frac{\mathrm{d}\omega'}{2\pi}$;
6. Divide by the symmetry factor.

Taking the net momentum-flow direction from right to left, the two bubble diagrams are demonstrated in Fig.2.4.

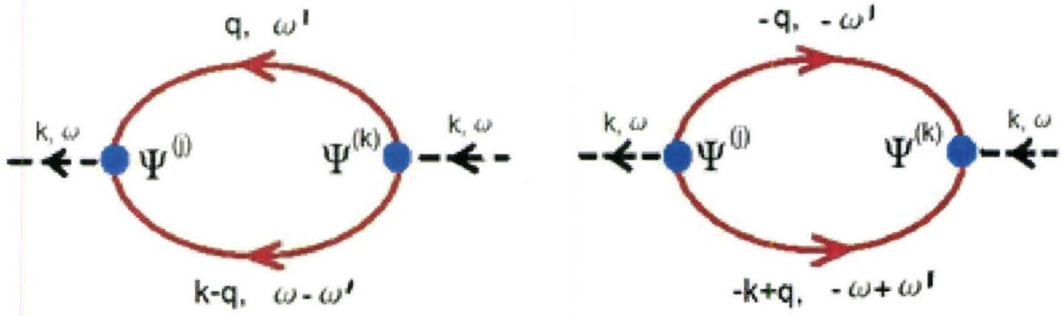

Figure 2.4: Schematic of the two bubble diagrams due to cubic interactions. The dashed lines represent the net momentum-flows.

Their analytic expressions are

$$-\frac{1}{2}\cdot\frac{2S}{N}\sum_{\mathbf{q}}\Psi^{(j)}_{\mathbf{1},\mathbf{2}}\Psi^{(k)}_{\mathbf{1},\mathbf{2}}\int_{-\infty}^{\infty}\frac{\mathrm{d}\omega'}{2\pi i}\,g_0(\mathbf{q},\omega')g_0(\mathbf{k}-\mathbf{q},\omega-\omega') \tag{2.51}$$

and

$$-\frac{1}{2}\cdot\frac{2S}{N}\sum_{\mathbf{q}}\Psi^{(j)}_{\mathbf{1},\mathbf{2}}\Psi^{(k)}_{\mathbf{1},\mathbf{2}}\int_{-\infty}^{\infty}\frac{\mathrm{d}\omega'}{2\pi i}\,g_0(-\mathbf{q},-\omega')g_0(-\mathbf{k}+\mathbf{q},-\omega+\omega'), \tag{2.52}$$

where the minus sign comes from $(i^{1/2})^2 = -1/i$; the prefactor $1/2$ is due to the symmetry factor "2" of the diagrams, and the vertex functions involved are determined by the external particles. Integrating over the internal frequency, they become

$$-\frac{S}{N}\sum_{\mathbf{q}}\frac{\Psi_{1,2}^{(j)}\Psi_{1,2}^{(k)}}{\omega_1+\omega_2-\omega-i0^+}, \quad \text{and} \quad -\frac{S}{N}\sum_{\mathbf{q}}\frac{\Psi_{1,2}^{(j)}\Psi_{1,2}^{(k)}}{\omega_1+\omega_2+\omega-i0^+}. \tag{2.53}$$

Both of the bubble diagrams go into each element of the self-energy matrix. Together with the right type of vertices, it is now possible to obtain the expressions for these elements:

$$\begin{aligned}
\Sigma^{+-}(\mathbf{k},\omega) &= -\frac{S}{N}\sum_{\mathbf{q}}\left[\frac{\left(\Psi_{1,2}^{(1)}\right)^2}{\omega_1+\omega_2-\omega-i0^+}+\frac{\left(\Psi_{1,2}^{(2)}\right)^2}{\omega_1+\omega_2+\omega-i0^+}\right],\\
\Sigma^{-+}(\mathbf{k},\omega) &= -\frac{S}{N}\sum_{\mathbf{q}}\left[\frac{\left(\Psi_{1,2}^{(2)}\right)^2}{\omega_1+\omega_2-\omega-i0^+}+\frac{\left(\Psi_{1,2}^{(1)}\right)^2}{\omega_1+\omega_2+\omega-i0^+}\right],\\
\Sigma^{++}(\mathbf{k},\omega) &= -\frac{S}{N}\sum_{\mathbf{q}}\left[\frac{\Psi_{1,2}^{(1)}\Psi_{1,2}^{(2)}}{\omega_1+\omega_2-\omega-i0^+}+\frac{\Psi_{1,2}^{(1)}\Psi_{1,2}^{(2)}}{\omega_1+\omega_2+\omega-i0^+}\right],\\
\Sigma^{--}(\mathbf{k},\omega) &= -\frac{S}{N}\sum_{\mathbf{q}}\left[\frac{\Psi_{1,2}^{(1)}\Psi_{1,2}^{(2)}}{\omega_1+\omega_2-\omega-i0^+}+\frac{\Psi_{1,2}^{(1)}\Psi_{1,2}^{(2)}}{\omega_1+\omega_2+\omega-i0^+}\right].
\end{aligned} \tag{2.54}$$

In the symmetric, antisymmetric and off-diagonal element notation, we have

$$\begin{aligned}
\Sigma_S^{(3)}(\mathbf{k},\omega) &= \frac{-S}{2N}\sum_{\mathbf{q}}\left[\left(\Psi_{1,2}^{(1)}\right)^2+\left(\Psi_{1,2}^{(2)}\right)^2\right]\left(\frac{1}{\omega_1+\omega_2-\omega-i0^+}+\frac{1}{\omega_1+\omega_2+\omega-i0^+}\right),\\
\Sigma_O^{(3)}(\mathbf{k},\omega) &= \frac{-S}{2N}\sum_{\mathbf{q}}\left[2\,\Psi_{1,2}^{(1)}\cdot\Psi_{1,2}^{(2)}\right]\left(\frac{1}{\omega_1+\omega_2-\omega-i0^+}+\frac{1}{\omega_1+\omega_2+\omega-i0^+}\right),\\
\Sigma_A^{(3)}(\mathbf{k},\omega) &= \frac{-S}{2N}\sum_{\mathbf{q}}\left[\left(\Psi_{1,2}^{(1)}\right)^2-\left(\Psi_{1,2}^{(2)}\right)^2\right]\left(\frac{1}{\omega_1+\omega_2-\omega-i0^+}-\frac{1}{\omega_1+\omega_2+\omega-i0^+}\right).
\end{aligned} \tag{2.55}$$

At this stage, it is clearly shown that all the self-energy elements are even functions of $\mathbf{k}$; $\Sigma_S^{(3)}$ and $\Sigma_O^{(3)}$ are even, or symmetric, functions of ω whereas $\Sigma_A^{(3)}$ is odd, or antisymmetric.

For later convenience, we introduce another set of definitions for the vertex functions:

$$\begin{aligned}
\Phi^{(1)}_{\mathbf{1,2}} \equiv & \Psi^{(1)}_{\mathbf{1,2}} + \Psi^{(2)}_{\mathbf{1,2}} \\
= & (C_1 + C_2)(u_1 u_2 - v_1 v_2) + (C_1 - C_2)(u_1 v_2 - v_1 u_2) \\
= & C_1(u_1 - v_1)(u_2 + v_2) + C_2(u_1 + v_1)(u_2 - v_2) \\
\Phi^{(2)}_{\mathbf{1,2}} \equiv & \Psi^{(1)}_{\mathbf{1,2}} - \Psi^{(2)}_{\mathbf{1,2}} \\
= & (C_1 + C_2)(u_1 u_2 + v_1 v_2) + (2C_3 - C_1 - C_2)(u_1 v_2 + v_1 u_2) \\
= & (C_1 + C_2)(u_1 - v_1)(u_2 - v_2) + 2C_3(u_1 v_2 + v_1 u_2).
\end{aligned} \tag{2.56}$$

In this case, the following relations hold,

$$\begin{aligned}
\left(\Psi^{(1)}_{\mathbf{1,2}}\right)^2 + \left(\Psi^{(2)}_{\mathbf{1,2}}\right)^2 &= \frac{1}{2}\left[\left(\Phi^{(1)}_{\mathbf{1,2}}\right)^2 + \left(\Phi^{(2)}_{\mathbf{1,2}}\right)^2\right], \\
2\,\Psi^{(1)}_{\mathbf{1,2}} \cdot \Psi^{(2)}_{\mathbf{1,2}} &= \frac{1}{2}\left[\left(\Phi^{(1)}_{\mathbf{1,2}}\right)^2 - \left(\Phi^{(2)}_{\mathbf{1,2}}\right)^2\right], \\
\left(\Psi^{(1)}_{\mathbf{1,2}}\right)^2 - \left(\Psi^{(2)}_{\mathbf{1,2}}\right)^2 &= \frac{1}{2}\left[2\,\Phi^{(1)}_{\mathbf{1,2}} \cdot \Phi^{(2)}_{\mathbf{1,2}}\right].
\end{aligned}$$

Obviously, the Φ's possess the same properties regarding the internal momenta as the Ψ's do. Complying with this set of definitions, (2.55) is written as

$$\begin{aligned}
\Sigma^{(3)}_S(\mathbf{k},\omega) &= \frac{-S}{4N}\sum_{\mathbf{q}}\left[\left(\Phi^{(1)}_{\mathbf{1,2}}\right)^2 + \left(\Phi^{(2)}_{\mathbf{1,2}}\right)^2\right]\left(\frac{1}{\omega_1 + \omega_2 - \omega - i0^+} + \frac{1}{\omega_1 + \omega_2 + \omega - i0^+}\right), \\
\Sigma^{(3)}_O(\mathbf{k},\omega) &= \frac{-S}{4N}\sum_{\mathbf{q}}\left[\left(\Phi^{(1)}_{\mathbf{1,2}}\right)^2 - \left(\Phi^{(2)}_{\mathbf{1,2}}\right)^2\right]\left(\frac{1}{\omega_1 + \omega_2 - \omega - i0^+} + \frac{1}{\omega_1 + \omega_2 + \omega - i0^+}\right), \\
\Sigma^{(3)}_A(\mathbf{k},\omega) &= \frac{-S}{4N}\sum_{\mathbf{q}}\left[2\,\Phi^{(1)}_{\mathbf{1,2}} \cdot \Phi^{(2)}_{\mathbf{1,2}}\right]\left(\frac{1}{\omega_1 + \omega_2 - \omega - i0^+} - \frac{1}{\omega_1 + \omega_2 + \omega - i0^+}\right).
\end{aligned} \tag{2.57}$$

Notice that since $\omega_{\mathbf{k}}$ is of order $\mathcal{O}(S^1)$, the one-loop self-energy is of order $\mathcal{O}(S^0)$.

A more elegant way to treat the cubic interaction is representing it in a matrix form, instead of the scalar ones we used first, in accordance with the matrix Green's

function. For this end, we have

$$
\begin{aligned}
H^{(3)} &= \sqrt{\frac{2S}{N}} \sum_{1,2} \delta_{1+2-3} \Big[\Psi^{(1)}_{1,2} \left(a^\dagger_3 \alpha_2 \alpha_1 + \alpha^\dagger_1 \alpha^\dagger_2 a_3 \right) + \Psi^{(2)}_{1,2} \left(a_{-3} \alpha_2 \alpha_1 + \alpha^\dagger_1 \alpha^\dagger_2 a^\dagger_{-3} \right) \Big] \\
&= \sqrt{\frac{2S}{N}} \sum_{1,2} \delta_{1+2-3} \Big[\Psi^{(1)}_{1,2} \left(a^\dagger_3 \alpha_2 \alpha_1 - \alpha^\dagger_{-1} \alpha^\dagger_{-2} a_{-3} \right) \\
&\qquad\qquad + \Psi^{(2)}_{1,2} \left(a_{-3} \alpha_2 \alpha_1 - \alpha^\dagger_{-1} \alpha^\dagger_{-2} a^\dagger_3 \right) \Big] \\
&= \sqrt{\frac{2S}{N}} \sum_{1,2} \delta_{1+2-3} \begin{bmatrix} a^\dagger_3 & a_{-3} \end{bmatrix} \begin{bmatrix} \Psi^{(1)}_{1,2} & -\Psi^{(2)}_{1,2} \\ \\ \Psi^{(2)}_{1,2} & -\Psi^{(1)}_{1,2} \end{bmatrix} \begin{bmatrix} \alpha_2 \alpha_1 \\ \\ \alpha^\dagger_{-1} \alpha^\dagger_{-2} \end{bmatrix},
\end{aligned} \tag{2.58}
$$

and it can also be written in the hermitian form

$$
\begin{aligned}
H^{(3)} &= \sqrt{\frac{2S}{N}} \sum_{1,2} \delta_{1+2-3} \Big[\Psi^{(1)}_{1,2} \left(a^\dagger_3 \alpha_2 \alpha_1 + \alpha^\dagger_1 \alpha^\dagger_2 a_3 \right) + \Psi^{(2)}_{1,2} \left(a_{-3} \alpha_2 \alpha_1 + \alpha^\dagger_1 \alpha^\dagger_2 a^\dagger_{-3} \right) \Big] \\
&= \sqrt{\frac{2S}{N}} \sum_{1,2} \delta_{1+2-3} \Big[\Psi^{(1)}_{1,2} \left(-a^\dagger_{-3} \alpha_{-2} \alpha_{-1} + \alpha^\dagger_1 \alpha^\dagger_2 a_3 \right) \\
&\qquad\qquad + \Psi^{(2)}_{1,2} \left(-a_3 \alpha_{-2} \alpha_{-1} + \alpha^\dagger_1 \alpha^\dagger_2 a^\dagger_{-3} \right) \Big] \\
&= \sqrt{\frac{2S}{N}} \sum_{1,2} \delta_{1+2-3} \begin{bmatrix} \alpha^\dagger_1 \alpha^\dagger_2 & \alpha_{-2} \alpha_{-1} \end{bmatrix} \begin{bmatrix} \Psi^{(1)}_{1,2} & \Psi^{(2)}_{1,2} \\ \\ -\Psi^{(2)}_{1,2} & -\Psi^{(1)}_{1,2} \end{bmatrix} \begin{bmatrix} a_3 \\ \\ a^\dagger_{-3} \end{bmatrix}.
\end{aligned} \tag{2.59}
$$

In terms of Φ's, the cubic vertex is written as

$$
\begin{bmatrix} a^\dagger_{\mathbf{k}} & a_{-\mathbf{k}} \end{bmatrix} \frac{\sqrt{2S}}{2} \mathbf{V}_{1,2}, \quad \text{and its hermitian,} \quad \mathbf{V}^\dagger_{1,2} \frac{\sqrt{2S}}{2} \begin{bmatrix} a_{\mathbf{k}} \\ \\ a^\dagger_{-\mathbf{k}} \end{bmatrix},
$$

where

$$
\mathbf{V}_{1,2} = \begin{bmatrix} V^{(u)}_{1,2} \\ \\ V^{(d)}_{1,2} \end{bmatrix} \equiv \begin{bmatrix} \Phi^{(1)}_{1,2} \left(\alpha_2 \alpha_1 - \alpha^\dagger_{-1} \alpha^\dagger_{-2} \right) + \Phi^{(2)}_{1,2} \left(\alpha_2 \alpha_1 + \alpha^\dagger_{-1} \alpha^\dagger_{-2} \right) \\ \\ \Phi^{(1)}_{1,2} \left(\alpha_2 \alpha_1 - \alpha^\dagger_{-1} \alpha^\dagger_{-2} \right) - \Phi^{(2)}_{1,2} \left(\alpha_2 \alpha_1 + \alpha^\dagger_{-1} \alpha^\dagger_{-2} \right) \end{bmatrix}
$$

In this way, we obtain the matrix self-energy directly

$$\boldsymbol{\Sigma}(\mathbf{k},\omega) = -i\frac{1}{N}\sum_{\mathbf{q}}\int_{-\infty}^{\infty} \mathrm{d}t'\, e^{i\omega(t'-t'')}\left(\frac{\sqrt{2S}}{2}\right)^2 \left\langle T \begin{bmatrix} V_{\mathbf{1,2}}^{(u)}(t') \\ \\ V_{\mathbf{1,2}}^{(d)}(t') \end{bmatrix} \begin{bmatrix} V_{\mathbf{1,2}}^{(u)\dagger}(t'') & V_{\mathbf{1,2}}^{(d)\dagger}(t'') \end{bmatrix} \right\rangle$$

$$= \begin{bmatrix} \Sigma_S(\mathbf{k},\omega) + \Sigma_A(\mathbf{k},\omega) & \Sigma_O(\mathbf{k},\omega) \\ \\ \Sigma_O(\mathbf{k},\omega) & \Sigma_S(\mathbf{k},\omega) - \Sigma_A(\mathbf{k},\omega) \end{bmatrix},$$

where the expressions of the Σ's are those defined in (2.57).

Finally, in terms of the one-loop self-energies due to quartic and cubic interactions, we have the dressed single-particle Green's function:

$$\mathbb{G}(\mathbf{k},\omega) = \begin{bmatrix} \frac{[-2SA_{\mathbf{k}}-\Sigma_S(\mathbf{k},\omega)]-[\omega-\Sigma_A(\mathbf{k},\omega)]}{D(\mathbf{k},\omega)} & \frac{2SB_{\mathbf{k}}+\Sigma_O(\mathbf{k},\omega)}{D(\mathbf{k},\omega)} \\ \\ \frac{2SB_{\mathbf{k}}+\Sigma_O(\mathbf{k},\omega)}{D(\mathbf{k},\omega)} & \frac{[-2SA_{\mathbf{k}}-\Sigma_S(\mathbf{k},\omega)]+[\omega-\Sigma_A(\mathbf{k},\omega)]}{D(\mathbf{k},\omega)} \end{bmatrix}, \tag{2.60}$$

which is symmetric in $\mathbf{k}$. To highlight the symmetry with respect to frequency, it is better to organize the components in another way:

$$\mathbb{G}(\mathbf{k},\omega) = \begin{bmatrix} G_S(\mathbf{k},\omega) + G_A(\mathbf{k},\omega) & G_O(\mathbf{k},\omega) \\ \\ G_O(\mathbf{k},\omega) & G_S(\mathbf{k},\omega) - G_A(\mathbf{k},\omega) \end{bmatrix}, \tag{2.61}$$

where G_S and G_O are symmetric in ω while G_A is odd.

Armed with the single-particle Green's function derived in this chapter, the calculations of the physical quantities connected to the experimental measurements are ready to be performed in the next chapter.

Chapter 3

Connection to Experimental Measurements

Understanding the link between experiment and the microscopic world is essential for theoretical studies. It is important to know how and what each measurement technique probes and how one begins to calculate the corresponding quantities from simple theoretical models in order to compare with experimental data, confirming or ruling out the mechanism suggested by the model.

In condensed matter physics, each measurement is fundamentally related to a given correlation function from which one extracts the information on the underlying excitation spectrum, the collective modes and the ground-state correlations of the material. In scattering experiments, the scattering particles couple to some microscopic variable $O(x)$ of the system under study, which results in a differential scattering cross section reflecting a measure of the autocorrelation function of $O(x)$ at the wavevecter $\mathbf{k}$ and frequency $\omega = E/\hbar$ inside the material,

$$\frac{\mathrm{d}^2\sigma}{\mathrm{d}\Omega \mathrm{d}\omega} \sim \int \mathrm{d}^4 x \langle O(\mathbf{x}, t) O(\mathbf{0}, 0) \rangle e^{-i(\mathbf{k}\cdot\mathbf{x} - \omega t)}.$$

For spin systems, inelastic neutron scattering is one of the main experimental approaches to studying electronic spin structures. In this chapter, we concentrate on how to relate the corresponding theoretical quantities of our spin system to experimentally measurable quantities in inelastic neutron scattering.

3.1 Linear Response and Correlation Functions

Experimentalists study the properties of a physical system by perturbing it and seeing how it responds. If the probe used couples to the system weakly enough, one can make the linear response approximation in which the change in the coupled variable is proportional to the external force or source current.

Let us perform a little thought experiment on a spin system at $T = 0$. Suppose there is an arbitrary weak source current turned on at $t \geq 0$. The source-dependent Hamiltonian becomes

$$\begin{aligned} H[j(t)] &= H_0 + H_s(t), \\ H_s(t) &= -\sum_{\mathbf{R},\alpha} j^{\alpha}_{\mathbf{R}}(t) S^{\alpha}_{\mathbf{R}}(t), \end{aligned} \tag{3.1}$$

where $\alpha = x, y, z$. Here H_0 is the unperturbed Hamiltonian, while $H_s(t)$ is the external source term which is taken as a perturbation in the following interaction picture so that

$$\begin{aligned} S_H(t) &= U^{\dagger}(t) S_I(t) U(t), \\ U(t) &= T \exp\left[-i \int_0^t \mathrm{d}t'\, H_s(t')\right], \end{aligned} \tag{3.2}$$

where T is the time-ordering operator. The time-ordered exponential represents the operator series

$$\begin{aligned} U(t) &= \sum_n \frac{(-i)^n}{n!} \int_0^t \mathrm{d}t_n \cdots \mathrm{d}t_1 T[H_s(t_n) \cdots H_s(t_1)] \\ &= 1 - i \int_0^t \mathrm{d}t'\, H_s(t') + \cdots . \end{aligned} \tag{3.3}$$

Thus,

$$\begin{aligned} S_H(t) &= \left[1 + i \int_0^t \mathrm{d}t'\, H_s(t') + \cdots\right] S_I(t) \left[1 - i \int_0^t \mathrm{d}t'\, H_s(t') + \cdots\right] \\ &= S_I(t) - i \int_0^t \mathrm{d}t'\, [S_I(t), H_s(t')] + \cdots , \end{aligned} \tag{3.4}$$

where the Heisenberg picture refers to the time evolution with respect to $H[j(t)]$ whereas the interaction picture is with respect to H_0. In this case, the expectation

value of the spin operator evolves under $H[j]$ as

$$\langle S^{\alpha}_{\mathbf{R}}(t)\rangle_j = \langle S^{\alpha}_{\mathbf{R}}(t)\rangle + i\int_0^t \mathrm{d}t' \sum_{\mathbf{R}',\alpha'} j^{\alpha'}_{\mathbf{R}'}(t')\langle\Big[S^{\alpha}_{\mathbf{R}}(t), S^{\alpha'}_{\mathbf{R}'}(t')\Big]\rangle + \cdots, \tag{3.5}$$

where we have dropped the subscript I with the implication that $\langle\cdots\rangle$ is defined with respect to H_0. Then by only considering the leading change in the observable, which is linear in the source current, we define the spin response function as

$$\mathcal{R}^{\alpha\alpha'}_{\mathbf{R}\mathbf{R}'}(t-t') = -i\theta(t-t')\langle\Big[S^{\alpha}_{\mathbf{R}}(t), S^{\alpha'}_{\mathbf{R}'}(t')\Big]\rangle, \tag{3.6}$$

which is essentially a retarded correlation function, sometimes also called the "dynamical susceptibility".

Now let us carry out a spectral decomposition of the response function. We begin by expanding the response function in terms of a complete set of energy eigenstates which satisfy

$$\begin{aligned} H|\lambda\rangle &= E_\lambda|\lambda\rangle, \\ \sum_\lambda |\lambda\rangle\langle\lambda| &= 1, \\ \langle\lambda|S(t)|\varsigma\rangle &= \langle\lambda|e^{iHt}Se^{-iHt}|\varsigma\rangle = e^{-i(E_\varsigma - E_\lambda)t}\langle\lambda|S|\varsigma\rangle, \end{aligned} \tag{3.7}$$

where $H = H_0$, the full Hamiltonian without the source term. Using the above results, (3.6) is expanded as follows,

$$\begin{aligned} \mathcal{R}^{\alpha\alpha'}_{\mathbf{R}\mathbf{R}'}(t-t') = -i\theta(t-t')\sum_\lambda \Big(&e^{-i(E_\lambda - E_0)(t-t')}\langle 0|S^{\alpha}_{\mathbf{R}}|\lambda\rangle\langle\lambda|S^{\alpha'}_{\mathbf{R}'}|0\rangle \\ &- e^{i(E_\lambda - E_0)(t-t')}\langle 0|S^{\alpha'}_{\mathbf{R}'}|\lambda\rangle\langle\lambda|S^{\alpha}_{\mathbf{R}}|0\rangle\Big). \end{aligned} \tag{3.8}$$

Translational invariance of the Hamiltonian yields $\mathcal{R}_{\mathbf{R}\mathbf{R}'} = \mathcal{R}(\mathbf{R}-\mathbf{R}')$. Therefore the space-time Fourier transform of $\mathcal{R}$ is

$$\begin{aligned} \mathcal{R}^{\alpha\alpha'}(\mathbf{k},\omega) &= \frac{1}{N}\sum_{\mathbf{R}\mathbf{R}'} e^{-i\mathbf{k}\cdot(\mathbf{R}-\mathbf{R}')}\int_{-\infty}^{\infty}\mathrm{d}t\, e^{i\omega t}\,\mathcal{R}^{\alpha\alpha'}(\mathbf{R}-\mathbf{R}',t) \\ &= \sum_\lambda\left[\frac{\langle 0|S^{\alpha}_{\mathbf{k}}|\lambda\rangle\langle\lambda|S^{\alpha'}_{-\mathbf{k}}|0\rangle}{\omega-(E_\lambda-E_0)+i0^+} - \frac{\langle 0|S^{\alpha'}_{-\mathbf{k}}|\lambda\rangle\langle\lambda|S^{\alpha}_{\mathbf{k}}|0\rangle}{\omega+(E_\lambda-E_0)+i0^+}\right], \end{aligned} \tag{3.9}$$

where

$$S^{\alpha}_{\mathbf{k}} = \frac{1}{\sqrt{N}} \sum_{\mathbf{R}} e^{-i\mathbf{k}\cdot\mathbf{R}} S^{\alpha}_{\mathbf{R}}. \tag{3.10}$$

Introducing positive and negative frequency spectral functions:

$$\begin{aligned} A^{\alpha\alpha'}(\mathbf{k},\omega') &= \sum_{\lambda} \langle 0|S^{\alpha}_{\mathbf{k}}|\lambda\rangle\langle\lambda|S^{\alpha'}_{-\mathbf{k}}|0\rangle\, \delta[\omega' - (E_\lambda - E_0)], \\ B^{\alpha\alpha'}(\mathbf{k},\omega') &= \sum_{\lambda} \langle 0|S^{\alpha'}_{-\mathbf{k}}|\lambda\rangle\langle\lambda|S^{\alpha}_{\mathbf{k}}|0\rangle\, \delta[\omega' - (E_\lambda - E_0)], \end{aligned} \tag{3.11}$$

(3.9) can be written as

$$\mathcal{R}^{\alpha\alpha'}(\mathbf{k},\omega) = \int_0^{\infty} \mathrm{d}\omega' \left[\frac{A^{\alpha\alpha'}(\mathbf{k},\omega')}{\omega - \omega' + i0^+} - \frac{B^{\alpha\alpha'}(\mathbf{k},\omega')}{\omega + \omega' + i0^+} \right]. \tag{3.12}$$

However, it is not easy to calculate retarded correlation functions directly in interacting many-body problems. It is generally more convenient to define an associated time-ordered correlation function of the same operators, such that diagrammatic perturbation theory can be applied to evaluate the time-ordered correlation function by means of single-particle Green's functions following certain Feynman rules. Hence, the remaining problem is to relate the time-ordered and retarded functions, using the spectral decomposition method.

Define the time-ordered spin correlation function as

$$\mathcal{C}^{\alpha\alpha'}_{\mathbf{R}\mathbf{R}'}(t-t') = -i\langle T S^{\alpha}_{\mathbf{R}}(t) S^{\alpha'}_{\mathbf{R}'}(t')\rangle, \tag{3.13}$$

which is also called the "causal" correlation function. The analysis is the same as that performed for the response function. Expand $\mathcal{C}^{\alpha\alpha'}_{\mathbf{R}\mathbf{R}'}(t-t')$ in terms of the energy eigenstates:

$$\begin{aligned} \mathcal{C}^{\alpha\alpha'}_{\mathbf{R}\mathbf{R}'}(t-t') &= -i\left[\theta(t-t')\langle S^{\alpha}_{\mathbf{R}}(t) S^{\alpha'}_{\mathbf{R}'}(t')\rangle + \theta(t'-t)\langle S^{\alpha'}_{\mathbf{R}'}(t') S^{\alpha}_{\mathbf{R}}(t)\rangle\right] \\ &= -i\sum_{\lambda}\Big[\theta(t-t') e^{-i(E_\lambda - E_0)(t-t')} \langle 0|S^{\alpha}_{\mathbf{R}}|\lambda\rangle\langle\lambda|S^{\alpha'}_{\mathbf{R}'}|0\rangle \\ &\quad + \theta(t'-t) e^{i(E_\lambda - E_0)(t-t')} \langle 0|S^{\alpha'}_{\mathbf{R}'}|\lambda\rangle\langle\lambda|S^{\alpha}_{\mathbf{R}}|0\rangle\Big]. \end{aligned} \tag{3.14}$$

Since either boson representations of spin operators, such as the Holstein-Primakoff one used here, or bilinear fermion representations render the commutation behavior of

spin operators as bosons, there is no sign change when exchanging the two operators in the above expression. Furthermore, by taking the Fourier transform, we obtain

$$\begin{aligned}\mathcal{C}^{\alpha\alpha'}(\mathbf{k},\omega) &= \frac{1}{N}\sum_{\mathbf{R}\mathbf{R}'} e^{-i\mathbf{k}\cdot(\mathbf{R}-\mathbf{R}')}\int_{-\infty}^{\infty} \mathrm{d}t\, e^{i\omega t}\,\mathcal{C}^{\alpha\alpha'}(\mathbf{R}-\mathbf{R}',t) \\ &= \sum_{\lambda}\left[\frac{\langle 0|S^{\alpha}_{\mathbf{k}}|\lambda\rangle\langle\lambda|S^{\alpha'}_{-\mathbf{k}}|0\rangle}{\omega-(E_\lambda-E_0)+i0^+} - \frac{\langle 0|S^{\alpha'}_{-\mathbf{k}}|\lambda\rangle\langle\lambda|S^{\alpha}_{\mathbf{k}}|0\rangle}{\omega+(E_\lambda-E_0)-i0^+}\right]. \end{aligned} \tag{3.15}$$

Writing it in the frequency representation gives

$$\mathcal{C}^{\alpha\alpha'}(\mathbf{k},\omega) = \int_0^{\infty}\mathrm{d}\omega'\left[\frac{A^{\alpha\alpha'}(\mathbf{k},\omega')}{\omega-\omega'+i0^+} - \frac{B^{\alpha\alpha'}(\mathbf{k},\omega')}{\omega+\omega'-i0^+}\right]. \tag{3.16}$$

By virtue of the identity

$$\frac{1}{x\pm i0^+} = \mathcal{P}\left(\frac{1}{x}\right) \mp i\pi\delta(x), \tag{3.17}$$

it is easy to find the relation between the real and imaginary parts of (3.12) and (3.16), which is

$$\begin{aligned}\mathrm{Re}\,\mathcal{R}(\mathbf{k},\omega) &= \mathrm{Re}\,\mathcal{C}(\mathbf{k},\omega), \\ \mathrm{Im}\,\mathcal{R}(\mathbf{k},\omega) &= \mathrm{sgn}(\omega)\,\mathrm{Im}\,\mathcal{C}(\mathbf{k},\omega),\end{aligned} \tag{3.18}$$

where $\mathrm{sgn}(\omega) = \omega/|\omega|$.

The real and imaginary parts of the response function are physically measurable quantities that describe the system's response and dissipation, while those of the causal function are theoretically calculable quantities. Therefore, (3.18) builds a bridge joining theory to experiment.

3.2 Dynamical Structure Factor

The fluctuations of a system may be characterized by time correlation functions of the dynamical variables. The space-time spin correlation is simply expressed as

$$\mathcal{S}^{\alpha\alpha'}_{\mathbf{R}\mathbf{R}'}(t-t') = \langle S^{\alpha}_{\mathbf{R}}(t) S^{\alpha'}_{\mathbf{R}'}(t')\rangle. \tag{3.19}$$

It is natural to use the same spectral decomposition analysis. First we have

$$\mathcal{S}^{\alpha\alpha'}_{\mathbf{R}\mathbf{R}'}(t-t') = \sum_{\lambda} e^{-i(E_\lambda - E_0)(t-t')} \langle 0|S^{\alpha}_{\mathbf{R}}|\lambda\rangle\langle\lambda|S^{\alpha'}_{\mathbf{R}'}|0\rangle. \tag{3.20}$$

Then the Fourier transform results in

$$\begin{aligned}\mathcal{S}^{\alpha\alpha'}(\mathbf{k},\omega) &= \frac{1}{N}\sum_{\mathbf{R}\mathbf{R}'} e^{-i\mathbf{k}\cdot(\mathbf{R}-\mathbf{R}')} \int_{-\infty}^{\infty} \frac{\mathrm{d}t}{2\pi}\, e^{i\omega t}\, \mathcal{S}^{\alpha\alpha'}(\mathbf{R}-\mathbf{R}',t) \\ &= \sum_{\lambda} \langle 0|S^{\alpha}_{\mathbf{k}}|\lambda\rangle\langle\lambda|S^{\alpha'}_{-\mathbf{k}}|0\rangle\, \delta\left[\omega - (E_\lambda - E_0)\right]. \end{aligned} \tag{3.21}$$

Here an extra prefactor $1/2\pi$ has been added to the Fourier transform for the sake of later convenience. This Fourier transformed correlation function, the dynamical correlation function, is sometimes called the "dynamical structure factor", which is real and describes the spontaneous fluctuations at momentum $\mathbf{k}$ and frequency ω and is measurable by scattering experiments. We may also notice that the dynamical structure factor contains only the positive frequency spectrum.

3.3 Fluctuation-dissipation Theorem

There is deep link between fluctuations about equilibrium and the response of a system to external forces. If the susceptibility of a system to external change is large, then the fluctuations about equilibrium are expected to be large. The imaginary part of the spectral response function is the dissipative part, which describes the damping of the external oscillations by exciting internal modes of the system. The mathematical relationship that quantifies this connection is called the "fluctuation-dissipation" theorem, whose classical form has been known for a long time. In quantum-mechanical terms, this relation is given as

$$\mathcal{S}(\mathbf{k},\omega) = -\frac{1}{\pi}\frac{1}{1-e^{-\omega/T}}\,\mathrm{Im}\,\mathcal{R}(\mathbf{k},\omega). \tag{3.22}$$

where we have taken $\hbar = k_B = 1$. At zero temperature, the second fraction on the right hand side becomes

$$\lim_{T\to 0}\frac{1}{1-e^{-\omega/T}} = \begin{cases} 1 & , \quad \omega \geq 0 \\ 0 & , \quad \omega < 0. \end{cases} \tag{3.23}$$

Then we obtain the zero-temperature version of the fluctuation-dissipation theorem:

$$\mathcal{S}(\mathbf{k},\omega) = -\frac{1}{\pi}\,\mathrm{Im}\,\mathcal{R}(\mathbf{k},\omega), \qquad \omega \geq 0. \tag{3.24}$$

Due to the relation (3.18), it can also be expressed as

$$\mathcal{S}(\mathbf{k},\omega) = -\frac{1}{\pi}\,\mathrm{Im}\,\mathcal{C}(\mathbf{k},\omega), \qquad \omega \geq 0. \tag{3.25}$$

Let us verify the above zero-temperature formula by writing down the explicit forms of $\mathrm{Im}\,\mathcal{R}(\mathbf{k},\omega)$ and $\mathrm{Im}\,\mathcal{C}(\mathbf{k},\omega)$, which are straightforward to derive from (3.9), (3.15) and (3.17),

$$\begin{aligned}
\mathrm{Im}\,\mathcal{R}(\mathbf{k},\omega) = -\pi \sum_{\lambda} \Big\{ & \langle 0|S^{\alpha}_{\mathbf{k}}|\lambda\rangle\langle\lambda|S^{\alpha'}_{-\mathbf{k}}|0\rangle\, \delta[\omega - (E_\lambda - E_0)] \\
& - \langle 0|S^{\alpha'}_{-\mathbf{k}}|\lambda\rangle\langle\lambda|S^{\alpha}_{\mathbf{k}}|0\rangle \delta[\omega + (E_\lambda - E_0)] \Big\}, \\
\mathrm{Im}\,\mathcal{C}(\mathbf{k},\omega) = -\pi \sum_{\lambda} \Big\{ & \langle 0|S^{\alpha}_{\mathbf{k}}|\lambda\rangle\langle\lambda|S^{\alpha'}_{-\mathbf{k}}|0\rangle\, \delta[\omega - (E_\lambda - E_0)] \\
& + \langle 0|S^{\alpha'}_{-\mathbf{k}}|\lambda\rangle\langle\lambda|S^{\alpha}_{\mathbf{k}}|0\rangle \delta[\omega + (E_\lambda - E_0)] \Big\}.
\end{aligned} \tag{3.26}$$

Comparing the positive frequency parts of these with (3.21), we see that the relations (3.24) and (3.25) do hold.

As we mentioned earlier, $\mathcal{C}(\mathbf{k},\omega)$ is a theoretically calculable quantity in diagrammatic perturbation theory, while $\mathcal{S}(\mathbf{k},\omega)$ is an experimentally measurable quantity. The relation (3.25) naturally offers the connection of our calculations to the experimental observations. Building on this, we will establish in the following section, for our specific problem, the formalism needed to compare with experiments.

3.4 Inelastic Neutron Scattering

Neutrons interact weakly with matter so that they provide an ideal probe of the bulk properties of matter.

The unpolarized inelastic neutron scattering cross section is given by

$$\frac{\mathrm{d}^2\sigma}{\mathrm{d}\omega \mathrm{d}\Omega} = |f_{\mathbf{k}}|^2 \sum_{\mu\nu} \left(\delta_{\mu\nu} - \hat{\mathbf{k}}_\mu \hat{\mathbf{k}}_\nu\right) \mathcal{S}^{\mu\nu}(\mathbf{k},\omega), \tag{3.27}$$

where $\mu, \nu = a, b, c$ label the crystallographic axes, $\hat{\mathbf{k}}_\mu$ denotes the μ-component of the unit vector in $\mathbf{k}$ direction, and $f_{\mathbf{k}}$, the magnetic form factor, is determined by the magnetic ions in the insulator of interest. In this case, the dynamical correlation functions are directly related to the measurements. To compare to experiments, we need to calculate the structure factor based on the nonlinear spin wave analysis performed in the last chapter.

The rotating coordinates description requires us to represent the dynamical structure factor in the crystallographic reference frame in terms of that in the local reference frame by means of the transformation (2.4), which yields

$$\begin{aligned}
\mathcal{S}^{aa}(\mathbf{k},\omega) &= \mathcal{S}^{xx}(\mathbf{k},\omega), \\
\mathcal{S}^{bb}(\mathbf{k},\omega) &= \mathcal{S}^{cc}(\mathbf{k},\omega) \\
&= \frac{1}{4}\left[\left(\mathcal{S}^{yy}(\mathbf{k}+\mathbf{Q},\omega)+\mathcal{S}^{zz}(\mathbf{k}+\mathbf{Q},\omega)\right)+i\left(\mathcal{S}^{yz}(\mathbf{k}+\mathbf{Q},\omega)-\mathcal{S}^{zy}(\mathbf{k}+\mathbf{Q},\omega)\right)\right] \\
&+ \frac{1}{4}\left[\left(\mathcal{S}^{yy}(\mathbf{k}-\mathbf{Q},\omega)+\mathcal{S}^{zz}(\mathbf{k}-\mathbf{Q},\omega)\right)-i\left(\mathcal{S}^{yz}(\mathbf{k}-\mathbf{Q},\omega)-\mathcal{S}^{zy}(\mathbf{k}-\mathbf{Q},\omega)\right)\right],
\end{aligned} \tag{3.28}$$

$$\begin{aligned}
&\mathcal{S}^{ab}(\mathbf{k},\omega) = \mathcal{S}^{ba}(\mathbf{k},\omega) = \mathcal{S}^{ac}(\mathbf{k},\omega) = \mathcal{S}^{ca}(\mathbf{k},\omega) = 0, \\
&\mathcal{S}^{bc}(\mathbf{k},\omega) = -\mathcal{S}^{cb}(\mathbf{k},\omega).
\end{aligned} \tag{3.29}$$

Clearly, the off-diagonal elements of the dynamical structure factor do not contribute to the cross section. Thus (3.27) is simplified as

$$\frac{\mathrm{d}^2\sigma}{\mathrm{d}\omega\mathrm{d}\Omega} = |f_{\mathbf{k}}|^2\left[(1-\hat{\mathbf{k}}_a^2)\mathcal{S}^{aa}(\mathbf{k},\omega)+(1+\hat{\mathbf{k}}_a^2)\mathcal{S}^{bb}(\mathbf{k},\omega)\right]. \tag{3.30}$$

The out-of-plane polarized structure factor corresponds to the transverse fluctuations in the long-range ordered ground state at the same wavevector. In contrast, the in-plane polarized part comprises three types of fluctuations at different wavevectors: modulated by $+\mathbf{Q}$ and $-\mathbf{Q}$. This mixing of various fluctuations and the shifting as well as splitting in the dependence on wavevectors are characteristic of noncollinear long-range order. Physically, $\mathcal{S}^{yy}$ refers to transverse fluctuations, the same as $\mathcal{S}^{xx}$, while $\mathcal{S}^{zz}$ portrays longitudinal fluctuations in the sense that z is the eigen-direction of spin in the ground state. What is more interesting is the contribution $\mathcal{S}^{yz}$, or $\mathcal{S}^{zy}$, which

depicts the non-trivial correlation between longitudinal and transverse fluctuations, unique to noncollinear order. In the second-quantization language and considering the leading-order contributions only, it can be pictured as follows. The transverse fluctuation is equivalent to a one-magnon scattering process and the longitudinal one is equivalent to a two-magnon process, within the framework of linear spin wave theory. The cross term implies a one magnon splitting into two magnon or two magnons combining into one magnon process, which, however, only exists beyond linear spin wave theory as the interaction between spin waves is required.

To evaluate these quantities, we turn to the relation obtained in the last section: $\mathcal{S}^{\alpha\beta} = -\mathrm{Im}\,\mathcal{C}^{\alpha\beta}/\pi$, where $\alpha, \beta = x, y, z$. Then (3.28) may be written in the following brief form,

$$\mathcal{S}^{aa}(\mathbf{k},\omega) = -\frac{1}{\pi}\,\mathrm{Im}\,\mathcal{C}^{xx}(\mathbf{k},\omega), \tag{3.31}$$

$$\begin{aligned}\mathcal{S}^{bb}(\mathbf{k},\omega) &= \mathcal{S}^{cc}(\mathbf{k},\omega)\\ &= -\frac{1}{\pi}\,\mathrm{Im}\Big[\mathcal{F}^{+}(\mathbf{k}+\mathbf{Q},\omega) + \mathcal{F}^{-}(\mathbf{k}-\mathbf{Q},\omega)\Big],\end{aligned} \tag{3.32}$$

where

$$\mathcal{F}^{\pm}(\mathbf{q},\omega) = \frac{1}{4}\Big[\mathcal{C}^{yy}(\mathbf{q},\omega) + \mathcal{C}^{zz}(\mathbf{q},\omega) \pm i\Big(\mathcal{C}^{yz}(\mathbf{q},\omega) - \mathcal{C}^{zy}(\mathbf{q},\omega)\Big)\Big] \tag{3.33}$$

represent the $+\mathbf{Q}$ and $-\mathbf{Q}$ shifted branches respectively. It is easy to see that

$$\mathcal{F}^{+}(-\mathbf{k}+\mathbf{Q},\omega) = \mathcal{F}^{-}(\mathbf{k}-\mathbf{Q},\omega), \quad \mathcal{F}^{-}(-\mathbf{k}-\mathbf{Q},\omega) = \mathcal{F}^{+}(\mathbf{k}+\mathbf{Q},\omega), \tag{3.34}$$

due to the properties, which will be proven:

$$\begin{aligned}\mathcal{C}^{\alpha\alpha}(-\mathbf{q},\omega) &= \mathcal{C}^{\alpha\alpha}(\mathbf{q},\omega),\\ \mathcal{C}^{\alpha\beta}(-\mathbf{q},\omega) &= -\mathcal{C}^{\alpha\beta}(\mathbf{q},\omega), \quad \alpha \neq \beta,\end{aligned}$$

i.e., the diagonal causal correlation functions are even functions of momentum whereas the off-diagonal ones are odd functions of momentum. Then the structure factor satisfies

$$\mathcal{S}^{\mu\mu}(\mathbf{k},\omega) = \mathcal{S}^{\mu\mu}(-\mathbf{k},\omega), \tag{3.35}$$

as expected from the inversion symmetry of the system.

Now we turn our attention to calculating the corresponding time-ordered correlation functions using diagrammatic perturbation theory. We concentrate on a series of correlations of the following form:

$$\mathcal{C}^{\alpha\beta}(\mathbf{k},\omega) = \frac{1}{N}\sum_{\mathbf{R}\mathbf{R}'} e^{-i\mathbf{k}\cdot(\mathbf{R}-\mathbf{R}')} \int_{-\infty}^{\infty} \mathrm{d}t\, e^{i\omega t}(-i) \left\langle T S^{\alpha}_{\mathbf{R}}(t) S^{\beta}_{\mathbf{R}'}(0) \right\rangle_H , \tag{3.36}$$

where the subscript H indicates that this quantity is to be evaluated in the Heisenberg picture. Usually, these correlation functions can not be calculated exactly for interacting many-body problems. However, for weakly interacting systems, we may use well-developed quantum field theory method to carry out a perturbative calculation. The general procedure, which has already been introduced, is as follows:

- First, the spin operators are represented by the corresponding field operators, the Holstein-Primakoff bosons here, i.e.

$$\begin{aligned} S^{x}_{\mathbf{R}} &= \frac{\sqrt{2S}}{2}\left[a_{\mathbf{R}} + a^{\dagger}_{\mathbf{R}} - \frac{1}{4S}(a^{\dagger}_{\mathbf{R}} a_{\mathbf{R}} a_{\mathbf{R}} + a^{\dagger}_{\mathbf{R}} a^{\dagger}_{\mathbf{R}} a_{\mathbf{R}}) + \cdots\right], \\ S^{y}_{\mathbf{R}} &= \frac{\sqrt{2S}}{2i}\left[a_{\mathbf{R}} - a^{\dagger}_{\mathbf{R}} - \frac{1}{4S}(a^{\dagger}_{\mathbf{R}} a_{\mathbf{R}} a_{\mathbf{R}} - a^{\dagger}_{\mathbf{R}} a^{\dagger}_{\mathbf{R}} a_{\mathbf{R}}) + \cdots\right], \\ S^{z}_{\mathbf{R}} &= S - a^{\dagger}_{\mathbf{R}} a_{\mathbf{R}}. \end{aligned} \tag{3.37}$$

- Second, the Gell-Mann Low theorem enables us to relate the operators in the Heisenberg picture to those in the interaction picture via the S-matrix,

$$\left\langle T S^{\alpha}_{\mathbf{R}}(t) S^{\beta}_{\mathbf{R}'}(0) \right\rangle_H = \frac{\left\langle T\, \mathbb{S}(\infty,-\infty) S^{\alpha}_{\mathbf{R}}(t) S^{\beta}_{\mathbf{R}'}(0) \right\rangle_I}{\langle \mathbb{S}(\infty,-\infty) \rangle}, \tag{3.38}$$

  where the S-matrix is

$$\mathbb{S}(\infty,-\infty) = T\exp\left[-i\int_{-\infty}^{\infty} \mathrm{d}t'\, V(t')\right]. \tag{3.39}$$

  Here V denotes the interaction operator in the interaction picture.

- Third, we expand the S-matrix as a power-series in V,

$$\mathbb{S}(\infty,-\infty) = \sum_n \frac{(-i)^n}{n!}\int_{-\infty}^{\infty} \mathrm{d}t_1 \cdots \mathrm{d}t_n T[V(t_1)\cdots V(t_n)]. \tag{3.40}$$

Then Wick's theorem allows us to implement the Feynman diagram expansion and due to the S-matrix in the denominator, only the connected diagrams need to be calculated.

- Finally, as a problem faced by any perturbative calculation, we need to decide at what order the truncation is made based on physical grounds for our specific problem.

As discussed in the preceding chapter, our perturbative expansion scheme is the $1/S$ expansion. In what follows, we include only the leading order effects in $1/S$ due to spin wave interactions.

3.4.1 Transverse Part

Figure 3.1: Schematic of the tadpole diagrams.

When evaluating the transverse correlation functions, we encounter the so-called "Tadpole" diagrams (illustrated in Fig. 3.1) which contain equal-time propagators due to the three-operator product in S^x, S^y. The existence of the non-zero Tadpoles is essentially a consequence of the HP boson condensing in the ground state. Physically, these Tadpoles represent the finite densities of all kinds of HP boson parings. For this reason, we can avoid evaluating those Tadpole diagrams, and instead, decouple the

cubic terms by making all possible pair averaging. For instance,

$$\begin{aligned} a^\dagger_{\mathbf{R}} a_{\mathbf{R}} a_{\mathbf{R}} + a^\dagger_{\mathbf{R}} a^\dagger_{\mathbf{R}} a_{\mathbf{R}} &= 2\langle a^\dagger_{\mathbf{R}} a_{\mathbf{R}}\rangle a_{\mathbf{R}} + \langle a_{\mathbf{R}} a_{\mathbf{R}}\rangle a^\dagger_{\mathbf{R}} + 2\langle a^\dagger_{\mathbf{R}} a_{\mathbf{R}}\rangle a^\dagger_{\mathbf{R}} + \langle a^\dagger_{\mathbf{R}} a^\dagger_{\mathbf{R}}\rangle a_{\mathbf{R}} \\ &= \left[\frac{1}{N}\sum_{\mathbf{q}} \left(2\langle a^\dagger_{\mathbf{q}} a_{\mathbf{q}}\rangle + \langle a_{\mathbf{q}} a_{-\mathbf{q}}\rangle\right)\right](a_{\mathbf{R}} + a^\dagger_{\mathbf{R}}) \\ &= \left[\frac{1}{N}\sum_{\mathbf{q}} (2v^2_{\mathbf{q}} + u_{\mathbf{q}} v_{\mathbf{q}})\right](a_{\mathbf{R}} + a^\dagger_{\mathbf{R}}). \end{aligned} \tag{3.41}$$

As a consequence,

$$\begin{aligned} S^x_{\mathbf{R}} &= \sqrt{\frac{S}{2}}\left[1 - \frac{1}{4SN}\sum_{\mathbf{q}} (2v^2_{\mathbf{q}} + u_{\mathbf{q}} v_{\mathbf{q}})\right](a_{\mathbf{R}} + a^\dagger_{\mathbf{R}}) \equiv \sqrt{\frac{S}{2}}\, t_x (a_{\mathbf{R}} + a^\dagger_{\mathbf{R}}), \\ S^y_{\mathbf{R}} &= -i\sqrt{\frac{S}{2}}\left[1 - \frac{1}{4SN}\sum_{\mathbf{q}} (2v^2_{\mathbf{q}} - u_{\mathbf{q}} v_{\mathbf{q}})\right](a_{\mathbf{R}} - a^\dagger_{\mathbf{R}}) \equiv -i\sqrt{\frac{S}{2}}\, t_y (a_{\mathbf{R}} - a^\dagger_{\mathbf{R}}), \end{aligned} \tag{3.42}$$

where t_x, t_y are constants. Therefore, the transverse correlation functions may be written as

$$\begin{aligned} \mathcal{C}^{xx}(\mathbf{k},\omega) &= \frac{1}{N}\sum_{\mathbf{R}\mathbf{R}'} e^{-i\mathbf{k}\cdot(\mathbf{R}-\mathbf{R}')} \int_{-\infty}^{\infty} \mathrm{d}t\, e^{i\omega t}(-i)\, \langle T S^x_{\mathbf{R}}(t) S^x_{\mathbf{R}'}(0)\rangle_H \\ &= \frac{S}{2} t_x^2 \Big[G^{-+}(\mathbf{k},\omega) + G^{+-}(\mathbf{k},\omega) + G^{--}(\mathbf{k},\omega) + G^{++}(\mathbf{k},\omega)\Big] \\ &= \frac{S}{2} t_x^2 \Big[2G_S(\mathbf{k},\omega) + 2G_O(\mathbf{k},\omega)\Big], \end{aligned} \tag{3.43}$$

which directly corresponds to the out-of-plane structure factor, and

$$\begin{aligned} \mathcal{C}^{yy}(\mathbf{k},\omega) &= \frac{1}{N}\sum_{\mathbf{R}\mathbf{R}'} e^{-i\mathbf{k}\cdot(\mathbf{R}-\mathbf{R}')} \int_{-\infty}^{\infty} \mathrm{d}t\, e^{i\omega t}(-i)\, \langle T S^y_{\mathbf{R}}(t) S^y_{\mathbf{R}'}(0)\rangle_H \\ &= \frac{S}{2} t_y^2 \Big[G^{-+}(\mathbf{k},\omega) + G^{+-}(\mathbf{k},\omega) - G^{--}(\mathbf{k},\omega) - G^{++}(\mathbf{k},\omega)\Big] \\ &= \frac{S}{2} t_y^2 \Big[2G_S(\mathbf{k},\omega) - 2G_O(\mathbf{k},\omega)\Big], \end{aligned} \tag{3.44}$$

which corresponds to the transverse component of the in-plane structure factor. Here the single-particle Green's functions are those we obtained in the last chapter.

3.4.2 Mixing Part

The non-zero correlation between transverse and longitudinal fluctuations can not happen in non-interacting spin-wave theory, but it can in 1st order perturbation theory because of the cubic terms in the Hamiltonian. As discussed in the section on the self-energy calculation (Sec. 2.3.2), there are two ways to manipulate the cubic interaction term: One is a scalar approach which is quite intuitive but a little tedious; the other is a matrix approach which is more elegant and concise. We will consider both, the former as an intuitive introduction and the latter as an abstract refinement.

Considering the leading order effect, one term in the mixing part is

$$\begin{aligned} i\mathcal{C}^{yz}(\mathbf{k},\omega) =& i\frac{1}{N}\sum_{\mathbf{R}\mathbf{R}'} e^{-i\mathbf{k}\cdot(\mathbf{R}-\mathbf{R}')}\int_{-\infty}^{\infty} \mathrm{d}t\, e^{i\omega t}(-i)\left\langle T S^{y}_{\mathbf{R}}(t) S^{z}_{\mathbf{R}'}(0)\right\rangle_{H} \\ =& -t_y\sqrt{\frac{S}{2}}\frac{1}{\sqrt{N}}\sum_{\mathbf{q}}\int_{-\infty}^{\infty}\mathrm{d}t\int_{-\infty}^{\infty}\mathrm{d}t'\, e^{i\omega t}(-i)^2 \\ & \times\left\langle T\left[H^{(3)}(t')\left(a_{\mathbf{k}}(t)-a^{\dagger}_{-\mathbf{k}}(t)\right)a^{\dagger}_{\mathbf{k}-\mathbf{q}}(0)a_{-\mathbf{q}}(0)\right]\right\rangle_{I}, \end{aligned} \tag{3.45}$$

where $H^{(3)}(t')$ is

$$\begin{aligned} H^{(3)}(t') = \sqrt{\frac{2S}{N}}\sum_{\mathbf{1}',\mathbf{2}'}\delta_{\mathbf{1}'+\mathbf{2}'-\mathbf{3}'}\Big[&\Psi^{(1)}_{\mathbf{1}',\mathbf{2}'}\left(a^{\dagger}_{\mathbf{3}'}(t')\alpha_{\mathbf{2}'}(t')\alpha_{\mathbf{1}'}(t')+\alpha^{\dagger}_{\mathbf{1}'}(t')\alpha^{\dagger}_{\mathbf{2}'}(t')a_{\mathbf{3}'}(t')\right) \\ &+\Psi^{(2)}_{\mathbf{1}',\mathbf{2}'}\left(a_{-\mathbf{3}'}(t')\alpha_{\mathbf{2}'}(t')\alpha_{\mathbf{1}'}(t')+\alpha^{\dagger}_{\mathbf{1}'}(t')\alpha^{\dagger}_{\mathbf{2}'}(t')a^{\dagger}_{-\mathbf{3}'}(t')\right)\Big]. \end{aligned}$$

As in the previous analysis, the two a-particles at $t=0$ in (3.45) will enter a bubble diagram, so we can transform them into α-particles and retain only the terms that contribute, that is,

$$\begin{aligned} a^{\dagger}_{\mathbf{k}-\mathbf{q}}a_{-\mathbf{q}} &= u_{\mathbf{k}-\mathbf{q}}v_{\mathbf{q}}\alpha^{\dagger}_{\mathbf{k}-\mathbf{q}}\alpha^{\dagger}_{\mathbf{q}}+v_{\mathbf{k}-\mathbf{q}}u_{\mathbf{q}}\alpha_{-(\mathbf{k}-\mathbf{q})}\alpha_{-\mathbf{q}} \\ &= \frac{1}{2}(u_{\mathbf{1}}v_{\mathbf{2}}+v_{\mathbf{1}}u_{\mathbf{2}})(\alpha^{\dagger}_{\mathbf{2}}\alpha^{\dagger}_{\mathbf{1}}+\alpha_{-\mathbf{2}}\alpha_{-\mathbf{1}}), \end{aligned} \tag{3.46}$$

where we have symmetrized the two-particle vertices, but not the interaction vertices, under the interchange of **1** and **2**. As usual, the factor $1/2$ can be ignored in the expressions for these vertices because of the cancellation. Diagrammatically, (3.46) may be sketched as shown in Fig. 3.2

Figure 3.2: Schematic of the two-particle non-interaction vertices. They are represented by black points.

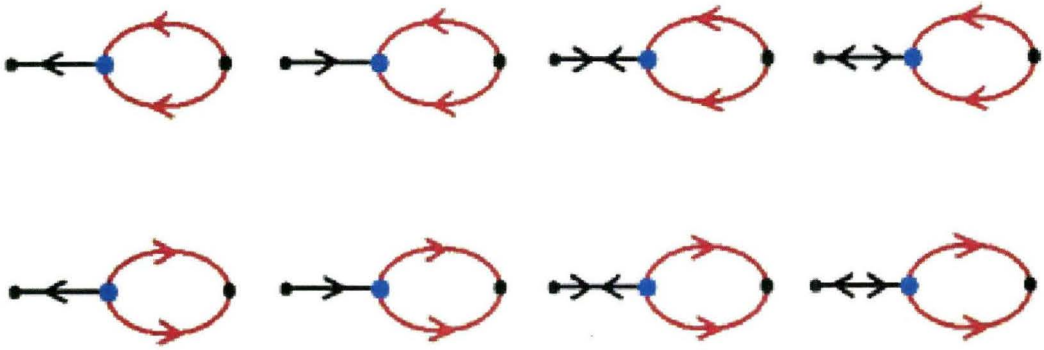

Figure 3.3: Schematic of the eight diagrams contributing to the expansion of (3.45).

In total, there are eight diagrams (illustrated in Fig. 3.3), or amplitudes, contributing to the expansion of (3.45). They give

$$i\mathcal{C}^{yz}(\mathbf{k},\omega) = t_y \frac{S}{2N} \sum_{\mathbf{q}} \tag{3.47}$$

$$\Big\{ \Big[G^{-+}(\mathbf{k},\omega)\Psi^{(1)}_{1,2} - G^{+-}(\mathbf{k},\omega)\Psi^{(2)}_{1,2} - G^{++}(\mathbf{k},\omega)\Psi^{(1)}_{1,2} + G^{--}(\mathbf{k},\omega)\Psi^{(2)}_{1,2} \Big] \times \frac{u_1 v_2 + v_1 u_2}{\omega_1 + \omega_2 - \omega - i0^+}$$
$$+ \Big[- G^{-+}(\mathbf{k},\omega)\Psi^{(2)}_{1,2} + G^{+-}(\mathbf{k},\omega)\Psi^{(1)}_{1,2} + G^{++}(\mathbf{k},\omega)\Psi^{(2)}_{1,2} - G^{--}(\mathbf{k},\omega)\Psi^{(1)}_{1,2} \Big] \times \frac{u_1 v_2 + v_1 u_2}{\omega_1 + \omega_2 + \omega - i0^+} \Big\}, \tag{3.48}$$

Using

$$\begin{aligned}
G^{-+}\Psi^{(1)} - G^{+-}\Psi^{(2)} &= \frac{1}{2}\Big[(G^{-+}+G^{+-})(\Psi^{(1)}-\Psi^{(2)}) + (G^{-+}-G^{+-})(\Psi^{(1)}+\Psi^{(2)})\Big] \\
&= G_S\Phi^{(2)} + G_A\Phi^{(1)}, \\
-G^{-+}\Psi^{(2)} + G^{+-}\Psi^{(1)} &= \frac{1}{2}\Big[(G^{-+}+G^{+-})(\Psi^{(1)}-\Psi^{(2)}) - (G^{-+}-G^{+-})(\Psi^{(1)}+\Psi^{(2)})\Big] \\
&= G_S\Phi^{(2)} - G_A\Phi^{(1)}, \\
G^{++}\Psi^{(1)} - G^{--}\Psi^{(2)} &= \frac{1}{2}(G^{++}+G^{--})(\Psi^{(1)}-\Psi^{(2)}) \\
&= G_O\Phi^{(2)},
\end{aligned}$$

we obtain:

$$\begin{aligned}
i\mathcal{C}^{yz}(\mathbf{k},\omega) = t_y\frac{S}{4N}\sum_{\mathbf{q}}\Big\{ & 2\Big[G_S(\mathbf{k},\omega) - G_O(\mathbf{k},\omega)\Big]\,\Phi^{(2)}_{\mathbf{1,2}}\,(u_{\mathbf{1}}v_{\mathbf{2}} + v_{\mathbf{1}}u_{\mathbf{2}}) \\
& \times\left(\frac{1}{\omega_{\mathbf{1}}+\omega_{\mathbf{2}}-\omega-i0^+} + \frac{1}{\omega_{\mathbf{1}}+\omega_{\mathbf{2}}+\omega-i0^+}\right) \\
& + 2G_A(\mathbf{k},\omega)\,\Phi^{(1)}_{\mathbf{1,2}}\,(u_{\mathbf{1}}v_{\mathbf{2}} + v_{\mathbf{1}}u_{\mathbf{2}}) \\
& \times\left(\frac{1}{\omega_{\mathbf{1}}+\omega_{\mathbf{2}}-\omega-i0^+} - \frac{1}{\omega_{\mathbf{1}}+\omega_{\mathbf{2}}+\omega-i0^+}\right)\Big\}.
\end{aligned}$$

Next we define the symmetric and antisymmetric functions of ω:

$$\begin{aligned}
M_S(\mathbf{k},\omega) =& \frac{S}{4N}\sum_{\mathbf{q}}\Phi^{(2)}_{\mathbf{1,2}}(u_{\mathbf{1}}v_{\mathbf{2}} + v_{\mathbf{1}}u_{\mathbf{2}})\left(\frac{1}{\omega_{\mathbf{1}}+\omega_{\mathbf{2}}-\omega-i0^+} + \frac{1}{\omega_{\mathbf{1}}+\omega_{\mathbf{2}}+\omega-i0^+}\right) \\
M_A(\mathbf{k},\omega) =& \frac{S}{4N}\sum_{\mathbf{q}}\Phi^{(1)}_{\mathbf{1,2}}(u_{\mathbf{1}}v_{\mathbf{2}} + v_{\mathbf{1}}u_{\mathbf{2}})\left(\frac{1}{\omega_{\mathbf{1}}+\omega_{\mathbf{2}}-\omega-i0^+} - \frac{1}{\omega_{\mathbf{1}}+\omega_{\mathbf{2}}+\omega-i0^+}\right),
\end{aligned} \tag{3.49}$$

which are of order $\mathcal{O}(S^0)$ and which describe a type of bubble diagrams with one cubic interaction vertex and one two-particle non-interaction vertex, as shown in Fig.3.4.

We can write the above formula as

$$i\mathcal{C}^{yz}(\mathbf{k},\omega) = t_y\Big\{2\Big[G_S(\mathbf{k},\omega) - G_O(\mathbf{k},\omega)\Big]M_S(\mathbf{k},\omega) + 2G_A(\mathbf{k},\omega)M_A(\mathbf{k},\omega)\Big\}. \tag{3.50}$$

Since M's are odd functions of $\mathbf{k}$, the mixing term is odd in $\mathbf{k}$, but even in ω.

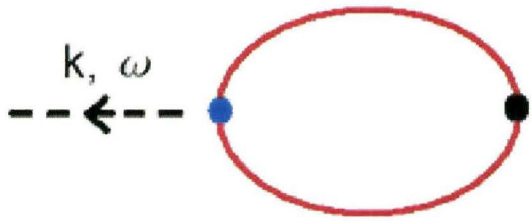

Figure 3.4: Schematic of the mixing bubble diagram generated by one cubic interaction vertex and one two-particle non-interaction vertex. The dashed line represents the net momentum-flow.

The other mixing term is

$$\begin{aligned}
-i\mathcal{C}^{zy}(\mathbf{k},\omega) &= -i\frac{1}{N}\sum_{\mathbf{R}\mathbf{R}'} e^{-i\mathbf{k}\cdot(\mathbf{R}-\mathbf{R}')}\int_{-\infty}^{\infty} \mathrm{d}t\, e^{i\omega t}(-i)\left\langle TS^z_{\mathbf{R}}(t)S^y_{\mathbf{R}'}(0)\right\rangle \\
&= -i\frac{1}{N}\sum_{\mathbf{R}\mathbf{R}'} e^{-i(-\mathbf{k})\cdot(\mathbf{R}'-\mathbf{R})}\int_{-\infty}^{\infty} \mathrm{d}t\, e^{i(-\omega)(-t)}(-i)\left\langle TS^y_{\mathbf{R}'}(0)S^z_{\mathbf{R}}(t)\right\rangle \\
&= -i\mathcal{C}^{yz}(-\mathbf{k},-\omega) = i\mathcal{C}^{yz}(\mathbf{k},\omega). \qquad (3.51)
\end{aligned}$$

Adding together gives

$$i\Big(\mathcal{C}^{yz}(\mathbf{k},\omega)-\mathcal{C}^{zy}(\mathbf{k},\omega)\Big) = 2t_y\Big\{2\Big[G_S(\mathbf{k},\omega)-G_O(\mathbf{k},\omega)\Big]M_S(\mathbf{k},\omega)+2G_A(\mathbf{k},\omega)M_A(\mathbf{k},\omega)\Big\}. \qquad (3.52)$$

Unlike the transverse and longitudinal parts, the mixing process is odd in momentum. This originates from the form of the cubic terms in the Hamiltonian, which depend on differences of neighboring spins.

Next, let us turn to the matrix approach introduced at the end of Sec. 2.3.2, where the cubic term is represented as $[a^\dagger_{\mathbf{k}},\ a_{-\mathbf{k}}]\frac{\sqrt{2S}}{2}\mathbf{V}$. Inserting this and (3.46) into (3.45),

it follows:

$$
\begin{aligned}
i\mathcal{C}^{yz}(\mathbf{k},\omega) =& -t_y\sqrt{\frac{S}{2}}\frac{\sqrt{2S}}{2}\frac{1}{N}\sum_{\mathbf{q}}(u_1v_2+v_1u_2)\int_{-\infty}^{\infty}\mathrm{d}t\int_{-\infty}^{\infty}\mathrm{d}t'\,e^{i\omega t}(-i)^2 \\
\times\Big\langle T\Big\{&\Big(a_{\mathbf{k}}(t)-a^{\dagger}_{-\mathbf{k}}(t)\Big)\begin{bmatrix}a^{\dagger}_{\mathbf{k}}(t') & a_{-\mathbf{k}}(t')\end{bmatrix}\begin{bmatrix}V^{(u)}_{\mathbf{1,2}}(t')\\ \\ V^{(d)}_{\mathbf{1,2}}(t')\end{bmatrix}\Big(\alpha^{\dagger}_{\mathbf{2}}(0)\alpha^{\dagger}_{\mathbf{1}}(0)+\alpha_{-\mathbf{2}}(0)\alpha_{-\mathbf{1}}(0)\Big)\Big\}\Big\rangle \\
=&\begin{bmatrix}G^{-+}(\mathbf{k},\omega)-G^{++}(\mathbf{k},\omega) & G^{--}(\mathbf{k},\omega)-G^{+-}(\mathbf{k},\omega)\end{bmatrix} \\
\times t_y\frac{S}{2N}\sum_{\mathbf{q}}(u_1v_2+v_1u_2)\int_{-\infty}^{\infty}&\mathrm{d}t'e^{i\omega t'}i\Big\langle T\begin{bmatrix}V^{(u)}_{\mathbf{1,2}}(t')\Big(\alpha^{\dagger}_{\mathbf{2}}(0)\alpha^{\dagger}_{\mathbf{1}}(0)+\alpha_{-\mathbf{2}}(0)\alpha_{-\mathbf{1}}(0)\Big)\\ \\ V^{(d)}_{\mathbf{1,2}}(t')\Big(\alpha^{\dagger}_{\mathbf{2}}(0)\alpha^{\dagger}_{\mathbf{1}}(0)+\alpha_{-\mathbf{2}}(0)\alpha_{-\mathbf{1}}(0)\Big)\end{bmatrix}\Big\rangle \\
=&\Big(G^{-+}(\mathbf{k},\omega)+G^{+-}(\mathbf{k},\omega)-G^{++}(\mathbf{k},\omega)-G^{--}(\mathbf{k},\omega)\Big)t_yM_S(\mathbf{k},\omega) \\
&+\Big(G^{-+}(\mathbf{k},\omega)-G^{+-}(\mathbf{k},\omega)\Big)t_yM_A(\mathbf{k},\omega) \\
=&t_y\Big\{2\Big[G_S(\mathbf{k},\omega)-G_O(\mathbf{k},\omega)\Big]M_S(\mathbf{k},\omega)+2G_A(\mathbf{k},\omega)M_A(\mathbf{k},\omega)\Big\},
\end{aligned}
$$

where the M's are defined in (3.49).

3.4.3 Longitudinal Part

Finally, we are left with the calculation of the longitudinal correlation function:

$$
\begin{aligned}
\mathcal{C}^{zz}(\mathbf{k},\omega) =&\frac{1}{N}\sum_{\mathbf{RR'}}e^{-i\mathbf{k}\cdot(\mathbf{R}-\mathbf{R'})}\int_{-\infty}^{\infty}\mathrm{d}t\,e^{i\omega t}(-i)\left\langle TS^z_{\mathbf{R}}(t)S^z_{\mathbf{R'}}(0)\right\rangle_H \\
=&\frac{1}{N}\sum_{\mathbf{qq'}}\int_{-\infty}^{\infty}\mathrm{d}t\,e^{i\omega t}(-i)\left\langle T\left[a^{\dagger}_{-\mathbf{q}}(t)a_{\mathbf{k}-\mathbf{q}}(t)a^{\dagger}_{\mathbf{k}-\mathbf{q'}}(0)a_{-\mathbf{q'}}(0)\right]\right\rangle_H.
\end{aligned}
$$

Performing the perturbative expansion gives

$$\begin{aligned}
\mathcal{C}^{zz}(\mathbf{k},\omega) = & \frac{1}{N}\sum_{\mathbf{q}\mathbf{q}'}\int_{-\infty}^{\infty} \mathrm{d}t\, e^{i\omega t}(-i)\left\langle T\left[a^{\dagger}_{-\mathbf{q}}(t)a_{\mathbf{k}-\mathbf{q}}(t)a^{\dagger}_{\mathbf{k}-\mathbf{q}'}(0)a_{-\mathbf{q}'}(0)\right]\right\rangle_I \\
& + \frac{1}{N}\sum_{\mathbf{q}\mathbf{q}'}\int_{-\infty}^{\infty}\mathrm{d}t\int_{-\infty}^{\infty}\mathrm{d}t'\, e^{i\omega t}(-i)^2 \\
& \times\left\langle T\left[H^{(4)}(t')a^{\dagger}_{-\mathbf{q}}(t)a_{\mathbf{k}-\mathbf{q}}(t)a^{\dagger}_{\mathbf{k}-\mathbf{q}'}(0)a_{-\mathbf{q}'}(0)\right]\right\rangle_I \\
& + \frac{1}{N}\sum_{\mathbf{q}\mathbf{q}'}\int_{-\infty}^{\infty}\mathrm{d}t\int_{-\infty}^{\infty}\mathrm{d}t'\int_{-\infty}^{\infty}\mathrm{d}t''\, e^{i\omega t}\frac{(-i)^3}{2} \\
& \times\left\langle T\left[H^{(3)}(t')H^{(3)}(t'')a^{\dagger}_{-\mathbf{q}}(t)a_{\mathbf{k}-\mathbf{q}}(t)a^{\dagger}_{\mathbf{k}-\mathbf{q}'}(0)a_{-\mathbf{q}'}(0)\right]\right\rangle_I \\
& + \ldots\ldots
\end{aligned} \tag{3.53}$$

Diagrammatically, these processes are illustrated in Fig. 3.5: The first diagram repre-

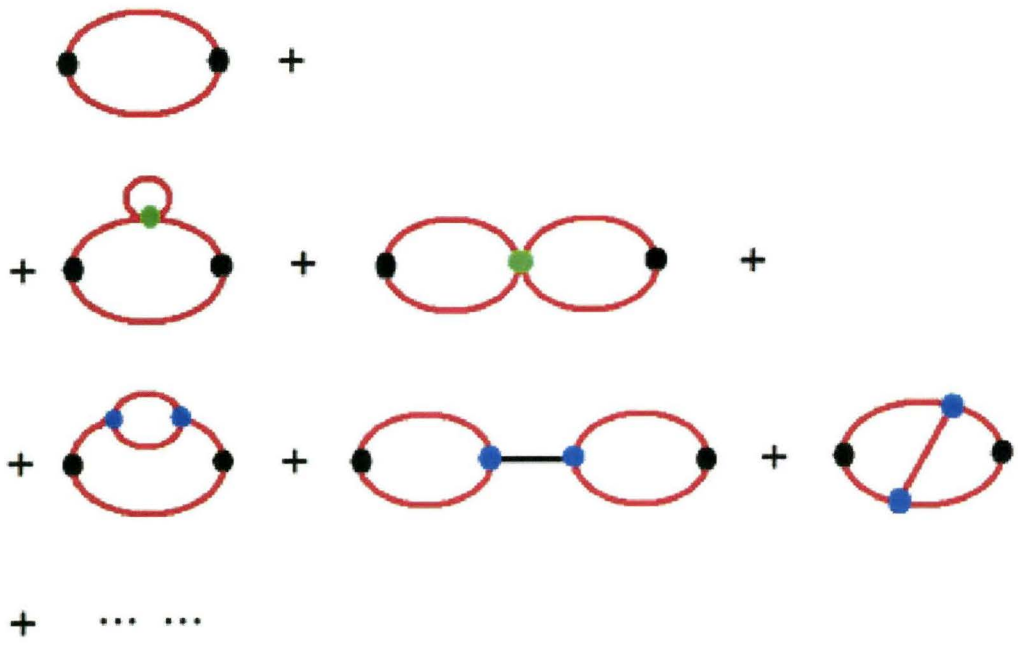

Figure 3.5: Schematic of the diagrams contributing to the two-particle correlation function. Here the quartic interaction vertices are denoted by green points.

sents none other than the bubble diagrams constructed by two two-particle vertices

and two α-propagators without interaction effects, whose analytic expression is readily obtained:

$$\mathcal{C}^{zz}_{\text{bare}}(\mathbf{k},\omega) = -\frac{1}{2N}\sum_{\mathbf{q}}(u_1 v_2 + v_1 u_2)^2 \left(\frac{1}{\omega_1+\omega_2-\omega-i0^+} + \frac{1}{\omega_1+\omega_2+\omega-i0^+}\right). \tag{3.54}$$

This is a non-interacting spin-wave result. Systematically, the sum of the first diagram on each line forms a single bubble diagram similar to the top one, but with dressed internal propagators.

The second diagram on the second line due to quartic interaction generates a series of ladder diagrams as shown in Fig. 3.6.

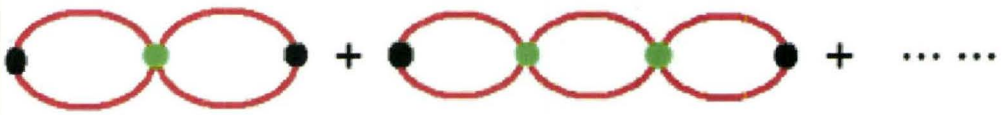

Figure 3.6: Schematic of the ladder diagrams.

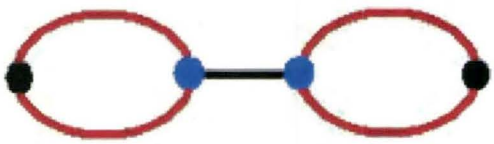

Figure 3.7: Schematic of the dumbbell diagram generated by two cubic interaction vertices for the two-particle correlation function.

What is intriguing is the "dumbbell" diagram (Fig.3.7) on the third line, because its intermediate states involve a one-particle process which might shift some scattering weight from the two-magnon process to the one-magnon process. It is handily calculable in the matrix approach based on the results from the mixing part. The intermediate part involving two cubic interactions and one a-particle propagator (as shown in Fig. 3.8) is expressed as

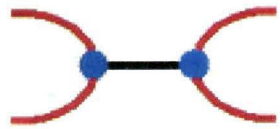

Figure 3.8: Schematic of the intermediate part in the dumbbell diagram generated by two cubic interaction vertices.

$$\left(\frac{\sqrt{2S}}{2}\right)^2 \int_{-\infty}^{\infty} \mathrm{d}t'\, e^{i\omega(t'-t'')}(-i) \left\langle T\left\{ \mathbf{V}^{\dagger}_{\mathbf{1,2}}(t') \begin{bmatrix} a_{\mathbf{k}}(t') \\ \\ a^{\dagger}_{-\mathbf{k}}(t') \end{bmatrix} \begin{bmatrix} a^{\dagger}_{\mathbf{k}}(t'') & a_{-\mathbf{k}}(t'') \end{bmatrix} \mathbf{V}_{\mathbf{1,2}}(t'') \right\} \right\rangle$$

$$= \frac{S}{2} \mathbf{V}^{\dagger}_{\mathbf{1,2}}(t') \begin{bmatrix} G^{-+}(\mathbf{k},\omega) & G^{--}(\mathbf{k},\omega) \\ \\ G^{++}(\mathbf{k},\omega) & G^{+-}(\mathbf{k},\omega) \end{bmatrix} \mathbf{V}_{\mathbf{1,2}}(t'').$$

Substituting this piece into the dumbbell diagram expression in (3.53), we have

$$\begin{aligned}
\mathcal{C}^{zz}_{\text{dumbbell}}(\mathbf{k},\omega) = \left(\sqrt{\frac{2}{S}}\right)^2 \Big\{ & G^{-+}(\mathbf{k},\omega)\Big[M_A(\mathbf{k},\omega) + M_S(\mathbf{k},\omega)\Big]^2 \\
& + G^{+-}(\mathbf{k},\omega)\Big[M_A(\mathbf{k},\omega) - M_S(\mathbf{k},\omega)\Big]^2 \\
& + \Big(G^{--}(\mathbf{k},\omega) + G^{++}(\mathbf{k},\omega)\Big)\Big[M_A(\mathbf{k},\omega)^2 - M_S(\mathbf{k},\omega)^2\Big] \Big\} \\
= \frac{2}{S} \Big\{ & \Big[G^{-+}(\mathbf{k},\omega) + G^{+-}(\mathbf{k},\omega) + G^{--}(\mathbf{k},\omega) + G^{++}(\mathbf{k},\omega)\Big] M_A(\mathbf{k},\omega)^2 \\
& + \Big[G^{-+}(\mathbf{k},\omega) + G^{+-}(\mathbf{k},\omega) - G^{--}(\mathbf{k},\omega) - G^{++}(\mathbf{k},\omega)\Big] M_S(\mathbf{k},\omega)^2 \\
& + \Big[G^{-+}(\mathbf{k},\omega) - G^{+-}(\mathbf{k},\omega)\Big] 2M_A(\mathbf{k},\omega) M_S(\mathbf{k},\omega) \Big\} \\
= \frac{2}{S} \Big\{ & 2\Big[G_S(\mathbf{k},\omega) + G_O(\mathbf{k},\omega)\Big] M_A(\mathbf{k},\omega)^2 \\
& + 2\Big[G_S(\mathbf{k},\omega) - G_O(\mathbf{k},\omega)\Big] M_S(\mathbf{k},\omega)^2 \\
& + 2G_A(\mathbf{k},\omega) \cdot 2M_A(\mathbf{k},\omega) M_S(\mathbf{k},\omega) \Big\},
\end{aligned}$$

where the prefactor $\sqrt{2/S}$ cancels the factor $\sqrt{S/2}$ in the M's which comes from S^y when evaluating the mixing part.

Chapter 4

Application to Cs_2CuCl_4

This chapter describes the application of the non-linear SWT formalism derived in the last two chapters to a real experimental system Cs_2CuCl_4, which is a quasi-2D $S = 1/2$ frustrated Heisenberg antiferromagnet on an anisotropic triangular lattice, in which neutron scattering measurements show the dynamical correlations to be dominated by a broad continuum [11].

Our numerical evaluation is performed using Mathematica. Adopting the experimentally determined bare exchange parameters: $J = 0.374$ meV along the b axis and $J' = 0.128$ meV along the zig-zag bonds, and neglecting the inter-layer couplings $J''/J = 0.045$ as well as the small Dzyaloshinskii-Moriya terms along the zig-zag bonds $D_a/J = 0.053$, we first turn to the single-site magnetization reduced by linear spin-wave fluctuations and the modified ordering wave vector within the LSWT framework. In non-linear SWT, the self-energies lead directly to renormalized magnon dispersion and damping. Furthermore, to compare with inelastic neutron scattering line shapes, we need to calculate spin structure factors at several momentum transfers. Weighted by the experimentally applied polarization factors, the in-plane and out-of-plane structure factors are added together to obtain the total scattering cross sections at those specific wavevector transfers.

4.1 Sublattice Magnetization

The $1/S$ correction to the local spin expectation value can be easily calculated within the LSWT framework. By numerical integration of Eq. (2.22), the first order correction to the classical value S is found to be

$$\Delta S = -0.435393, \tag{4.1}$$

which reduces the local magnetization from 0.5 to 0.0646068. The large spin reduction reflects the large quantum fluctuations in this system, and since this is purely due to longitudinal fluctuations, it also implies that the longitudinal susceptibility may be large, which is relevant to the two-magnon scattering process. On the other hand, for the $1/S$ expansion scheme itself, the large first-order correction naturally raises a question: Will the higher-order corrections kill the finite magnetization destroying the long-range order?

The measured spin reduction[11] is $\Delta S = -0.125$ which is much smaller than the LSWT result. This enhancement of the local spin moment is puzzling as it is too large to be attributed to the inter-layer couplings and the DM interaction not included in this calculation, which can quench some of the low-energy fluctuations and partially stabilize the spin ordering.

4.2 Shift of the Ordering Wavevector

Another LSWT result is the shift of the ordering wave vector $\mathbf{Q}$, which is acquired by minimizing the LSWT ground-state energy with respect to $\mathbf{Q}$. From (2.24) and (2.25), we have

$$\mathbb{M}^{-1} = \begin{bmatrix} \frac{4J}{4J^2-J'^2} & 0 \\ 0 & \frac{4J}{J'^2} \end{bmatrix} \quad \text{and} \quad \mathbf{L} = \begin{bmatrix} L_x \\ 0 \end{bmatrix},$$

where

$$L_x = -\sum_{\mathbf{q}} \frac{A_{\mathbf{q}} + B_{\mathbf{q}}}{\Omega_{\mathbf{q}}} \Big[J \sin 2\pi(q_x + Q_c) + J' \sin \pi(q_x + Q_c) \cos \pi q_y \Big].$$

Apparently, $\det \mathbb{M}^{-1} > 0$, when $J' < 2J$; when $J' = 2J$, $\det \mathbb{M}^{-1}$ diverges, which indicates a possible phase transition point[12, 13]; when $J' > 2J$, ΔQ_x changes sign, if this formalism still holds and L_x is non-negative. It can be shown that for the isotropic triangular lattice, i.e. $J' = J$, $L_x = 0$ so that $\Delta\mathbf{Q} = \mathbf{0}$. In the case at hand, $M_{xx}^{-1} = 0.363048, L_x = 0.0739398$. Then we find

$$\Delta Q_x = -0.0324141.$$

The shifted ordering wave vector becomes

$$\mathbf{Q}_0 = (0.522325, 0).$$

Compared to the classical one

$$\mathbf{Q}_c = (0.554740, 0),$$

we see that quantum fluctuations decrease the incommensuration from $\epsilon_c = 0.054740$ to $\epsilon_0 = 0.022325$, and $\epsilon_0/\epsilon_c = 0.407837$. This renormalization of the incommensuration is even stronger than the large experimental value[11] $\epsilon_0 = 0.030$, and $\epsilon_0/\epsilon_c = 0.56$.

4.3 Excitation Spectrum

Now, let us turn our attention to the non-linear SWT calculation. First of all, one of the physical properties encoded in the dressed Green's function is the renormalized excitation spectrum, which can be determined by exploring its pole structure. In our calculation, the correction to the bare dispersion relation is only retained to leading order in $1/S$, since to complete the higher order corrections requires inclusion of higher-order $\Delta\mathbf{Q}$-effect and other two-loop diagrams. For this reason, the excitation position we locate is just slightly different from the real pole position of the Green's functions as long as the higher-order-in-$1/S$ terms in the denominator are relatively small. Otherwise, the perturbative expansion itself becomes problematic.

To compare with the experimental data, we take a special momentum direction $(0, k, 0)$ in which to study the renormalized excitation spectrum, where the momentum

transfer is expressed in reciprocal lattice units of $(2\pi/a, 2\pi/b, 2\pi/c)$. As shown in (2.37), besides the self-energy contributions, the shift of the ordering wave vector directly gives rise to a modification of the spectrum:

$$\omega_{\mathbf{k}}^{\Delta\mathbf{Q}} = \sqrt{(A_{\mathbf{k}} + \Delta A_{\mathbf{k}})^2 - (B_{\mathbf{k}} + \Delta B_{\mathbf{k}})^2}.$$

We can see from Fig. 4.1 that this modification is rather large around $(0, 1, 0)$, but hardly noticeable in other areas.

The $1/S$ renormalized excitation dispersion relation $\omega_{\mathbf{k}}^{1/S}$ and damping $\Gamma_{\mathbf{k}}$ are shown in Fig. 4.1 as well as the comparison with the bare dispersion relation $\omega_{\mathbf{k}}^{0}$ and the $1/S$ $\Delta\mathbf{Q}$-modified one $\omega_{\mathbf{k}}^{\Delta\mathbf{Q}}$. Although there exist well-defined quasiparticles in most of the low-energy regime, the non-negligible damping of some medium- to high-energy excitations implies the failure of the magnon description at those wave vectors. But still, in the vicinity of the Goldstone modes, the magnetic excitations remain as long-lived single particles, which to some extent explains the appearance of sharp peak feature in the low-energy regime measured by the neutron experiments[11]. Moreover, the large damping of those medium- to high-energy excitations can not only broaden the excitation peaks in the inelastic scattering, but also induce a high-energy tail which might explain the extended continuum features in the experimental data.

However, we find that, compared with the experimentally measured excitation energies (as shown in Fig. 4.2), the calculated are much lower in energy except those Goldstone modes.

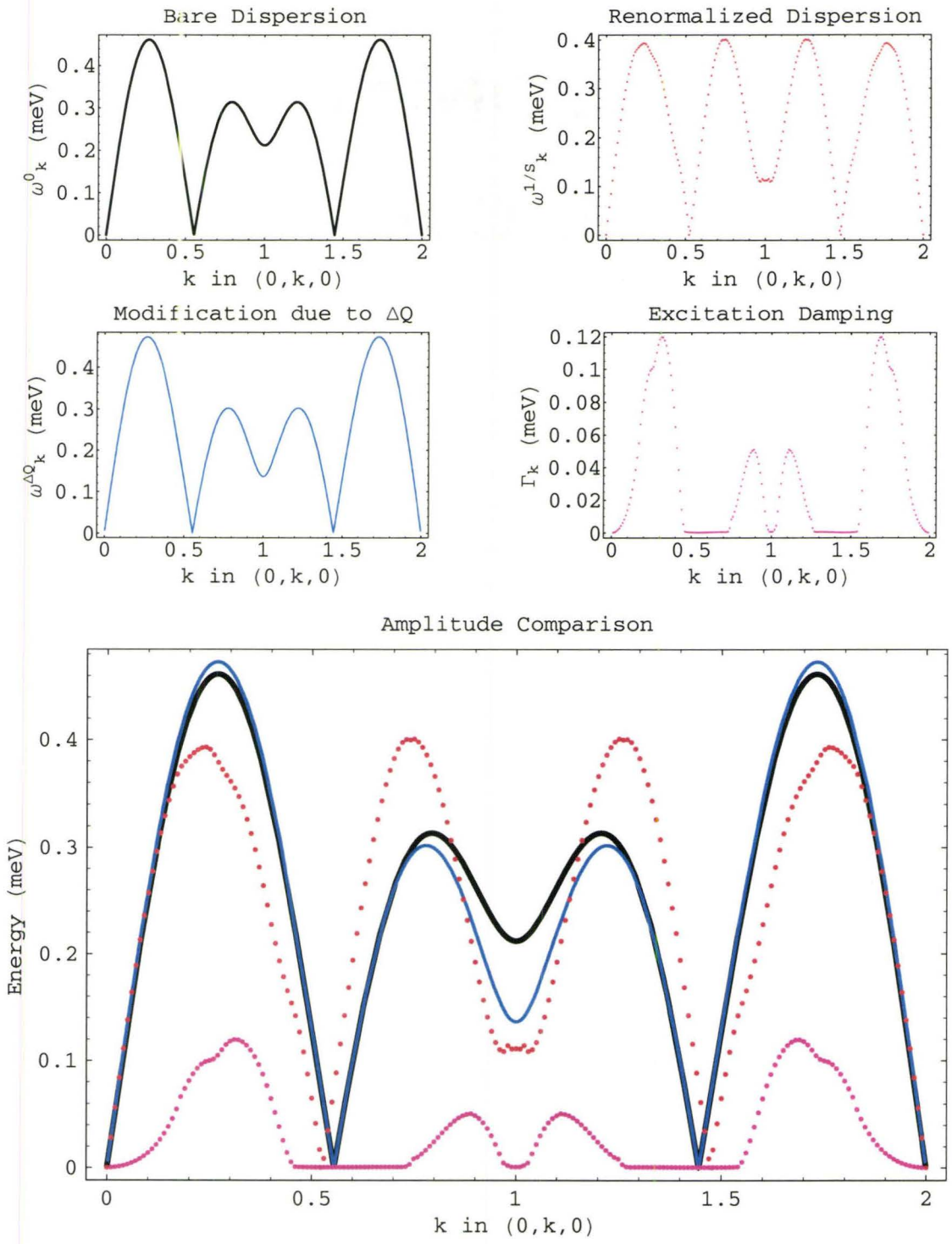

Figure 4.1: The red dotted line represents the $1/S$ renormalized excitation dispersion relation, while the pink dotted line exhibits the corresponding excitation damping at those wave vectors. As a comparison, the bare and $\Delta\mathbf{Q}$-modified dispersion relation are also shown in terms of black and blue solid line respectively.

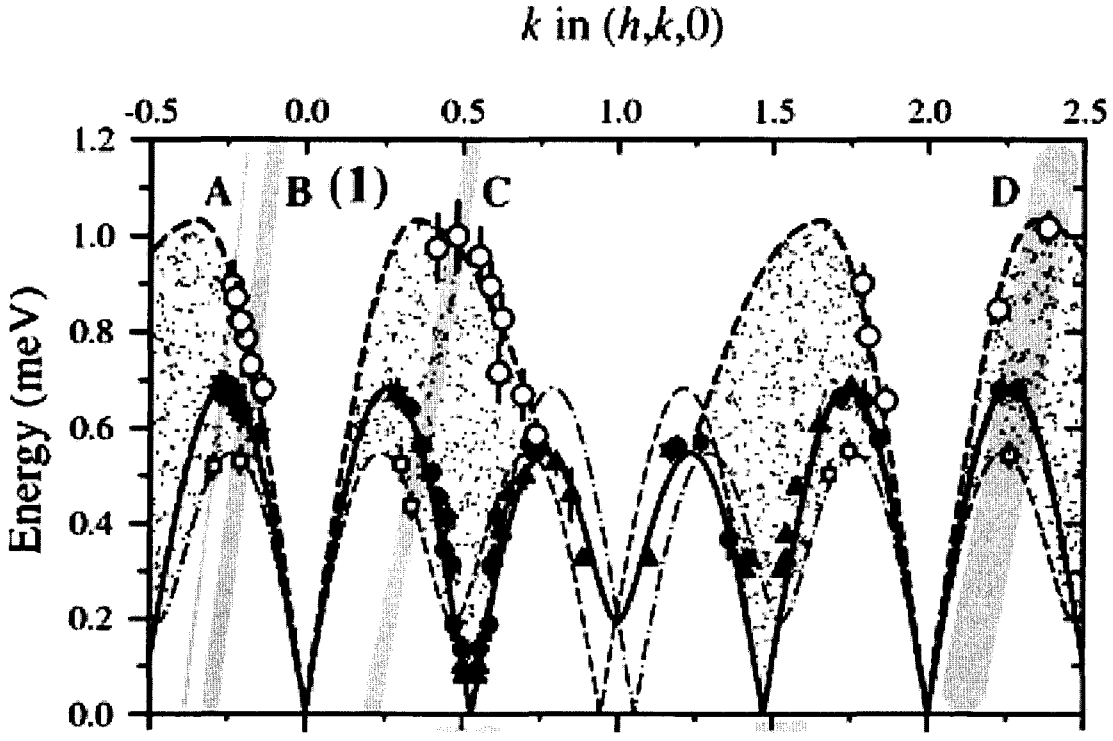

Figure 4.2: The solid points are experimentally measured excitation energies Ref. [11].

4.4 Spin Structure Factor

Neutron scattering experiments directly measure the scattering cross-section intensity. The dynamical spin correlation functions are obtained from the scattering intensity distribution versus the energy transfer in inelastic scattering measurements. The experimental results on Cs_2CuCl_4 by Coldea and co-workers include energy scans at several non-equivalent positions in the Brillouin zone with different polarization factors to explore the properties of the excitations in this spin system. Likewise, we calculate the spin structure factors at those wave-vector transfers to determine the theoretical cross sections.

Based on physical consideration, we will take the full expressions of the correlation functions, without keeping the final results only to the sub-leading order in $1/S$ as we did for the spectra calculation. Thus, our results for spin structure factors do not follow the $1/S$ order criterion strictly.

4.4.1 Numerical Results

In Table 4.1, capital letters A-H indicate location of energy scans with parameters listed, where the wavevector transfer $\mathbf{k} = (h, k, l)$ is expressed in reciprocal lattice units of $(2\pi/a, 2\pi/b, 2\pi/c)$. The energy lattice spacing we used is $\Delta\omega = 0.01\text{meV}$.

To illustrate the relative intensity of the different components of the line shape, the different processes in the scattering are displayed separately first and then added together. Taking the G point as an example, first of all, the two processes in the in-plane two-magnon scattering, the bare two-magnon process and the dumbbell two-magnon process, are shown in separate figures in the left panel of Fig. 4.3; The total two-magnon scattering intensity is shown in the upper-right corner, and the lower-right corner exhibits the relative contributions of the two components, together with the total. As discussed in Sec. 3.4, the in-plane structure factor involves multiple components: transverse, longitudinal and mixing parts, which correspond to different excitations. Naively, the transverse part is related to one-magnon excitations with two-magnon intermediate states that damp the single mode and induce some high-

Scan	k(rlu)	l(rlu)	p_b	p_a
A	-0.389	0	1.95	0.05
B	-0.30	0	1.98	0.02
C	0.21	0	1.75	0.25
D	2.11	0	1.05	0.95
E	-0.33	0.78	1	1
F	-0.39	1.66	1	1
G	0.5	1.53	1	1
H	0.28	1.205	1	1

Table 4.1: Scan parameters: wave vector $\mathbf{k} = (0, k, l)$ and polarization factors (p_b, p_a) at this point. Slightly different from Ref.[11], instead of choosing energy-trajectories for the wavevector transfers, we pick up constant wavevector transfers without energy dependence. And since the interlayer coupling is neglected in our calculation, h is set to zero. Here p_b, p_a describe in-plane and out-of-plane polarization respectively.

energy structure in the one-magnon dynamical correlations. This process is shown in the upper-left graph of Fig. 4.4. From the expression for the transverse correlation (3.44), the small prefactor t_y, which is 0.611617 in this case, further suppresses the weight of this part, reflecting the large fluctuations. In the same graph panel, the mixing and longitudinal parts are shown in the lower-left and upper-right corner respectively. A comparison of all these three in-plane parts is made in the lower-right diagram.

Finally, we put the in-plane and out-of-plane structure factor in Fig. 4.5. Similar to the in-plane transverse part, there is a prefactor suppression for the out-of-plane correlation: $t_x = 0.517597$ in the case at hand. Weighted by the specific polarization factors at the point, the total cross-section intensity is evaluated as:

$$I(\mathbf{k}, \omega) = p_b \, \mathcal{S}^{bb}(\mathbf{k}, \omega) + p_a \, \mathcal{S}^{aa}(\mathbf{k}, \omega), \tag{4.2}$$

which is shown in the upper-right corner of graph panel 4.5. A comparison of the two components as well as the total result is given in the lower-right graph.

In the same pattern, the line shapes at all the other points are shown in the following figures.

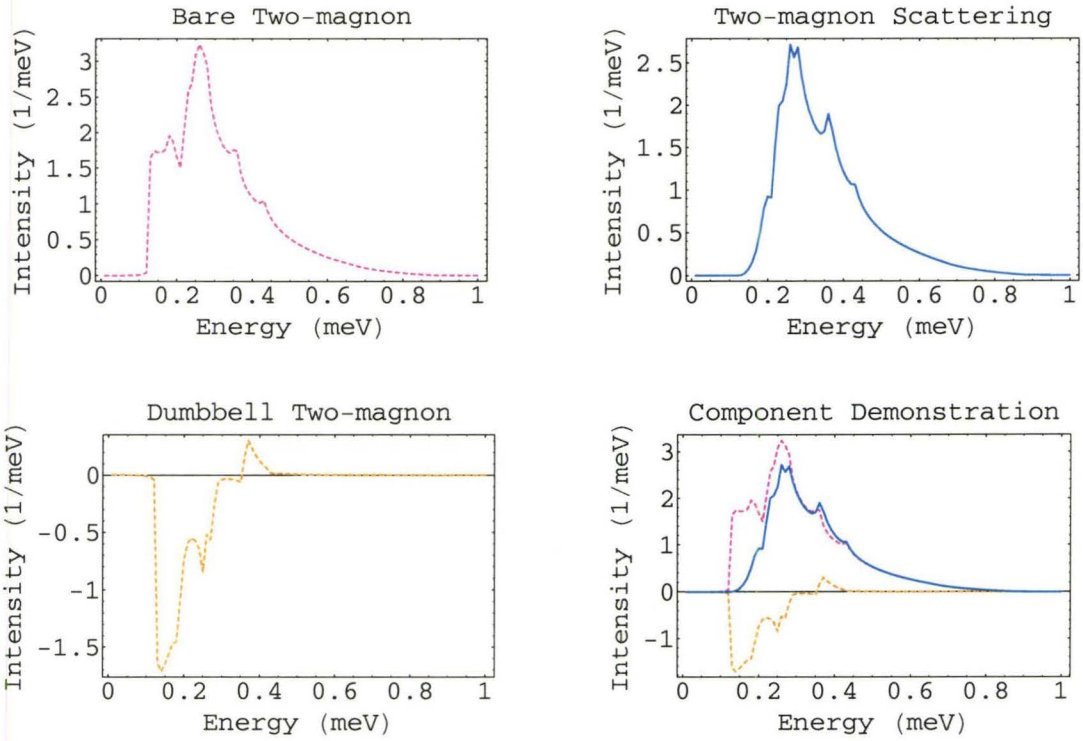

Figure 4.3: In-plane two-magnon scattering at G point. The two dashed lines in the upper- and lower-left graph are the bare and interactive two-magnon scattering intensities respectively. The solid blue line in the upper-right corner is the total two-magnon part after summing those two sub-parts. All the components and the resultant amplitude are gathered in the lower-right graph.

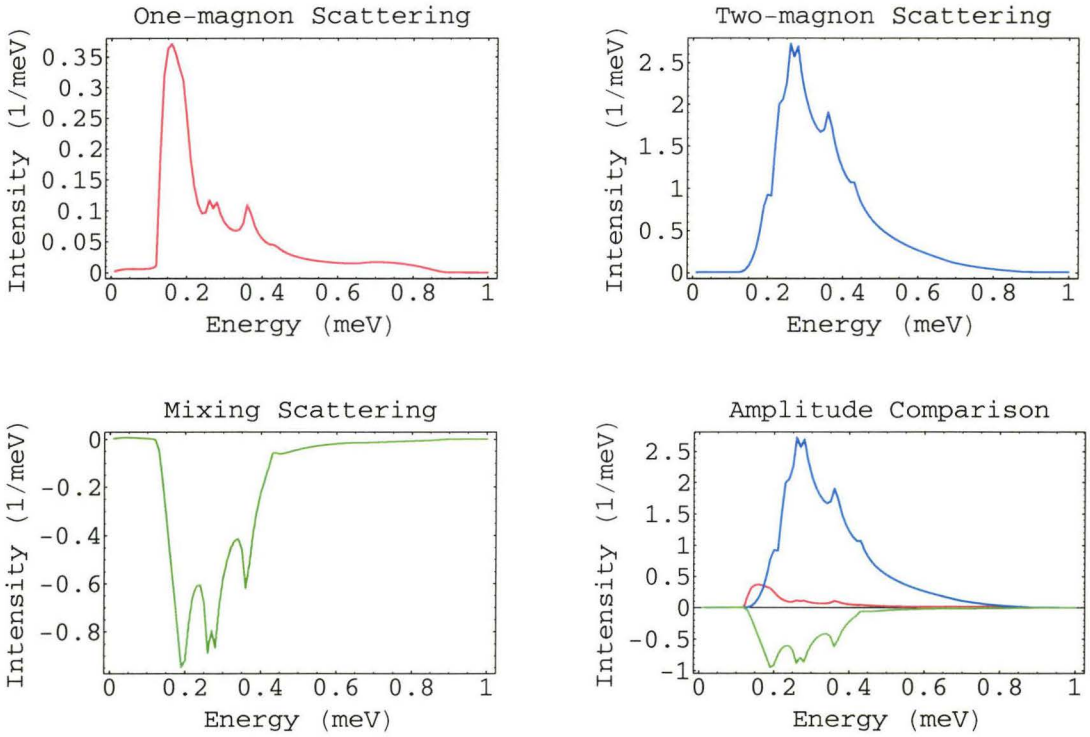

Figure 4.4: Three in-plane scattering processes at G point. The red, blue and green curves are representing the scattering intensities of transverse, longitudinal and mixing processes occurring in the in-plane correlation. The graph in the lower-right corner is a comparison of all these three amplitudes.

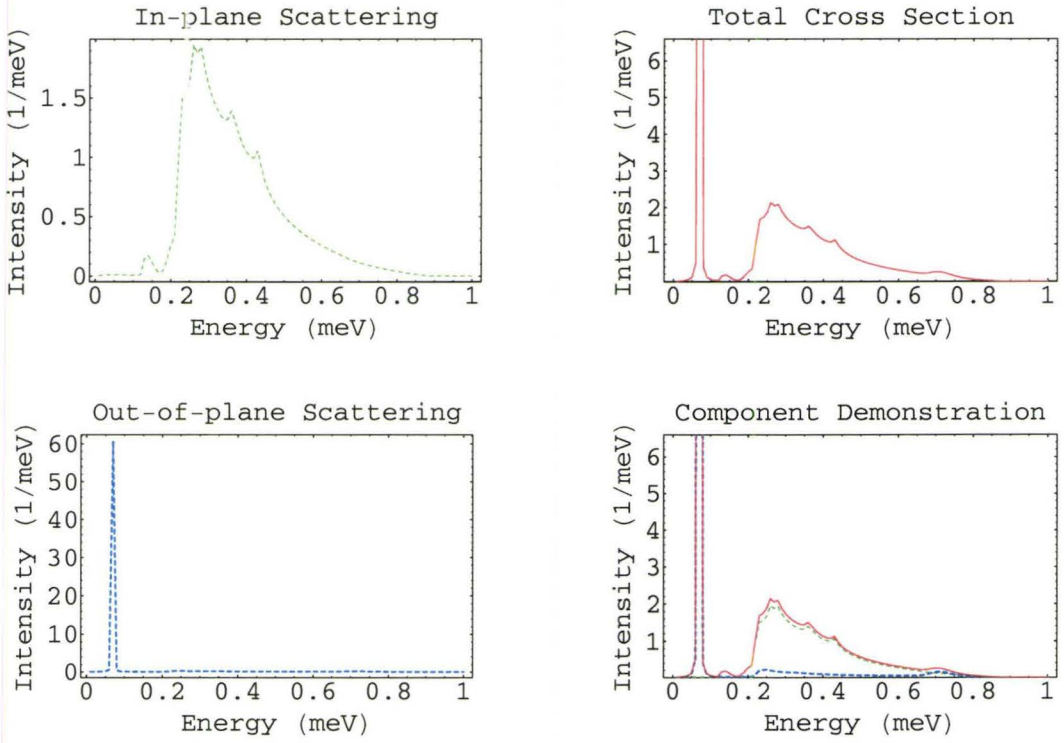

Figure 4.5: Structure factors and cross section at G point. The in-plane and out-of-plane structure factors are denoted by dashed green and blue line in the upper- and lower-left graph. Total cross-section intensity is plotting as solid red line shown in the upper-right graph. And the comparison is given in the lower-right corner.

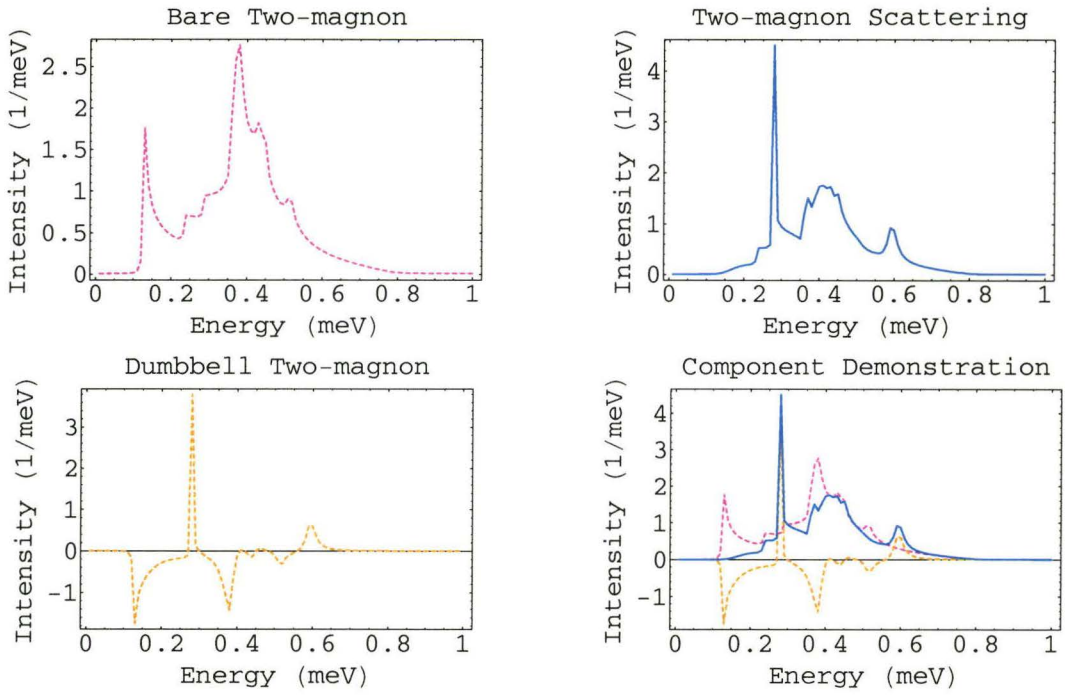

Figure 4.6: In-plane two-magnon scattering at A point.

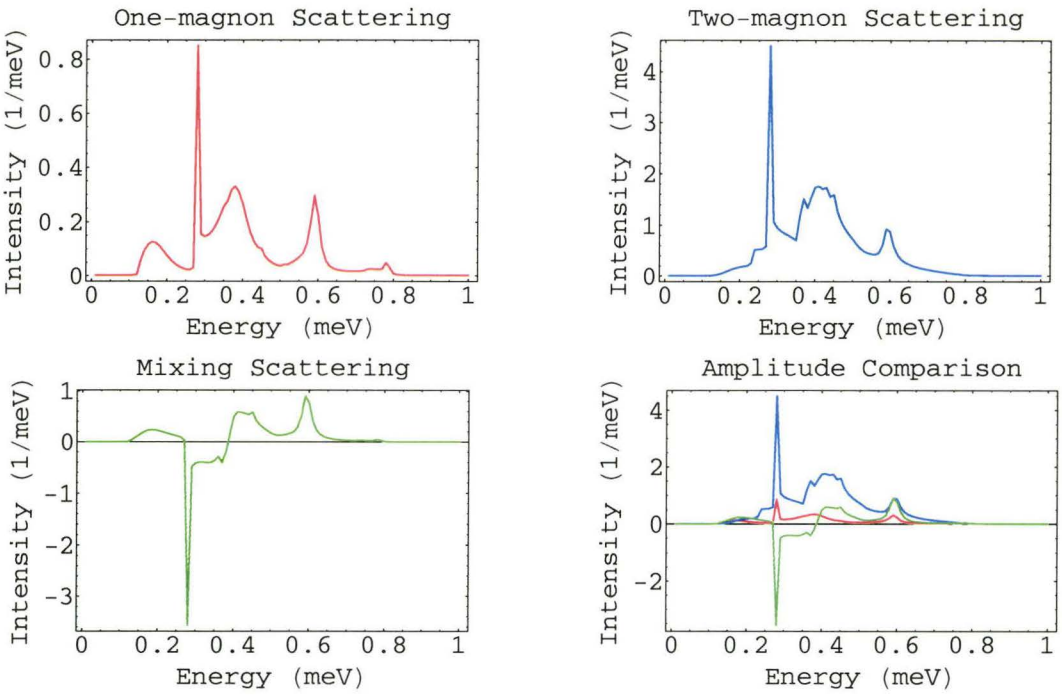

Figure 4.7: Three in-plane scattering processes at A point.

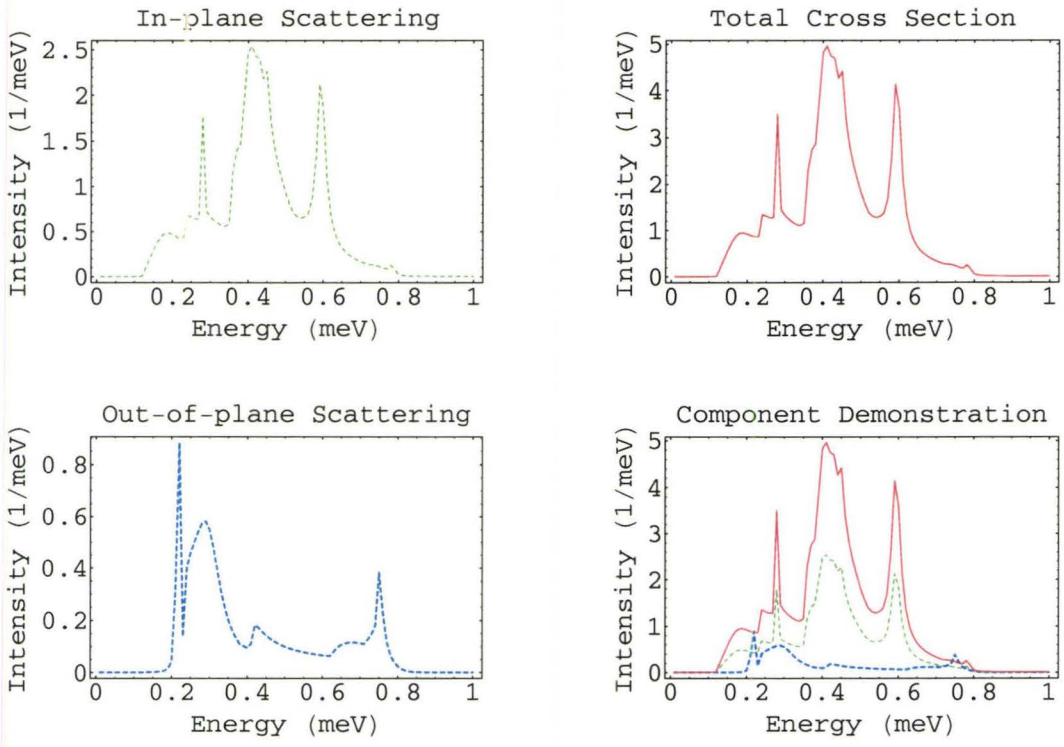

Figure 4.8: Structure factors and cross section at A point.

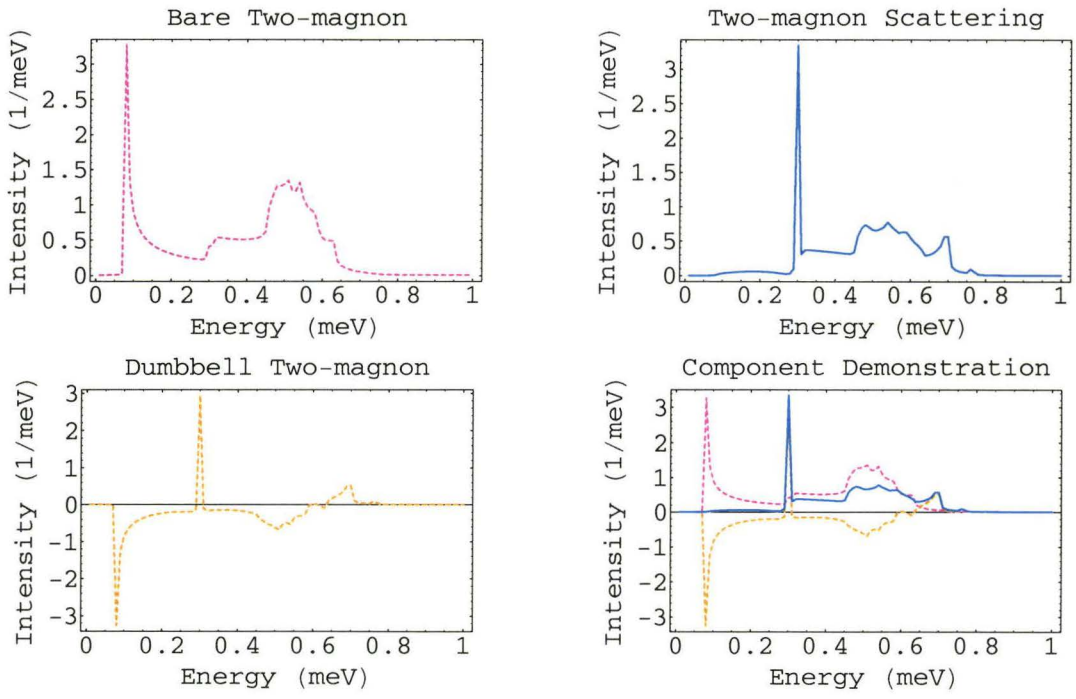

Figure 4.9: In-plane two-magnon scattering at B point.

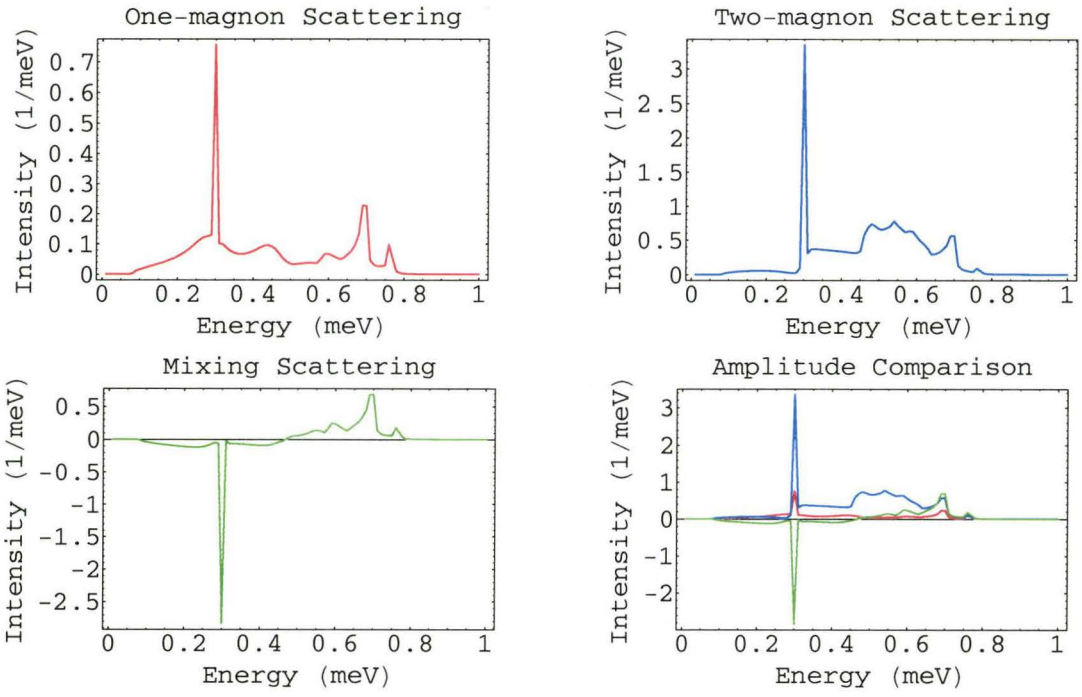

Figure 4.10: Three in-plane scattering processes at B point.

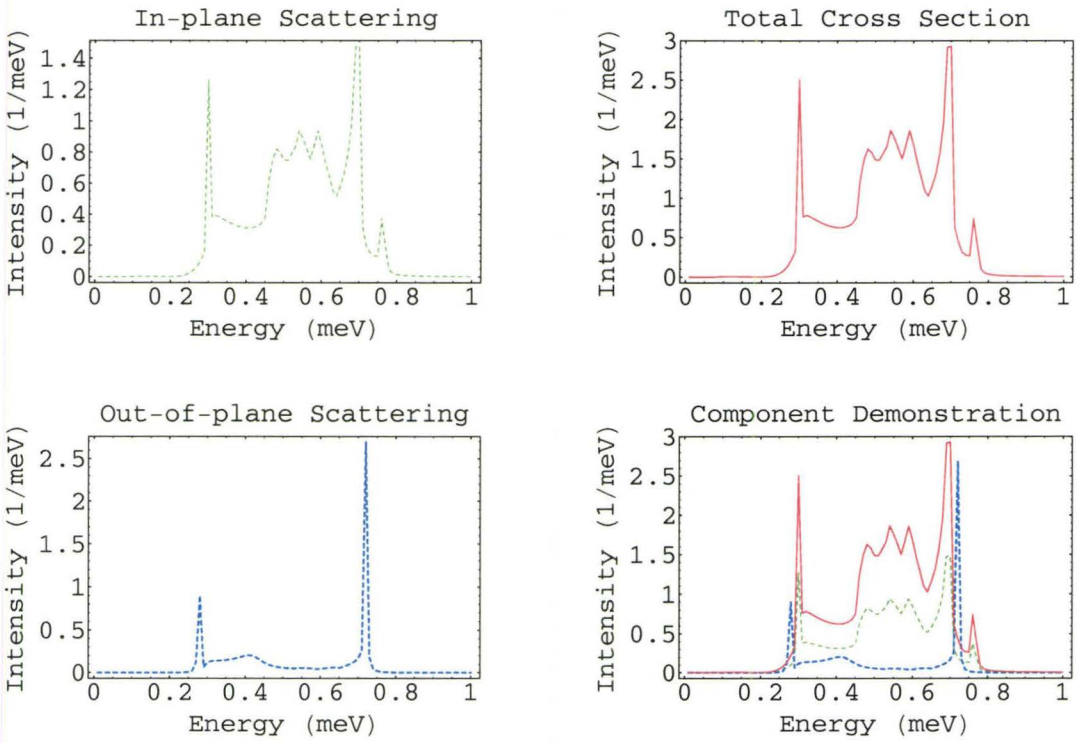

Figure 4.11: Structure factors and cross section at B point.

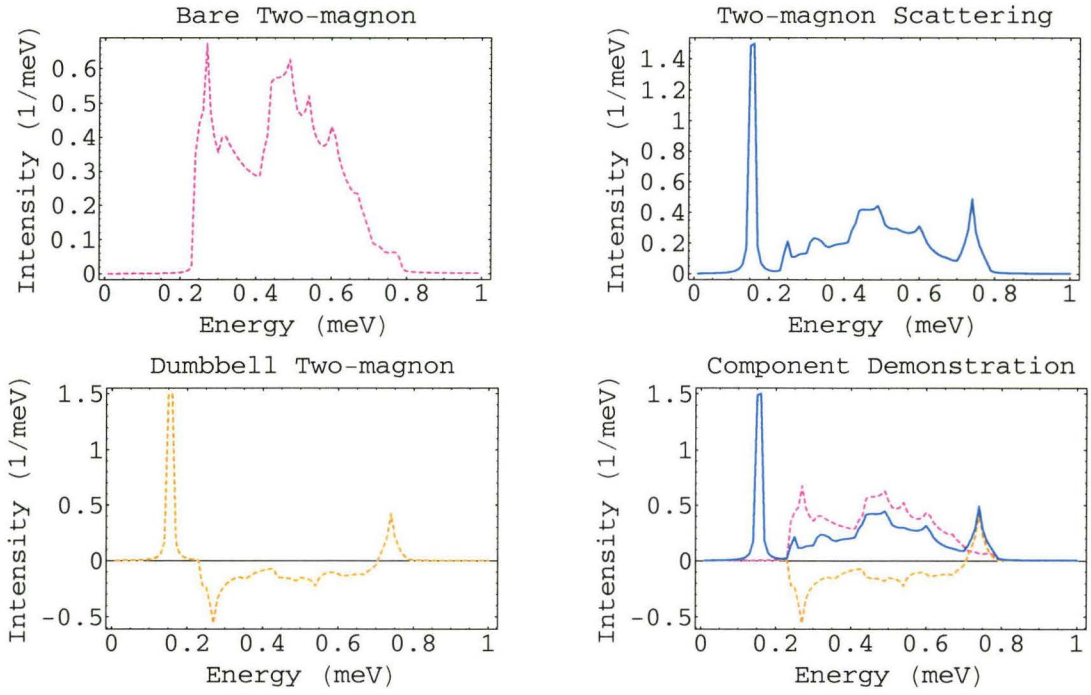

Figure 4.12: In-plane two-magnon scattering at C point.

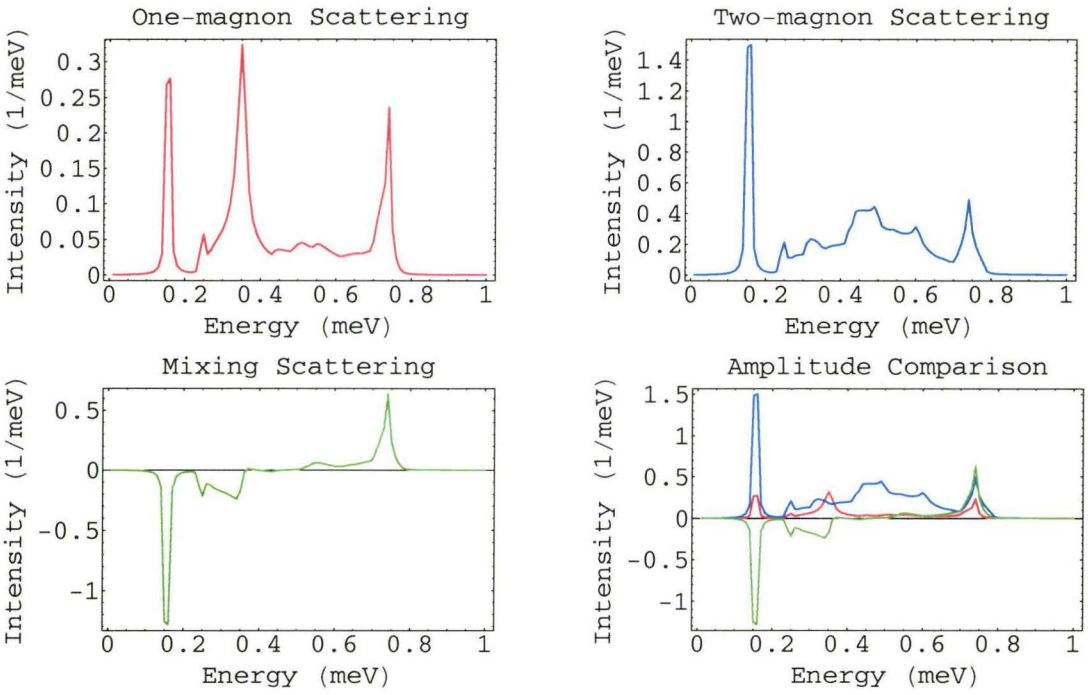

Figure 4.13: Three in-plane scattering processes at C point.

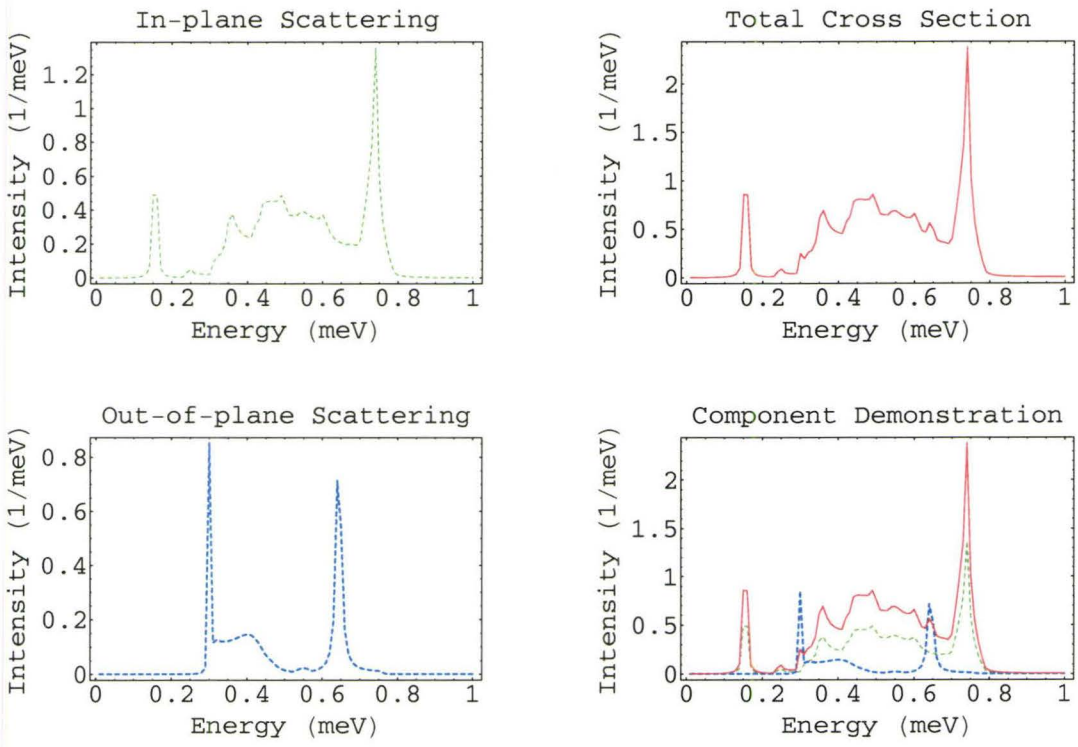

Figure 4.14: Structure factors and cross section at C point.

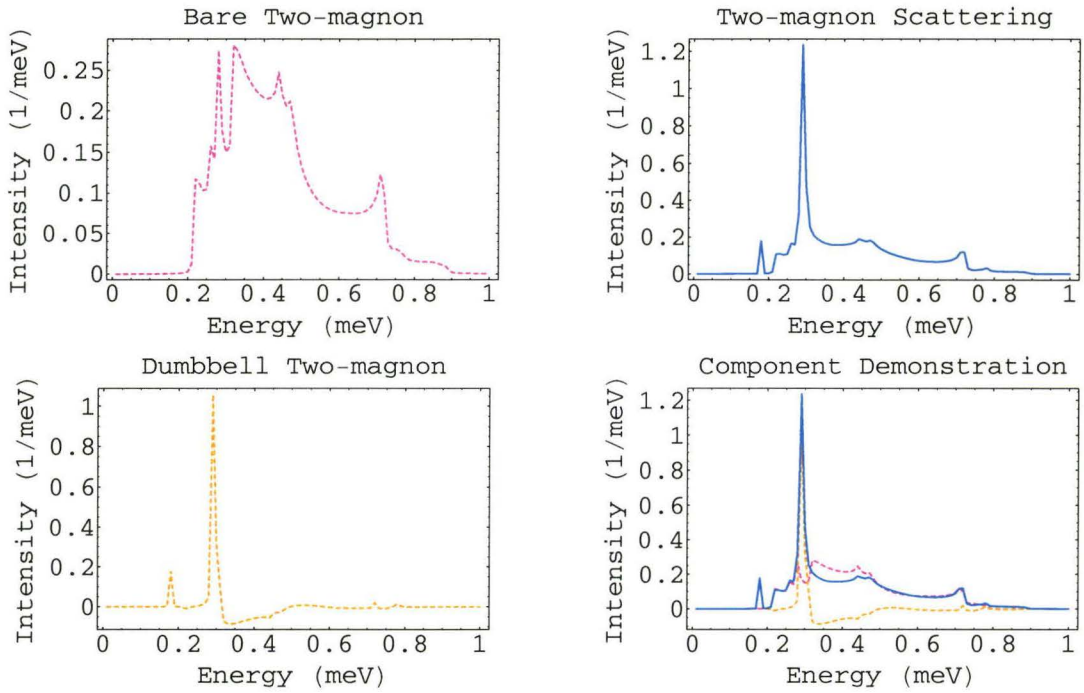

Figure 4.15: In-plane two-magnon scattering at D point.

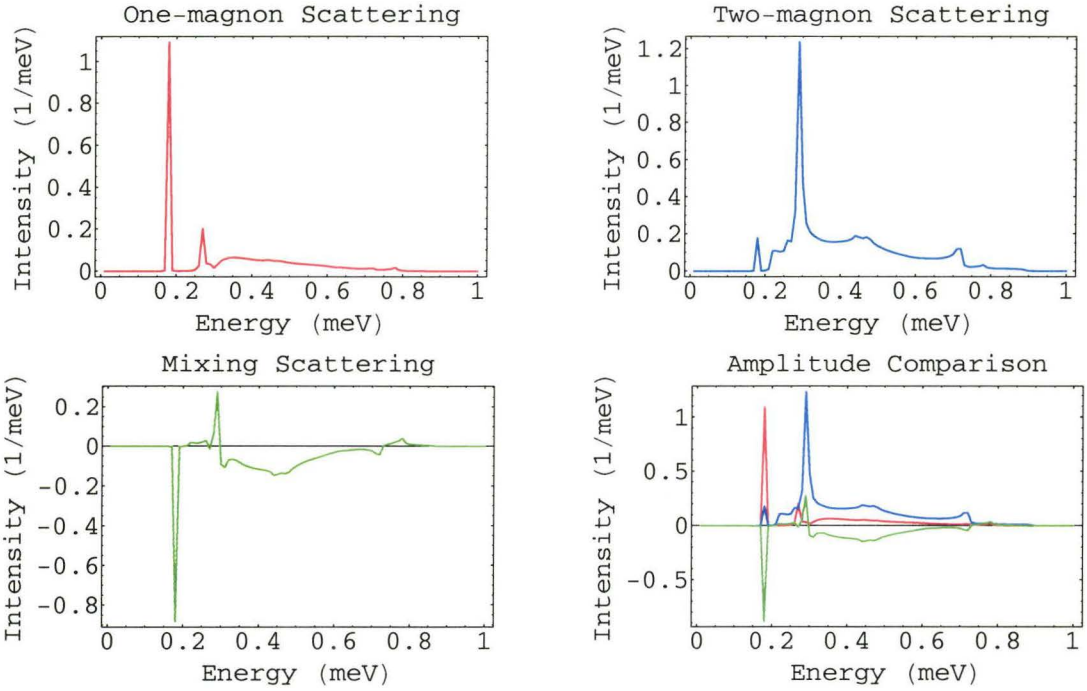

Figure 4.16: Three in-plane scattering processes at D point.

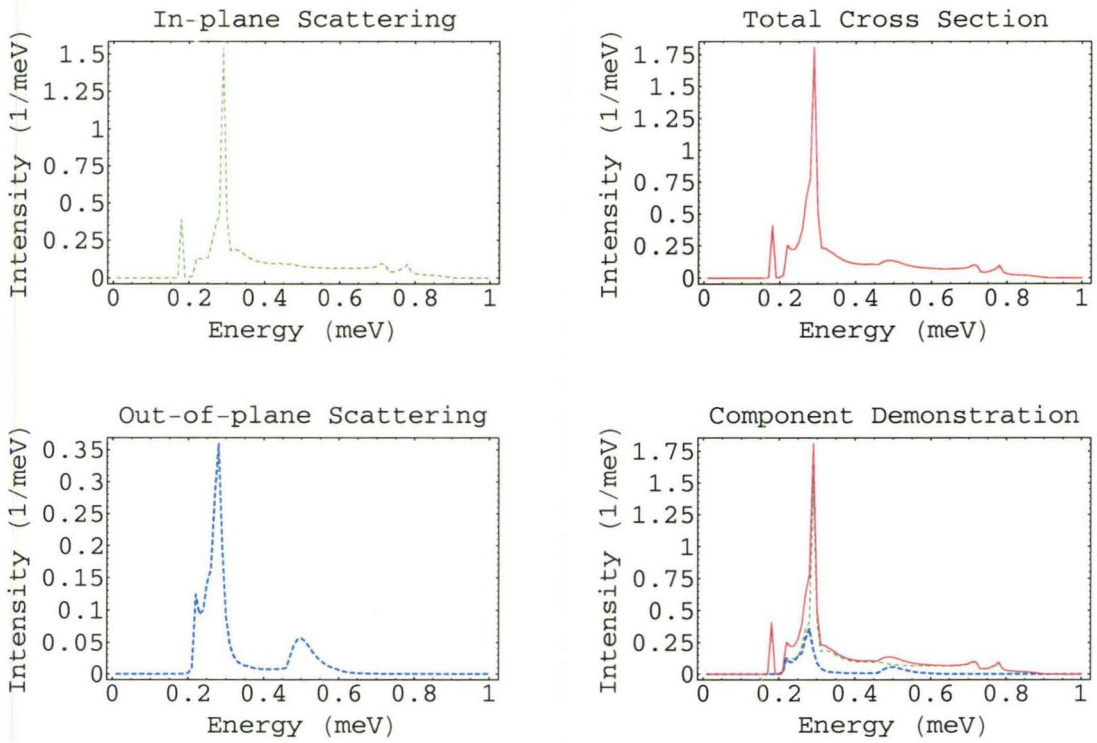

Figure 4.17: Structure factors and cross section at D point.

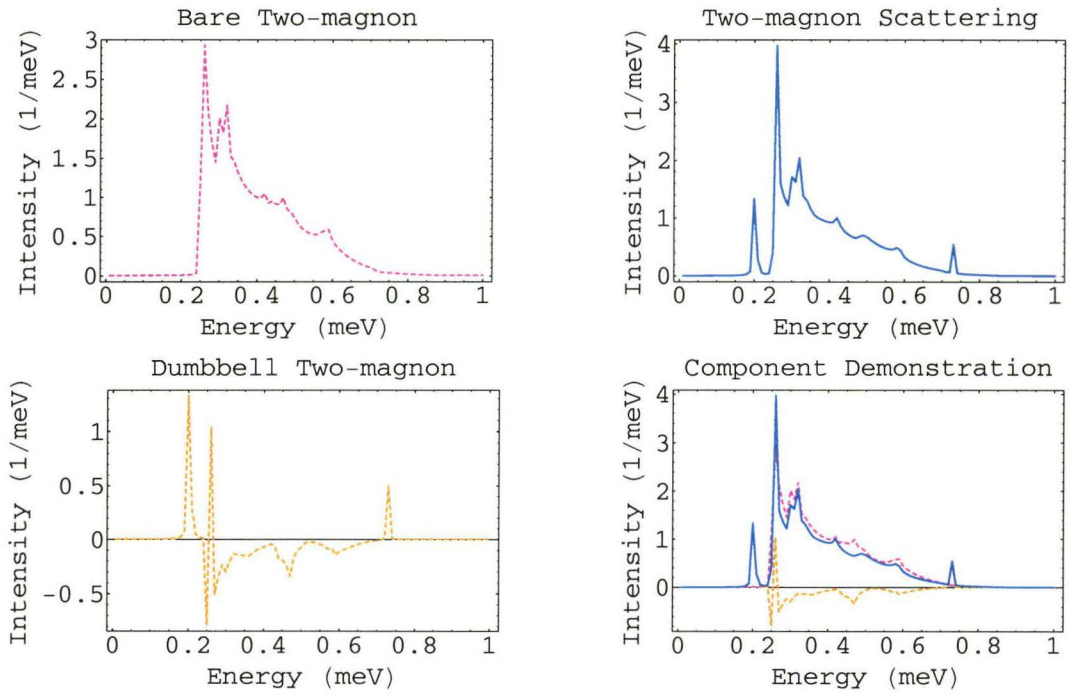

Figure 4.18: In-plane two-magnon scattering at E point.

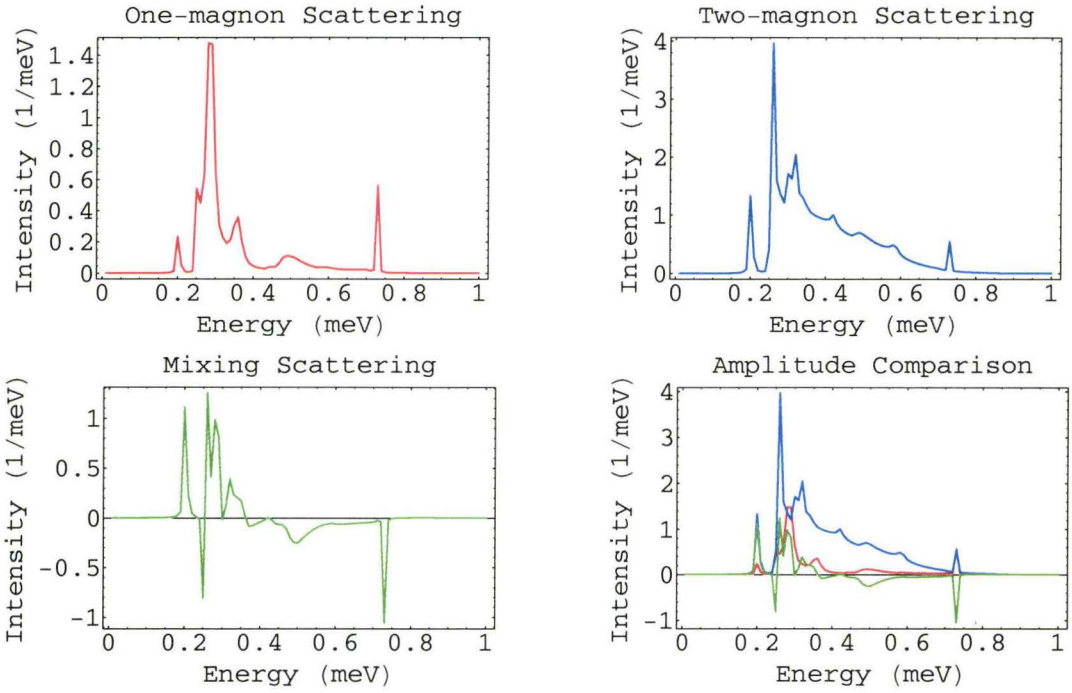

Figure 4.19: Three in-plane scattering processes at E point.

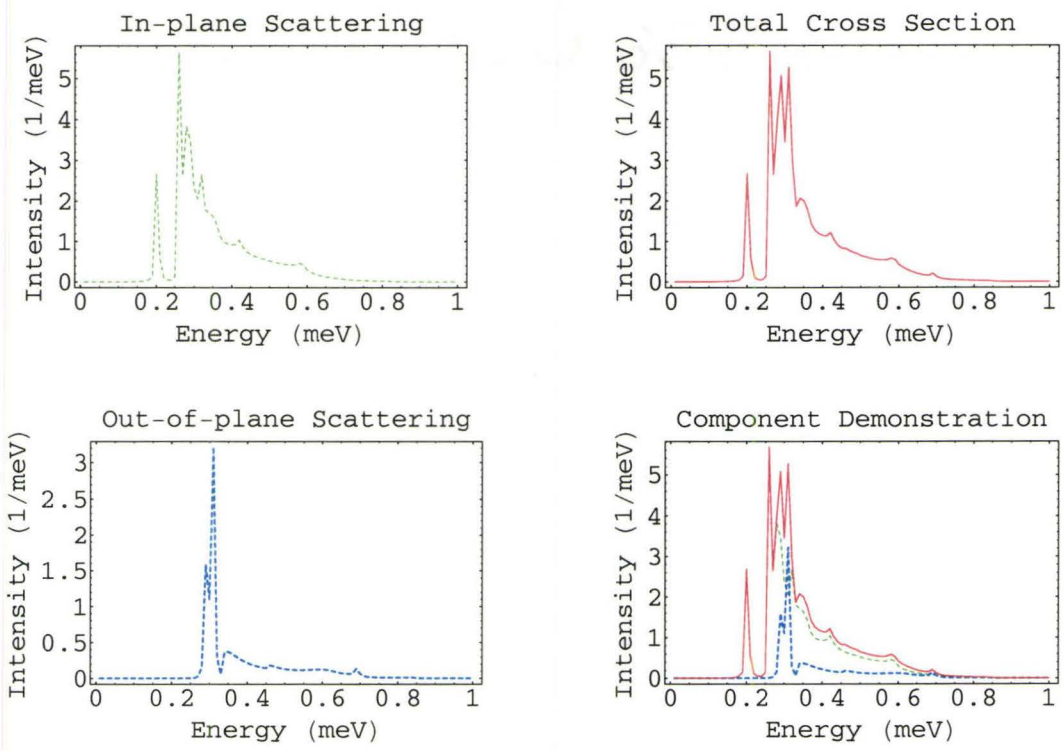

Figure 4.20: Structure factors and cross section at E point.

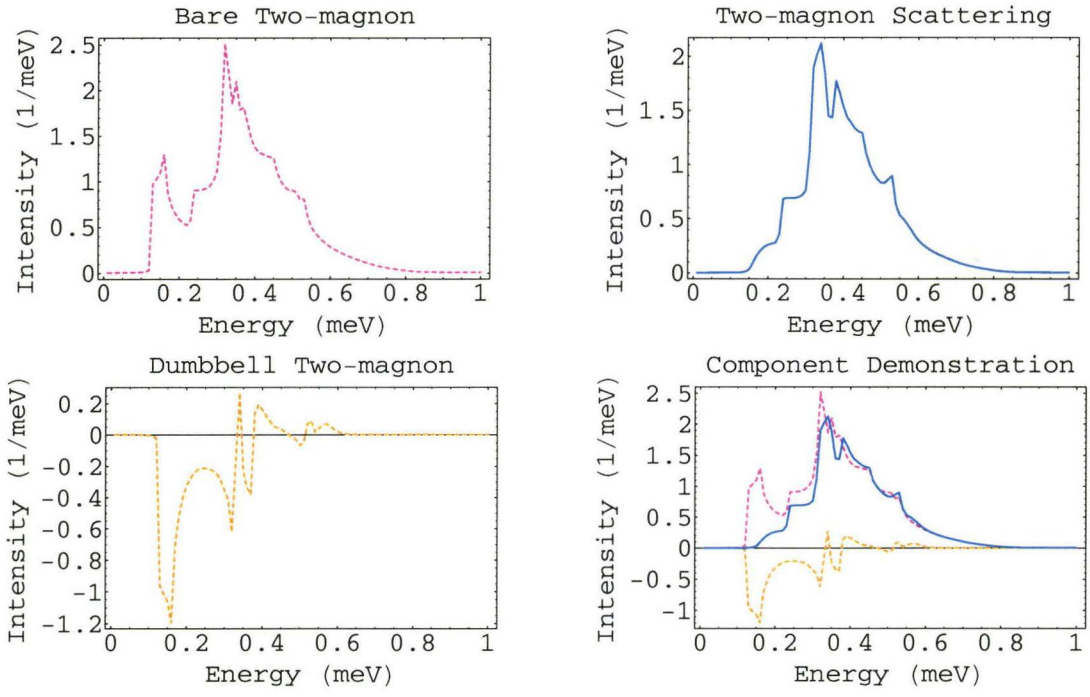

Figure 4.21: In-plane two-magnon scattering at F point.

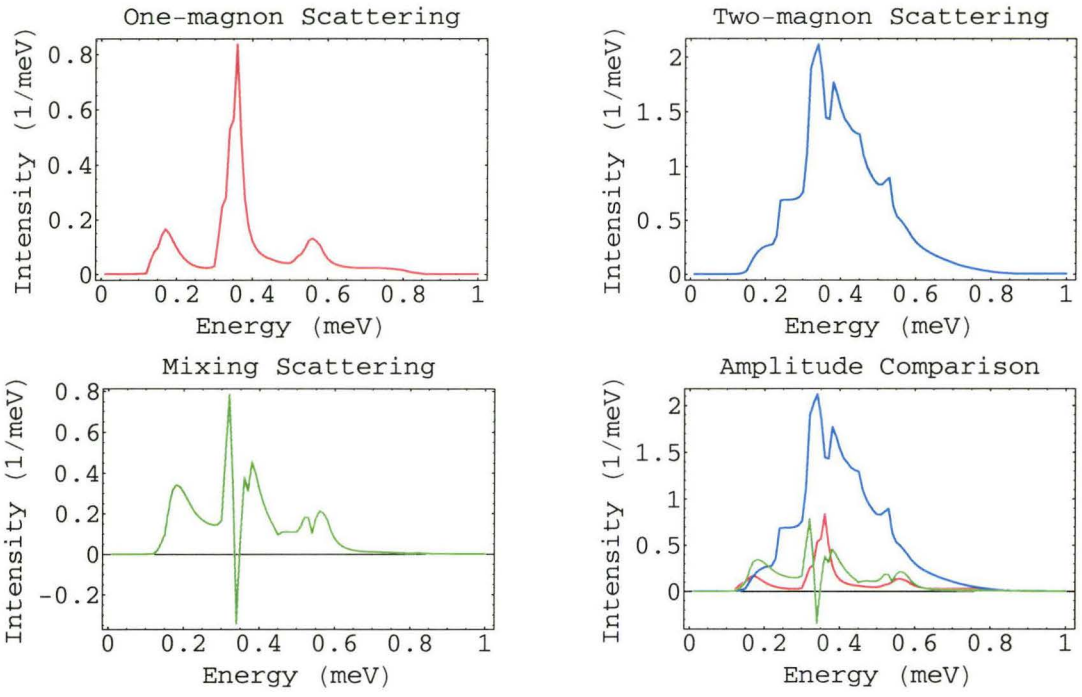

Figure 4.22: Three in-plane scattering processes at F point.

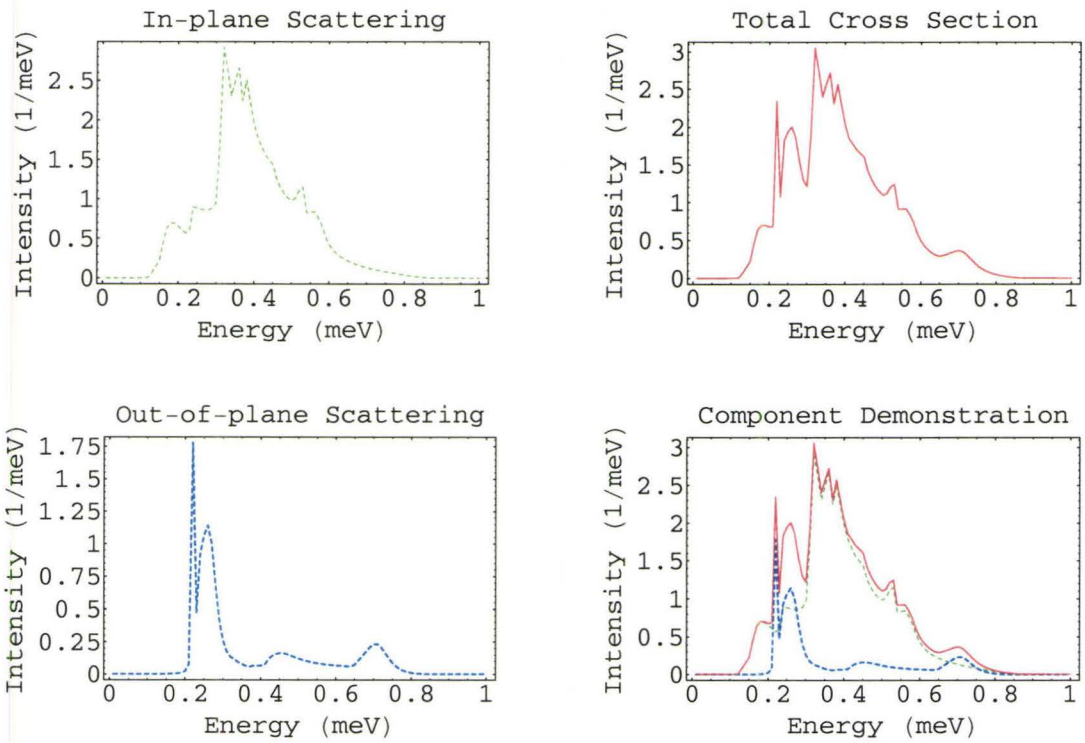

Figure 4.23: Structure factors and cross section at F point.

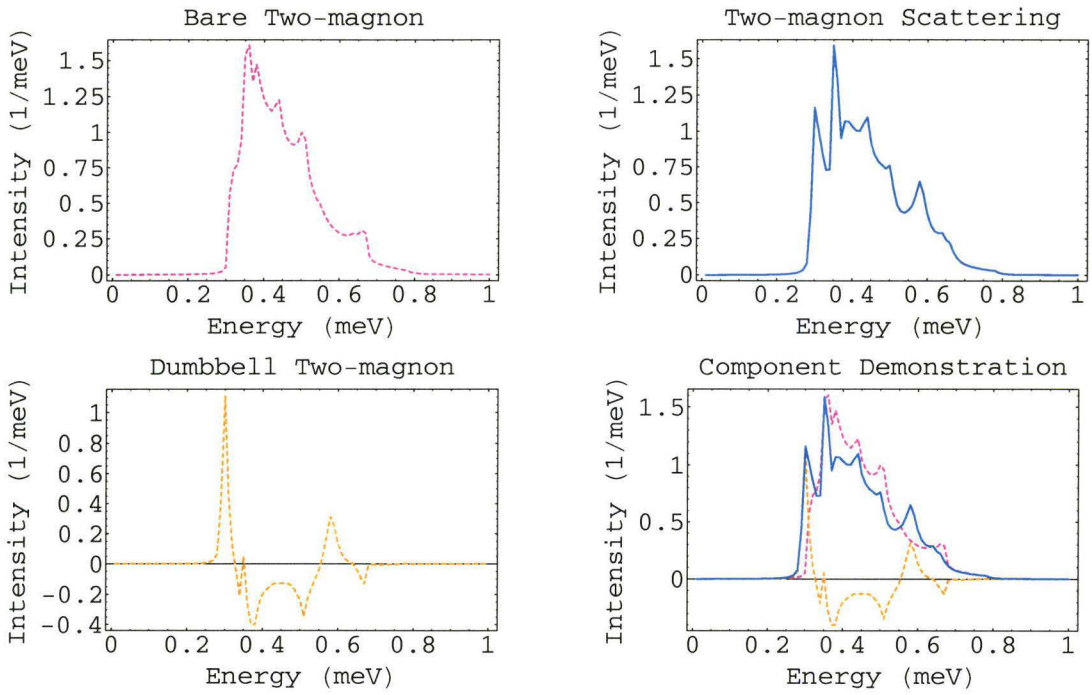

Figure 4.24: In-plane two-magnon scattering at H point.

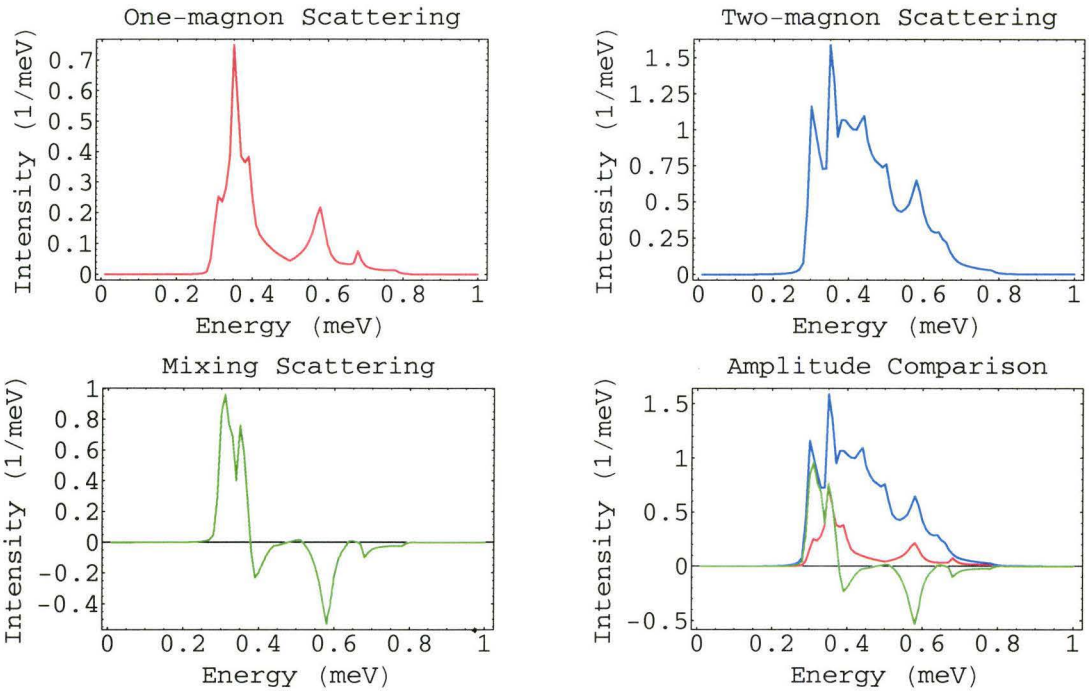

Figure 4.25: Three in-plane scattering processes at H point.

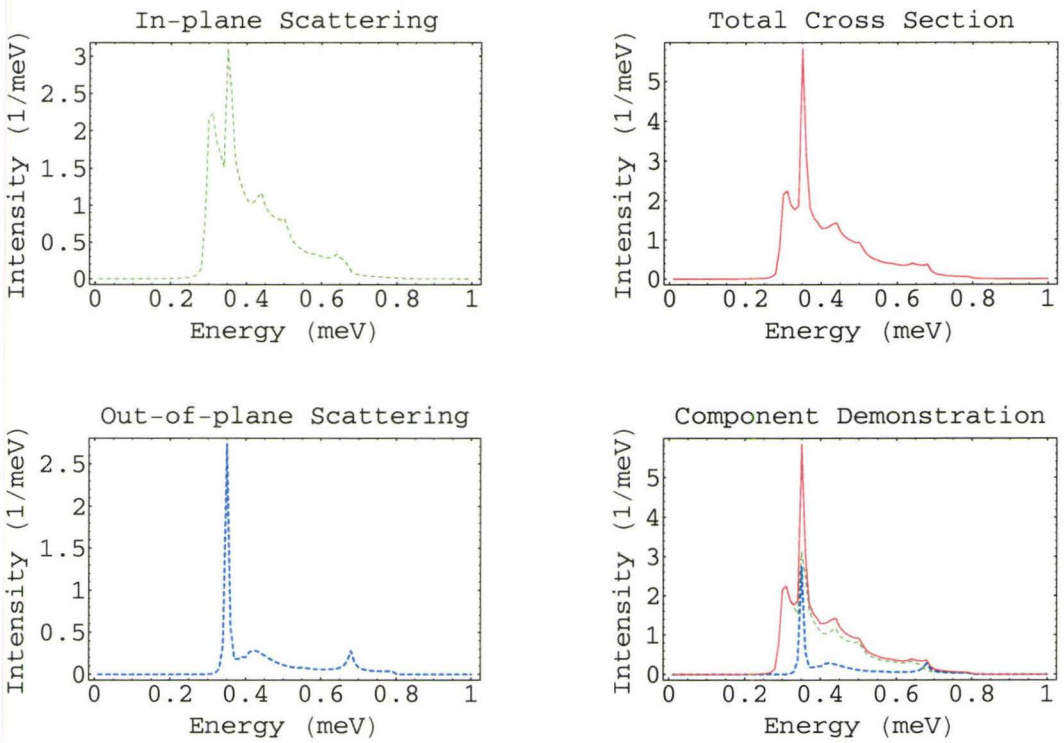

Figure 4.26: Structure factors and cross section at H point.

4.4.2 Line Shape Analysis

In the in-plane component graph panels, it is clearly seen that the two-magnon scattering process carries a large weight of the intensity and forms an extensive shape, spanning from the medium- to the high-energy regime with a sharp lower threshold. This is not surprising because the longitudinal fluctuations are expected to be large as discussed in Sec. 4.1. By comparison, the one-magnon processes both for the in-plane transverse part and the out-of-plane polarized part are rather small, which on the one hand is a consequence of the frequency-dependent self-energy, and on the other hand, due to the small prefactor suppression:

$$t_y = 0.611617, \quad t_x = 0.517597.$$

The mixing process results in a re-distribution of the scattering weight as shown in the diagrams.

With different polarization factors, A,B and C points mainly reflect the in-plane structure factor while D to H measurements are almost unpolarized. However, since the two-magnon process is extremely large, all of them exhibit a noticeable continuum extended into a high-energy tail. The G point is somewhat special because there is a sharp peak showing up in the low-energy regime at about 0.07 meV, which is the out-of-plane polarized principal mode with almost no damping. Above an energy gap, starting at 0.2 meV, another peak appears decaying slowly with energy. This agrees quite well with the experimental observation except that the position of the peak and the ending of the tail are a little lower. Also agreeing with the observation at the H point, the principal peak merges into the continuum. Although the polarizations at the A and F points are different, the line shapes are not so different from each other since the two-magnon contribution is dominant in both cases.

However, in spite of some similarity between the calculated and measured line shape, there exist significant discrepancies. For convenience, we put the calculated cross sections at these points together (see Fig. 4.27) to make a comparison with the experimental data (see Fig. 4.28). First, the energy region for the theoretical scattering occurrence is generally lower than the experimental ones. This is consistent with the calculated spectrum which is also shifted to lower energy than is measured.

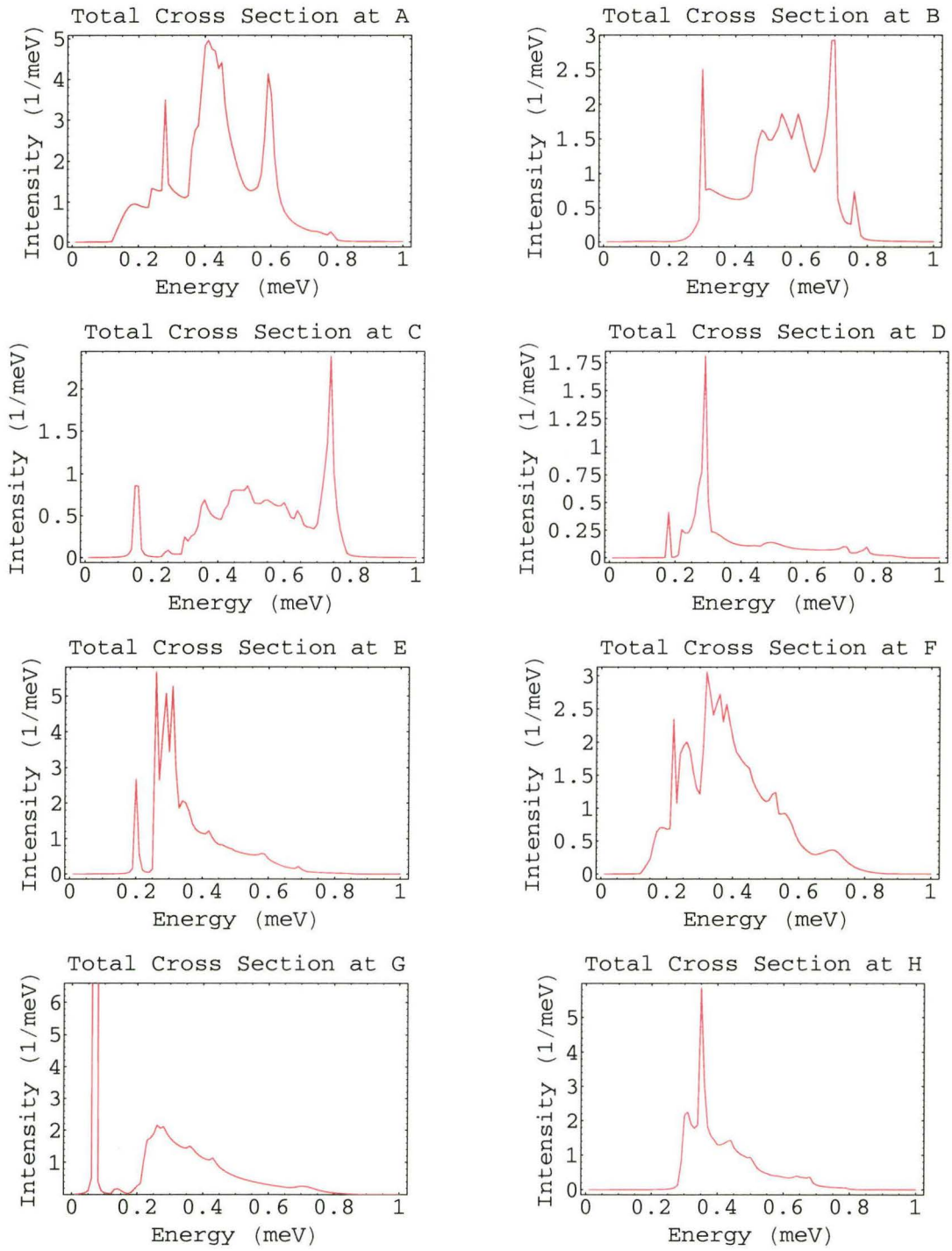

Figure 4.27: Total cross sections at A-H points.

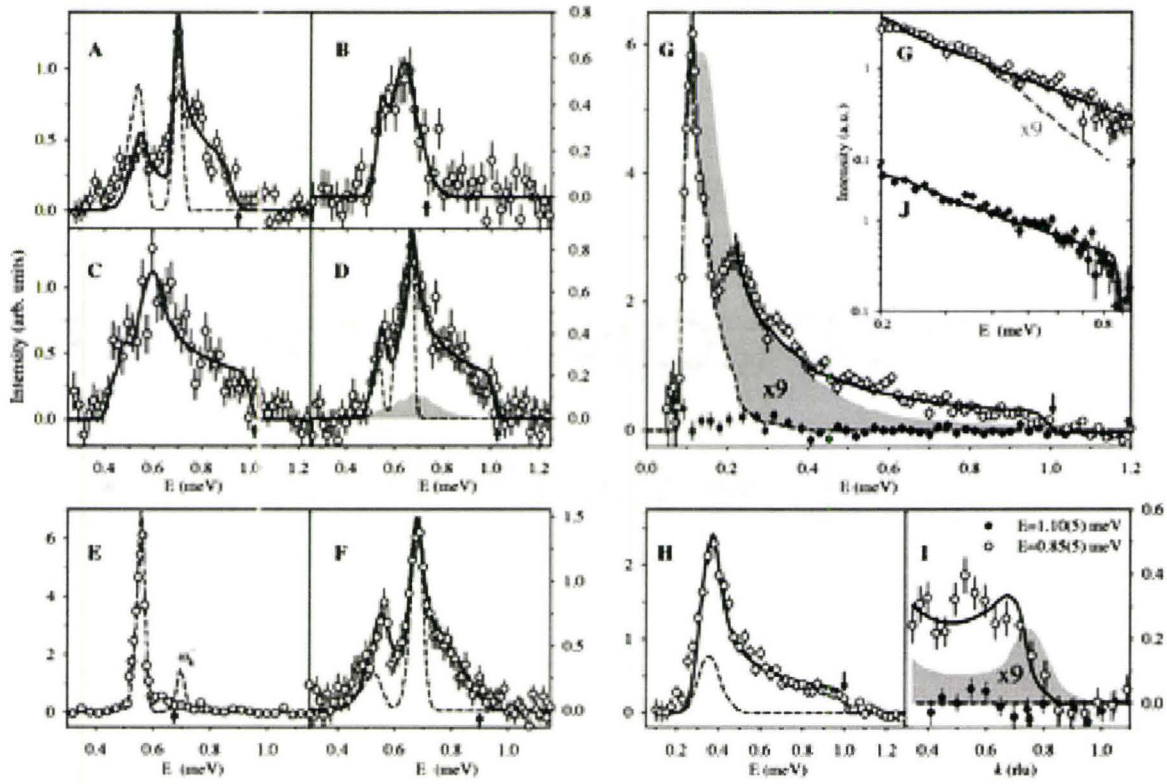

Figure 4.28: Experimental measurements at A-H points (Ref. [11]).

Second, the theoretical line shape at the E point is remarkably different from the experimental result: instead of having a single sharp peak, it is still dominated by a continuum due to the large two-magnon scattering intensity. This disagreement motivates us to investigate the situation where there are Dzyaloshinskii-Moriya terms in the Hamiltonian that reduce the multiple magnon process. Taking the experimental value of this DM coupling 0.020 meV [11], we perform the numerical work at the E point with the result shown in Fig. 4.29, 4.30, 4.31.

The line shape with DM terms is quite different from that without DM terms (as shown in Fig. 4.32). Particularly, the two-magnon scattering intensity is greatly reduced such that the continuum carries a much smaller weight.

Finally, there are unphysical peaks appearing at high energies in some graphs, which have been discussed in Ref. [15].

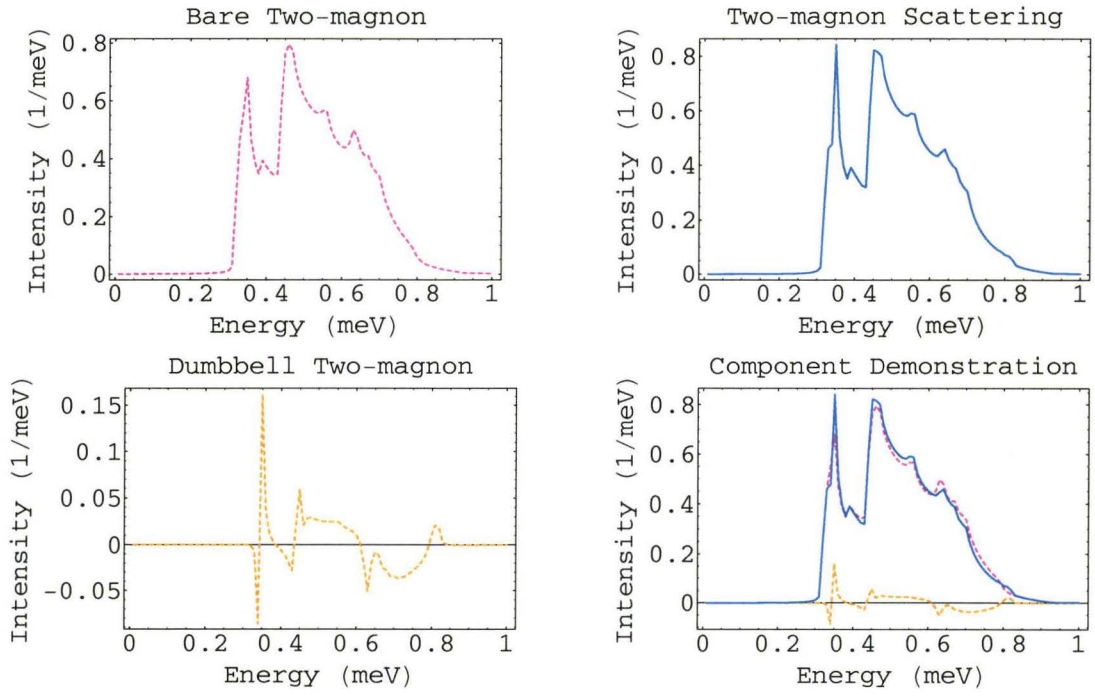

Figure 4.29: In-plane two-magnon scattering at E point with DM terms.

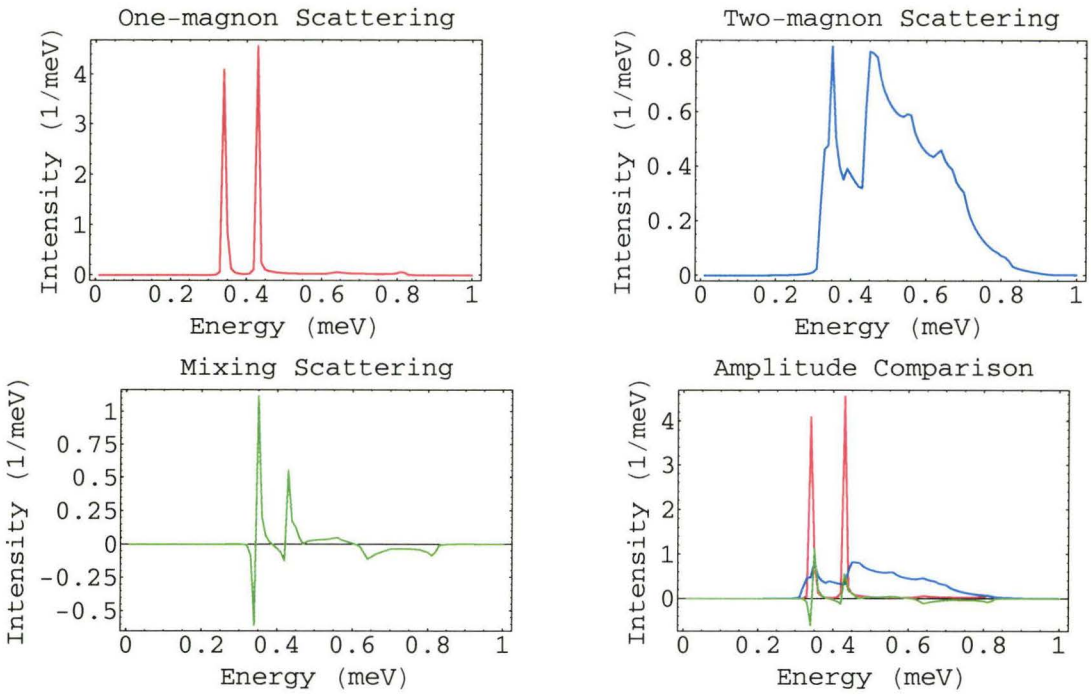

Figure 4.30: Three in-plane scattering processes at E point with DM terms.

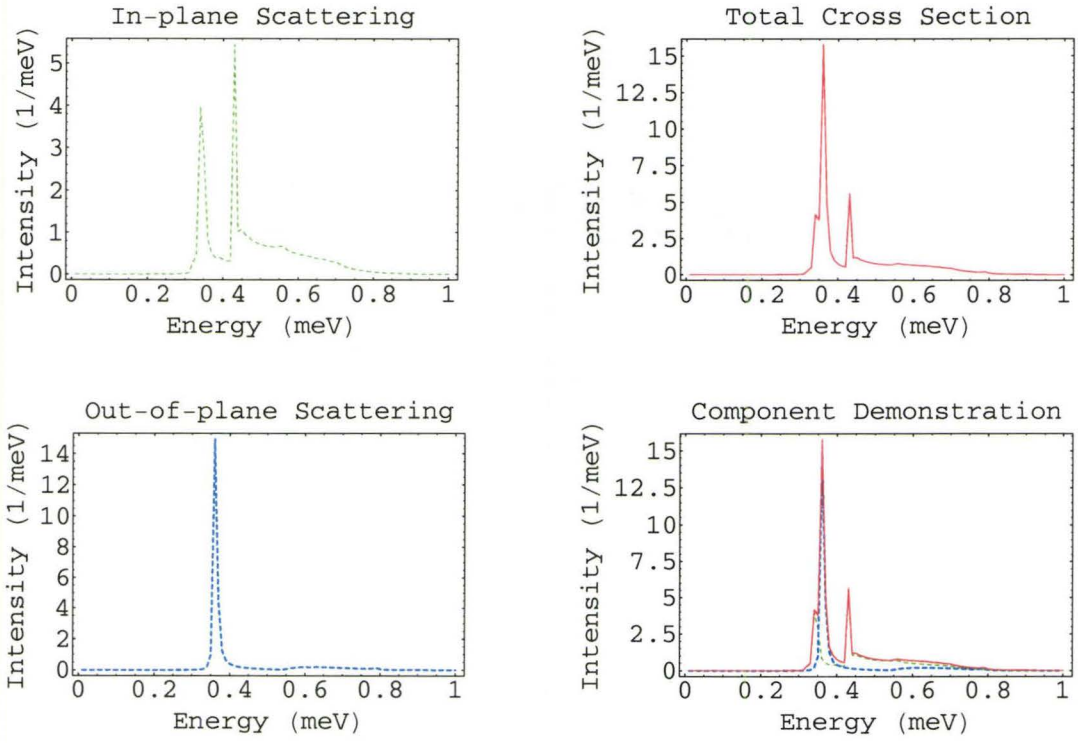

Figure 4.31: Structure factors and cross section at E point with DM terms.

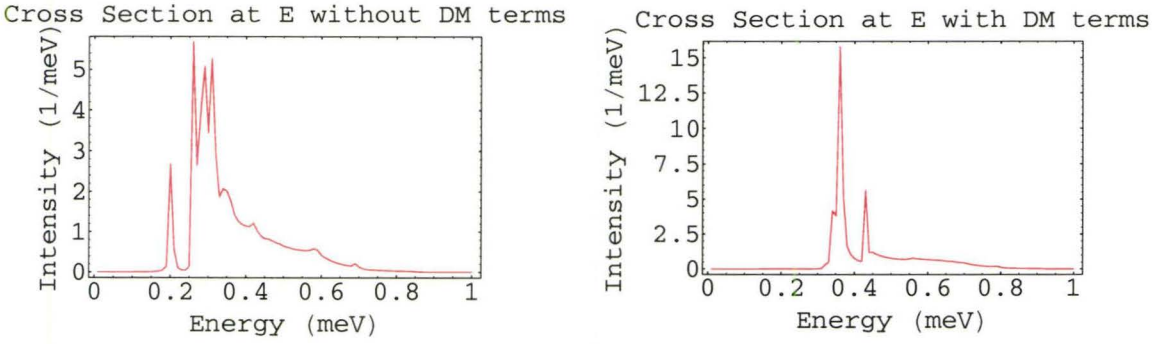

Figure 4.32: Cross Section at E point without and with DM interactions respectively.

Chapter 5

Conclusion

In this work we have used nonlinear spin wave theory to calculate the dynamical spin structure factor as well as the renormalized excitation spectrum in the spiral ordered phase of J-J' Heisenberg antiferromagnet on the anisotropic triangular lattice. The application to a real experimental system, Cs_2CuCl_4, has been initially made. We found that to the first sub-leading contribution in a $1/S$ expansion, quantum fluctuations are rather large, which give rise to considerable renormalization of the magnon dispersion relation as well as noticeable excitation damping in some regions of the Brillouin zone. More significantly, we found a strong continuum in the dynamical structure factor, which is mainly due to multi-magnon scattering processes. However, our results have crucial discrepancies compared with the experimental observations. First, the energy regimes where continua occur are generally lower than the experimentally observed. Second, there are remarkable differences between the line shapes at some wave vectors especially at the saddle point E. Third, the theoretically calculated $1/S$-renormalized excitation spectrum can not explain the experimental data since the overall energy scale is much smaller than that measured.

In spite of these disagreements, there remain quite a few similarities on the qualitative level, e.g. the notable scattering continua. Also, our comparison to experiment is at a preliminary stage as it did not choose energy-trajectories for the wavevector transfers and did not perform wavevector averages when computing the structure factor. Furthermore, the precision of the numerics needs to be improved in light of

the oscillating signals in some of the graphs. Therefore, it would be necessary to make more progress on the numerical evaluation for a complete comparison to the measurements.

Another speculation from this work is a question about the Hamiltonian: Does the minimal Hamiltonian really capture all the essential physics? Veillette et al.'s work[15] shows that the DM interaction enhances the sublattice magnetization and suppresses the fluctuations so that the ordered phase is more stable. Purely starting from the minimal Hamiltonian, we obtain a fragile ordered phase which could be destroyed by higher-order corrections and make the perturbative expansion problematic.

Finally, we have to point out that since this 2D calculation is restricted to zero temperature, we have nothing to say about the temperature dependence of the continuum, while the experiment shows its survival to relatively high temperature (above T_N) as convincing evidence for a spin liquid state.

All in all, the nature of Cs_2CuCl_4's low temperature magnetic phase is still not well understood. Both additional experimental and theoretical work would be desirable.

Bibliography

[1] P. W. Anderson, Mater. Res. Bull. **8**, 153 (1973).

[2] P. W. Anderson, Science **235**, 1196 (1987).

[3] S. Sachdev, Phys. Rev. B **45**, 12377 (1992).

[4] R. Moessner and S. L. Sondhi, Phys. Rev. Lett. **86**, 1881 (2001).

[5] V. Kalmeyer and R. B. Laughlin, Phys. Rev. Lett. **59**, 2095 (1987).

[6] R. Coldea, D. A. Tennant, R. A. Cowley, D. F. McMorrow, B. Dorner, and Z. Tylczynski, J. Phys.: Condens. Matter **8**, 7473 (1996).

[7] R. Coldea, D. A. Tennant, R. A. Cowley, D. F. McMorrow, B. Dorner, and Z. Tylczynski, Phys. Rev. Lett. **79**, 151 (1997).

[8] R. Coldea, D. A. Tennant, R. A. Cowley, D. F. McMorrow, B. Dorner, and Z. Tylczynski, Journal of Magnetism and Magnetic Materials **177-181**, 659 (1998).

[9] R. Coldea, D. A. Tennant, A. M. Tsvelik, and Z. Tylczynski, Phys. Rev. Lett. **86**, 1335 (2001).

[10] R. Coldea, D. A. Tennant, K. Habicht, P. Smeibidl, C. Wolters, and Z. Tylczynski, Phys. Rev. Lett. **88**, 137203 (2002).

[11] R. Coldea, D. A. Tennant, and Z. Tylczynski, Phys. Rev. B **68**, 134424 (2003).

[12] A. E. Trumper, Phys. Rev. B **60**, 2987 (1999).

[13] J. Merino, R. H. McKenzie, J. B. Marston, and C. H. Chung, J. Phys.: Condens. Matter **60**, 2987 (1999).

[14] M. Y. Veillette, J. T. Chalker, and R. Coldea, Phys. Rev. B **71**, 214426 (2005).

[15] M. Y. Veillette, A. J. A. James, and F. H. L. Essler, cond-mat/0506667 (unpublished).

[16] W. Zheng, R. H. McKenzie, and R. R. P. Singh, Phys. Rev. B **59**, 14367 (1999).

[17] W. Zheng, R. R. P. Singh, R. H. McKenzie, and R. Coldea, Phys. Rev. B **71**, 134422 (2005).

[18] W. Zheng, J. O. Fjaerestad, R. R. P. Singh, R. H. McKenzie, and R. Coldea, cond-mat/0506400 (unpublished).

[19] M. Bocquet, F. H. L. Essler, A. M. Tsvelik, and A. O. Gogolin, Phys. Rev. B **64**, 094425 (2001).

[20] S. Yunoki and S. Sorella, Phys. Rev. Lett. **92**, 157003 (2004).

[21] M. Casula, S. Yunoki, C. Attaccalite, and S. Sorella, cond-mat/0411745 (unpublished).

[22] Y. Zhou and X. G. Wen, cond-mat/0210662 (unpublished).

[23] C. H. Chung, J. B. Marston, and R. H. McKenzie, J. Phys.: Condens. Matter **13**, 5159 (2001).

[24] C. H. Chung, K. Voelker, and Y. B. Kim, Phys. Rev. B **68**, 094412 (2003).

[25] S. Takei, C. H. Chung, and Y. B. Kim, Phys. Rev. B **70**, 104402 (2004).

[26] S. V. Isakov, T. Senthil, and Y. B. Kim, cond-mat/0503241 (unpublished).

[27] S. Florens, L. Fritz, and M. Vojta, cond-mat/0507188 (unpublished).

[28] M. Q. Weng, D. N. Sheng, Z. Y. Weng, and R. J. Bursill, cond-mat/0508186 (unpublished).

[29] J. Alicea, O. I. Motrunich, and M. P. A. Fisher, cond-mat/0508536 (unpublished).

[30] N. D. Mermin and H. Wagner, Phys. Rev. Lett. **22**, 1133 (1966).

[31] T. Jolicoeur, Phys. Rev. B **40**, 2727 (1989).

[32] S. J. Miyake, J. Phys. Soc. Jpn **61**, 983 (1992).

[33] R. Deutscher and H. U. Everts, Z. Phys. B **93**, 77 (1993).

[34] A. V. Chubukov, S. Sachdev, and T. Senthil, J. Phys: Condens. Matter **6**, 8891 (1994).

[35] F. Bloch, Z. Physik **61**, 206 (1930).

[36] F. Bloch, Z. Physik **74**, 295 (1932).

[37] T. Holstein and H. Primakoff, Phys. Rev. **58**, 1098 (1940).

[38] P. W. Anderson, Phys. Rev. **86**, 694 (1952).

[39] R. Kubo, Phys. Rev. **87**, 568 (1952).

[40] T. Oguchi, Phys. Rev. **117**, 117 (1960).

[41] F. Dyson, Phys. Rev. **102**, 1217 (1956).

[42] F. Dyson, Phys. Rev. **102**, 1230 (1956).

[43] N. B. Ivanov and D. Sen, *Quantum Magnetism* (Springer-Verlag GmbH, 2004), vol. 645, pp. 195 – 226.

[44] Y. L. Wang, S. Shtrikman, and H. Callen, Phys. Rev. **148**, 419 (1966).

[45] E. Rastelli, L. Reatto, and A. Tassi, J. Appl. Phys. **55**, 1871 (1984).

[46] A. V. Chubukov, J. Phys. C: Solid State Phys. **17**, L991 (1984).

[47] E. Rastelli, L. Reatto, and A. Tassi, J. Phys. C: Solid State Phys. **18**, 353 (1985).

[48] E. Rastelli and A. Tassi, J. Phys. C: Solid State Phys. **19**, 1993 (1986).

[49] T. Ohyama and H. Shiba, J. Phys. Soc. Jpn **62**, 3277 (1993).

Appendix A

Goldstone Modes

Here we show that the excitation spectrum defined by (2.37) exhibits the Goldstone modes. The appearance of Goldstone modes is one of the phenomena stemming from spontaneous continuous symmetry breaking in the ground state of a system whose dynamics is controlled by a symmetric Hamiltonian. The $1/S$-expansion of the Heisenberg model is expected to maintain spin rotational symmetry order by order in $1/S$. Thus, our renormalized excitation spectrum, which includes all the contributions to order $\mathcal{O}(S^1)$ and $\mathcal{O}(S^0)$, is expected to preserve these zero modes.

In linear spin wave theory, where only the contribution of order $\mathcal{O}(S^1)$ is counted, the Goldstone modes occur at $\mathbf{k} = \mathbf{0},\ \mathbf{Q}_c$ due to the facts that

$$A_{\mathbf{k}} - B_{\mathbf{k}} \xrightarrow{\mathbf{k}\to\mathbf{0}} \sum_{i,j} \frac{1}{2} M^0_{ij} \Delta k_i \Delta k_j, \quad A_{\mathbf{k}} + B_{\mathbf{k}} \xrightarrow{\mathbf{k}\to\mathbf{0}} \text{finite}, \tag{A.1}$$

where $i, j = x, y$, $\Delta k_{i,j} = k_{i,j} - 0$ and

$$M^0_{ij} = \left. \frac{\partial^2 J_{\mathbf{k}}}{\partial k_i \partial k_j} \right|_{\mathbf{k}=\mathbf{0}},$$

and

$$A_{\mathbf{k}} - B_{\mathbf{k}} \xrightarrow{\mathbf{k}\to\mathbf{Q}_c} \text{finite}, \quad A_{\mathbf{k}} + B_{\mathbf{k}} \xrightarrow{\mathbf{k}\to\mathbf{Q}_c} \sum_{i,j} \frac{1}{2} M_{ij} \Delta k_i \Delta k_j, \tag{A.2}$$

where $i, j = x, y$, $\Delta k_{i,j} = k_{i,j} - Q^c_{i,j}$ and M_{ij} is defined in (2.25), i.e.,

$$M_{ij} = \left. \frac{\partial^2 J_{\mathbf{k}}}{\partial k_i \partial k_j} \right|_{\mathbf{k}=\mathbf{Q}_c}.$$

Hence

$$\omega_{\mathbf{k}} = 2S\Omega_{\mathbf{k}} = 2S\sqrt{(A_{\mathbf{k}} - B_{\mathbf{k}})(A_{\mathbf{k}} + B_{\mathbf{k}})}$$

is linear around the two Goldstone modes because both the constant and linear terms in the relevant factor $A_{\mathbf{k}} - B_{\mathbf{k}}$ or $A_{\mathbf{k}} + B_{\mathbf{k}}$ vanish.

A straightforward property of the LSWT ground state is that the ordering wavevector $\mathbf{Q}$ is shifted by a $\mathcal{O}(S^{-1})$ amount. This new value of $\mathbf{Q}$ will contribute to the next order perturbative calculation. Hence, we need to examine the Goldstone modes at wave vectors $\mathbf{0}$ and the shifted $\mathbf{Q} = \mathbf{Q}_c + \Delta\mathbf{Q} \equiv \mathbf{Q}_0$ for the $1/S$-renormalized excitation spectrum.

For the convenience of analysis, the correction to the bare dispersion relation, Eq. (2.37), is written in the following way:

$$\Delta\omega_{\mathbf{k}} = F_{\mathbf{k}}^{(1)} + F_{\mathbf{k}}^{(2)} + F_{\mathbf{k}}^{(3)} + \mathrm{Re}\Sigma_A(\mathbf{k}, \omega_{\mathbf{k}}),$$

$$\begin{aligned}
F_{\mathbf{k}}^{(1)} &\equiv \frac{2S\Delta A_{\mathbf{k}} \cdot (A_{\mathbf{k}} + B_{\mathbf{k}})^{1/2}}{(A_{\mathbf{k}} - B_{\mathbf{k}})^{1/2}}, \\
F_{\mathbf{k}}^{(2)} &\equiv \frac{\mathrm{Re}\Big[\Sigma_S(\mathbf{k}, \omega_{\mathbf{k}}) - \Sigma_O(\mathbf{k}, \omega_{\mathbf{k}})\Big] \cdot (A_{\mathbf{k}} + B_{\mathbf{k}})^{1/2}}{2(A_{\mathbf{k}} - B_{\mathbf{k}})^{1/2}}, \\
F_{\mathbf{k}}^{(3)} &\equiv \frac{(A_{\mathbf{k}} - B_{\mathbf{k}})^{1/2} \cdot \mathrm{Re}\Big[\Sigma_S(\mathbf{k}, \omega_{\mathbf{k}}) + \Sigma_O(\mathbf{k}, \omega_{\mathbf{k}})\Big]}{2(A_{\mathbf{k}} + B_{\mathbf{k}})^{1/2}}.
\end{aligned} \tag{A.3}$$

First, we consider the vicinity of the zone center: $\mathbf{k} \to \mathbf{0}$, where we have

$$\begin{aligned}
(A_{\mathbf{k}} + B_{\mathbf{k}})^{1/2} &\to \text{finite}, \\
\mathrm{Re}\Big[\Sigma_S(\mathbf{k}, \omega_{\mathbf{k}}) + \Sigma_O(\mathbf{k}, \omega_{\mathbf{k}})\Big] &\to \text{finite}, \\
(A_{\mathbf{k}} - B_{\mathbf{k}})^{1/2} &\to \left(\sum_{i,j} \frac{1}{2} M_{ij}^0 \Delta k_i \Delta k_j\right)^{1/2}, \\
2S\Delta A_{\mathbf{k}} &\to \sum_{i,j} \frac{1}{2} \left.\frac{\partial^2 (2S\Delta A_{\mathbf{k}})}{\partial k_i \partial k_j}\right|_{\mathbf{k}=\mathbf{0}} \Delta k_i \Delta k_j, \\
\mathrm{Re}\Big[\Sigma_S(\mathbf{k}, \omega_{\mathbf{k}}) - \Sigma_O(\mathbf{k}, \omega_{\mathbf{k}})\Big] &\to \mathcal{O}\left(|\Delta k|^2\right), \\
\mathrm{Re}\Sigma_A(\mathbf{k}, \omega_{\mathbf{k}}) &\to \mathcal{O}\left(|\Delta k|^2\right).
\end{aligned} \tag{A.4}$$

Then

$$
\begin{aligned}
F_{\mathbf{k}}^{(1)} &\to \mathcal{O}\left(|\Delta k|^1\right), \\
F_{\mathbf{k}}^{(2)} &\to \mathcal{O}\left(|\Delta k|^1\right), \\
F_{\mathbf{k}}^{(3)} &\to \mathcal{O}\left(|\Delta k|^1\right).
\end{aligned} \tag{A.5}
$$

From this we find

$$
\widetilde{\omega}_{\mathbf{k}} = \omega_{\mathbf{k}} + \Delta\omega_{\mathbf{k}} \xrightarrow{\mathbf{k}\to\mathbf{0}} \mathcal{O}\left(|\Delta k|\right). \tag{A.6}
$$

And at this point we could, in principle, calculate the renormalized spin-wave velocities.

Next, let us consider the excitation energy at $\mathbf{Q}_c$, where we have

$$
\begin{aligned}
(A_{\mathbf{k}} - B_{\mathbf{k}})^{1/2}\Big|_{\mathbf{k}=\mathbf{Q}_c} &= \text{finite}, \\
2S\Delta A_{\mathbf{k}}\Big|_{\mathbf{k}=\mathbf{Q}_c} &= \text{finite}, \\
\mathrm{Re}\Big[\Sigma_S(\mathbf{k},\omega_{\mathbf{k}}) - \Sigma_O(\mathbf{k},\omega_{\mathbf{k}})\Big]\Big|_{\mathbf{k}=\mathbf{Q}_c} &= \text{finite}, \\
(A_{\mathbf{k}} + B_{\mathbf{k}})^{1/2}\Big|_{\mathbf{k}=\mathbf{Q}_c} &= 0, \\
\mathrm{Re}\Sigma_A(\mathbf{k},\omega_{\mathbf{k}})\Big|_{\mathbf{k}=\mathbf{Q}_c} &= 0.
\end{aligned} \tag{A.7}
$$

Then

$$
\begin{aligned}
F_{\mathbf{k}}^{(1)}\Big|_{\mathbf{k}=\mathbf{Q}_c} &= 0, \\
F_{\mathbf{k}}^{(2)}\Big|_{\mathbf{k}=\mathbf{Q}_c} &= 0.
\end{aligned} \tag{A.8}
$$

The part $F_{\mathbf{k}}^{(3)}$ at $\mathbf{k} = \mathbf{Q}_c$ is of the " $\frac{0}{0}$ " type, which should be evaluated in the limiting case. In the numerator, the self-energy part includes both the quartic and cubic interaction contributions. It is easy to show that

$$
\begin{aligned}
\Sigma_S^{(4)}(\mathbf{k}) + \Sigma_O^{(4)}(\mathbf{k}) =& \frac{1}{N}\sum_{\mathbf{q}} \frac{1}{\Omega_{\mathbf{q}}}\Big[-\Omega_{\mathbf{q}}^2 + (A_{\mathbf{q}} - B_{\mathbf{q}})(A_{\mathbf{k}-\mathbf{q}} - B_{\mathbf{k}-\mathbf{q}})\Big] \\
&+ (A_{\mathbf{k}} + B_{\mathbf{k}})\Big[1 - \frac{1}{N}\sum_{\mathbf{q}} \frac{1}{\Omega_{\mathbf{q}}}\Big(A_{\mathbf{q}} - \frac{1}{2}B_{\mathbf{q}}\Big)\Big].
\end{aligned} \tag{A.9}
$$

At $\mathbf{k} \to \mathbf{Q}_c$, it becomes

$$\Sigma_S^{(4)}(\mathbf{k})+\Sigma_O^{(4)}(\mathbf{k}) = \frac{1}{N}\sum_{\mathbf{q}} \frac{1}{\Omega_{\mathbf{q}}}\Big[-\Omega_{\mathbf{q}}^2+(A_{\mathbf{q}}-B_{\mathbf{q}})(A_{\mathbf{k}-\mathbf{q}}-B_{\mathbf{k}-\mathbf{q}})\Big] + \mathcal{O}\left((\Delta k)^2\right). \quad \text{(A.10)}$$

Since $\omega_{\mathbf{Q}_c} = 0$, at $\mathbf{k} \to \mathbf{Q}_c$, the cubic part simply becomes

$$\mathrm{Re}\Big[\Sigma_S^{(3)}(\mathbf{k},0) + \Sigma_O^{(3)}(\mathbf{k},0)\Big] = -\frac{1}{N}\sum_{\mathbf{q}} \frac{\left[\Phi_{\mathbf{1},\mathbf{2}}^{(1)}\right]^2}{2(\Omega_{\mathbf{1}}+\Omega_{\mathbf{2}})}, \quad \text{(A.11)}$$

where $\mathbf{1} = \mathbf{q}$, $\mathbf{2} = \mathbf{k} - \mathbf{q}$, and

$$\Phi_{\mathbf{1},\mathbf{2}}^{(1)} = (C_{\mathbf{1}} + C_{\mathbf{2}})(u_{\mathbf{1}}u_{\mathbf{2}} - v_{\mathbf{1}}v_{\mathbf{2}}) + (C_{\mathbf{1}} - C_{\mathbf{2}})(u_{\mathbf{1}}v_{\mathbf{2}} - v_{\mathbf{1}}u_{\mathbf{2}}).$$

Using the relation (2.16):

$$C_{\mathbf{k}} = (A_{\mathbf{k}} - B_{\mathbf{k}}) - (A_{\mathbf{k}-\mathbf{Q}_c} + B_{\mathbf{k}-\mathbf{Q}_c}),$$

the cubic couplings $C_{\mathbf{1}}, C_{\mathbf{2}}$ can be expressed as

$$C_{\mathbf{q}} = \Big[(A_{\mathbf{q}} - B_{\mathbf{q}}) - (A_{\mathbf{k}-\mathbf{q}} + B_{\mathbf{k}-\mathbf{q}})\Big] + \Big[(A_{\mathbf{k}-\mathbf{q}} + B_{\mathbf{k}-\mathbf{q}}) - (A_{\mathbf{q}-\mathbf{Q}_c} + B_{\mathbf{q}-\mathbf{Q}_c})\Big],$$
$$C_{\mathbf{k}-\mathbf{q}} = \Big[(A_{\mathbf{k}-\mathbf{q}} - B_{\mathbf{k}-\mathbf{q}}) - (A_{\mathbf{q}} + B_{\mathbf{q}})\Big] + \Big[(A_{\mathbf{q}} + B_{\mathbf{q}}) - (A_{\mathbf{k}-\mathbf{q}-\mathbf{Q}_c} + B_{\mathbf{k}-\mathbf{q}-\mathbf{Q}_c})\Big].$$

Define

$$\psi(\mathbf{1},\mathbf{2}) \equiv (A_{\mathbf{2}} + B_{\mathbf{2}}) - (A_{\mathbf{Q}_c-\mathbf{1}} + B_{\mathbf{Q}_c-\mathbf{1}}),$$

then,

$$\psi(\mathbf{2},\mathbf{1}) = (A_{\mathbf{1}} + B_{\mathbf{1}}) - (A_{\mathbf{Q}_c-\mathbf{2}} + B_{\mathbf{Q}_c-\mathbf{2}}).$$

We write the couplings as

$$C_{\mathbf{1}} = \Big[(A_{\mathbf{1}} - B_{\mathbf{1}}) - (A_{\mathbf{2}} + B_{\mathbf{2}})\Big] + \psi(\mathbf{1},\mathbf{2}),$$
$$C_{\mathbf{2}} = \Big[(A_{\mathbf{2}} - B_{\mathbf{2}}) - (A_{\mathbf{1}} + B_{\mathbf{1}})\Big] + \psi(\mathbf{2},\mathbf{1}).$$

Substituting the above expressions into (A.11), after a little algebra, we find that

$$\mathrm{Re}\Big[\Sigma_S^{(3)}(\mathbf{k},0) + \Sigma_O^{(3)}(\mathbf{k},0)\Big] = \frac{1}{N}\sum_{\mathbf{q}} \frac{1}{\Omega_{\mathbf{q}}}\Big[2\Omega_{\mathbf{q}}^2 - 2(A_{\mathbf{q}}A_{\mathbf{k}-\mathbf{q}} + B_{\mathbf{q}}B_{\mathbf{k}-\mathbf{q}})$$
$$+2(A_{\mathbf{q}} + B_{\mathbf{q}})\,\psi(\mathbf{q},\mathbf{k}-\mathbf{q}) - 2(A_{\mathbf{q}} - B_{\mathbf{q}})\,\psi(\mathbf{k}-\mathbf{q},\mathbf{q}) + \mathcal{O}(\psi^2)\Big].$$

Together with the quartic part, we arrive at

$$\mathrm{Re}\left[\Sigma_S(\mathbf{k},0)+\Sigma_O(\mathbf{k},0)\right]=\frac{1}{N}\sum_{\mathbf{q}}\frac{1}{\Omega_{\mathbf{q}}}\Big[\Omega_{\mathbf{q}}^2-(A_{\mathbf{q}}+B_{\mathbf{q}})(A_{\mathbf{k}-\mathbf{q}}+B_{\mathbf{k}-\mathbf{q}})$$
$$+2(A_{\mathbf{q}}+B_{\mathbf{q}})\,\psi(\mathbf{q},\mathbf{k}-\mathbf{q})-2(A_{\mathbf{q}}-B_{\mathbf{q}})\,\psi(\mathbf{k}-\mathbf{q},\mathbf{q})+\mathcal{O}(\psi^2)\Big]+\mathcal{O}\left((\Delta k)^2\right).$$

Since $A_{\mathbf{q}}, B_{\mathbf{q}}$ and $\Omega_{\mathbf{q}}$ are all even functions of $\mathbf{q}$, the expression above can be written as

$$\mathrm{Re}\left[\Sigma_S(\mathbf{k},0)+\Sigma_O(\mathbf{k},0)\right]=\frac{1}{N}\sum_{\mathbf{q}}\frac{1}{\Omega_{\mathbf{q}}}\Big[\Omega_{\mathbf{q}}^2-\frac{1}{2}(A_{\mathbf{q}}+B_{\mathbf{q}})(A_{\mathbf{k}-\mathbf{q}}+B_{\mathbf{k}-\mathbf{q}}+A_{\mathbf{k}+\mathbf{q}}+B_{\mathbf{k}+\mathbf{q}})$$
$$+2(A_{\mathbf{q}}+B_{\mathbf{q}})\,\psi(\mathbf{q},\mathbf{k}-\mathbf{q})-2(A_{\mathbf{q}}-B_{\mathbf{q}})\,\psi(\mathbf{k}-\mathbf{q},\mathbf{q})+\mathcal{O}(\psi^2)\Big]+\mathcal{O}\left((\Delta k)^2\right).$$

When $\mathbf{k}\to\mathbf{Q}_c$, we have

$$\begin{aligned}
&A_{\mathbf{k}-\mathbf{q}}+B_{\mathbf{k}-\mathbf{q}}+A_{\mathbf{k}+\mathbf{q}}+B_{\mathbf{k}+\mathbf{q}}=J_{\mathbf{k}-\mathbf{q}}+J_{\mathbf{k}+\mathbf{q}}-2J_{\mathbf{Q}_c}\\
&\approx J_{\mathbf{Q}_c-\mathbf{q}}+J_{\mathbf{Q}_c+\mathbf{q}}-2J_{\mathbf{Q}_c}+\sum_i\left.\frac{\partial(J_{\mathbf{k}-\mathbf{q}}+J_{\mathbf{k}+\mathbf{q}})}{\partial k_i}\right|_{\mathbf{k}=\mathbf{Q}_c}\Delta k_i+\mathcal{O}\left((\Delta k)^2\right)\\
&=2(A_{\mathbf{q}}-B_{\mathbf{q}})+\sum_i\left.\frac{\partial(J_{\mathbf{k}-\mathbf{q}}+J_{\mathbf{k}+\mathbf{q}})}{\partial k_i}\right|_{\mathbf{k}=\mathbf{Q}_c}\Delta k_i+\mathcal{O}\left((\Delta k)^2\right);
\end{aligned}$$

$$\begin{aligned}
\psi(\mathbf{q},\mathbf{k}-\mathbf{q})&=J_{\mathbf{k}-\mathbf{q}}-J_{\mathbf{Q}_c-\mathbf{q}}\approx\sum_i\left.\frac{\partial J_{\mathbf{k}-\mathbf{q}}}{\partial k_i}\right|_{\mathbf{k}=\mathbf{Q}_c}\Delta k_i+\mathcal{O}\left((\Delta k)^2\right),\\
\psi(\mathbf{k}-\mathbf{q},\mathbf{q})&=J_{\mathbf{q}}-J_{\mathbf{k}-\mathbf{Q}_c-\mathbf{q}}\approx-\sum_i\left.\frac{\partial J_{\mathbf{k}-\mathbf{Q}_c-\mathbf{q}}}{\partial k_i}\right|_{\mathbf{k}=\mathbf{Q}_c}\Delta k_i+\mathcal{O}\left((\Delta k)^2\right)\\
&=\sum_i\left.\frac{\partial J_{\mathbf{k}}}{\partial k_i}\right|_{\mathbf{k}=\mathbf{q}}\Delta k_i+\mathcal{O}\left((\Delta k)^2\right).
\end{aligned}$$

The last term is an odd function of $\mathbf{q}$ so that it vanishes after the summation over $\mathbf{q}$.

From these we obtain

$$\begin{aligned}\mathrm{Re}\left[\Sigma_S(\mathbf{k},0)+\Sigma_O(\mathbf{k},0)\right] =& \frac{1}{N}\sum_{\mathbf{q}}\frac{1}{\Omega_{\mathbf{q}}}\Bigg[\Omega_{\mathbf{q}}^2 \quad \Omega_{\mathbf{q}}^2 \\ & \frac{1}{2}(A_{\mathbf{q}}+B_{\mathbf{q}})\sum_i \left.\frac{\partial(J_{\mathbf{k}-\mathbf{q}}+J_{\mathbf{k}+\mathbf{q}})}{\partial k_i}\right|_{\mathbf{k}=\mathbf{Q}_c}\Delta k_i \\ & + 2(A_{\mathbf{q}}+B_{\mathbf{q}})\sum_i \left.\frac{\partial J_{\mathbf{k}-\mathbf{q}}}{\partial k_i}\right|_{\mathbf{k}=\mathbf{Q}_c}\Delta k_i\Bigg] + \mathcal{O}\left((\Delta k)^2\right) \\ =& \sum_i \frac{1}{N}\sum_{\mathbf{q}}\frac{A_{\mathbf{q}}+B_{\mathbf{q}}}{\Omega_{\mathbf{q}}}\left.\frac{\partial J_{\mathbf{k}+\mathbf{q}}}{\partial k_i}\right|_{\mathbf{k}=\mathbf{Q}_c}\Delta k_i + \mathcal{O}\left((\Delta k)^2\right),\end{aligned}$$

that is,

$$\mathrm{Re}\left[\Sigma_S(\mathbf{k},0)+\Sigma_O(\mathbf{k},0)\right] = \sum_i L_i\Delta k_i + \mathcal{O}\left((\Delta k)^2\right) \tag{A.12}$$

Thus,

$$\lim_{\mathbf{k}\to\mathbf{Q}_c} F_{\mathbf{k}}^{(3)} = \lim_{\mathbf{k}\to\mathbf{Q}_c}\frac{(A_{\mathbf{k}} \quad B_{\mathbf{k}})^{1/2} \quad \sum_i L_i\Delta k_i}{(\sum_{i,j} 2M_{ij}\Delta k_i\Delta k_j)^{1/2}}$$

Since $L_y = 0, M_{xy} = M_{yx} = 0$ in our case, the formula is simplified as

$$\lim_{\mathbf{k}\to\mathbf{Q}_c} F_{\mathbf{k}}^{(3)} = \lim_{\mathbf{k}\to\mathbf{Q}_c}\frac{(A_{\mathbf{k}} \quad B_{\mathbf{k}})^{1/2} \quad (L_x\Delta k_x)}{\left[2M_{xx}(\Delta k_x)^2 + 2M_{yy}(\Delta k_y)^2\right]^{1/2}}$$

The region between $\mathbf{Q}_0$ and $\mathbf{Q}_c$ can not be discussed in the analytic approach because the slope in the k_x direction changes sign when the non-analytical point $\mathbf{Q}$ is shifted from $\mathbf{Q}_c$ to $\mathbf{Q}_0$. Based on this analyticity consideration, we choose $\mathbf{k}$-approaching $\mathbf{Q}_c$ from the right along k_x direction in the limiting evaluation, i.e.

$$\begin{aligned}\lim_{(k_x,0)\to(Q_c^+,0)} F_{\mathbf{k}}^{(3)} &= \lim_{(k_x,0)\to(Q_c^+,0)}\frac{(A_{\mathbf{k}} \quad B_{\mathbf{k}})^{1/2} \quad (L_x\Delta k_x)}{\left[2M_{xx}(\Delta k_x)^2\right]^{1/2}} \\ &= (A_{\mathbf{Q}_c} \quad B_{\mathbf{Q}_c})^{1/2}\lim_{(k_x,0)\to(Q_c^+,0)}\frac{L_x\Delta k_x}{\left(2M_{xx}\right)^{1/2}|\Delta k_x|} \\ &= (A_{\mathbf{Q}_c} \quad B_{\mathbf{Q}_c})^{1/2}\left(\frac{1}{2}M_{xx}\right)^{1/2}M_{xx}^{-1}L_x\end{aligned}$$

Recall that

$$\Delta Q_x = Q_c \quad Q_0 = \frac{1}{2S}M_{xx}^{-1}L_x,$$

so that

$$\lim_{(k_x,0)\to(Q_c^+,0)} F_{\mathbf{k}}^{(3)} = 2S(A_{\mathbf{Q}_c} \quad B_{\mathbf{Q}_c})^{1/2}\Big(\frac{1}{2}M_{xx}\Big)^{1/2}(Q_c \quad Q_0)$$

Thus we have

$$\begin{aligned}\widetilde{\omega}_{\mathbf{Q}_c} = \omega_{\mathbf{Q}_c} + \Delta\omega_{\mathbf{Q}_c} &= 2S\Big[\frac{1}{2}M_{xx}(A_{\mathbf{Q}_c} \quad B_{\mathbf{Q}_c})\Big]^{1/2}(Q_c \quad Q_0) \\ &= 2S\Big[\frac{1}{2}M_{xx}(A_{\mathbf{Q}_c} \quad B_{\mathbf{Q}_c})\Big]^{1/2}|\Delta\mathbf{Q}| \end{aligned} \tag{A.13}$$

Therefore, at $\mathbf{k} = \mathbf{Q}_c$, the $1/S$-renormalized excitation acquires a finite positive energy gap which is linear in momentum with respect to the new Goldstone mode position $\mathbf{Q}_0$ and is of order $\mathcal{O}(S^0)$ This feature is consistent with our order-by-order symmetry argument.

Finally, we turn to the new $\mathbf{Q}$-value of the Goldstone mode to investigate the excitation energy at $\mathbf{k} = \mathbf{Q}_0$.

It is easy to see that

$$\begin{aligned}(A_{\mathbf{k}} \quad B_{\mathbf{k}})^{1/2}\Big|_{\mathbf{k}=\mathbf{Q}_0} &= \text{finite}, \\ 2S\Delta A_{\mathbf{k}}\Big|_{\mathbf{k}=\mathbf{Q}_0} &= \text{finite}, \\ \mathrm{Re}\Big[\Sigma_S(\mathbf{k},\omega_{\mathbf{k}}) \quad \Sigma_O(\mathbf{k},\omega_{\mathbf{k}})\Big]\Big|_{\mathbf{k}=\mathbf{Q}_0} &= \text{finite}. \end{aligned} \tag{A.14}$$

Due to the wave vector dependence in the neighborhood of $\mathbf{Q}_c$, the other terms in (A.3) behave as

$$\begin{aligned}\mathrm{Re}\Sigma_A(\mathbf{k},\omega_{\mathbf{k}})\Big|_{\mathbf{k}=\mathbf{Q}_0} &\sim \mathcal{O}(|\Delta\mathbf{Q}|), \\ (A_{\mathbf{k}} + B_{\mathbf{k}})^{1/2}\Big|_{\mathbf{k}=\mathbf{Q}_0} &\sim \mathcal{O}(|\Delta\mathbf{Q}|), \\ \mathrm{Re}\left[\Sigma_S(\mathbf{k},\omega_{\mathbf{k}}) + \Sigma_O(\mathbf{k},\omega_{\mathbf{k}})\right] &\sim \mathcal{O}(|\Delta\mathbf{Q}|) \end{aligned}$$

Since $|\Delta\mathbf{Q}|$ is of order $\mathcal{O}(S^{-1})$, for the solution of $\Delta\omega_{\mathbf{k}} \sim \mathcal{O}(S^0)$, we still have

$$\begin{aligned} F_{\mathbf{k}}^{(1)}\Big|_{\mathbf{k}=\mathbf{Q}_0} &= 0, \\ F_{\mathbf{k}}^{(2)}\Big|_{\mathbf{k}=\mathbf{Q}_0} &= 0, \\ \mathrm{Re}\Sigma_A(\mathbf{k},\omega_{\mathbf{k}})\Big|_{\mathbf{k}=\mathbf{Q}_0} &= 0. \end{aligned} \tag{A.15}$$

But the last term becomes

$$\begin{aligned} F_{\mathbf{k}}^{(3)}\Big|_{\mathbf{k}=\mathbf{Q}_0} =& \frac{(A_{\mathbf{Q}_0}-B_{\mathbf{Q}_0})^{1/2}\cdot\sum_i L_i\Delta Q_i}{(\sum_{i,j}2M_{ij}\Delta Q_i\Delta Q_j)^{1/2}} \\ =& \frac{(A_{\mathbf{Q}_0}-B_{\mathbf{Q}_0})^{1/2}\cdot L_x\Delta Q_x}{(2M_{xx})^{1/2}|\Delta Q_x|}. \end{aligned}$$

Since $\Delta Q_x = Q_0 - Q_c < 0$, we obtain

$$\begin{aligned} \Delta\omega_{\mathbf{Q}_0} =& -(A_{\mathbf{Q}_0}-B_{\mathbf{Q}_0})^{1/2}\Big(\frac{1}{2}M_{xx}\Big)^{1/2}M_{xx}^{-1}L_x \\ =& -2S\Big[\frac{1}{2}M_{xx}(A_{\mathbf{Q}_0}-B_{\mathbf{Q}_0})\Big]^{1/2}|\Delta\mathbf{Q}|. \end{aligned}$$

From the LSWT, the bare excitation energy at $\mathbf{Q}_0$ is

$$\begin{aligned} \omega_{\mathbf{Q}_0} =& 2S(A_{\mathbf{Q}_0}-B_{\mathbf{Q}_0})^{1/2}(A_{\mathbf{Q}_0}+B_{\mathbf{Q}_0})^{1/2} \\ =& 2S\Big[\frac{1}{2}M_{xx}(A_{\mathbf{Q}_0}-B_{\mathbf{Q}_0})\Big]^{1/2}|\Delta\mathbf{Q}|. \end{aligned}$$

Therefore we have

$$\widetilde{\omega}_{\mathbf{Q}_0} = \omega_{\mathbf{Q}_0} + \Delta\omega_{\mathbf{Q}_0} = 0, \tag{A.16}$$

which demonstrates that $\mathbf{Q}_0$ is, indeed, a zero mode.

In conclusion, Goldstone modes occur at $\mathbf{k} = \mathbf{0}$ and $\pm\mathbf{Q}_0$ in the $1/S$-renormalized excitation spectrum as expected by symmetry.